NEUTRAL BIDENDATE GUANIDINE-BASED ZINC COMPLEXES FOR THE RING OPENING POLYMERIZATION OF LACTIDE

BRANDON S. KHAN

A THESIS SUBMITTED TO THE FACULTY OF GRADUATE STUDIES IN PARTIAL FUFILMENT OF THE REQUIERMENTS FOR THE DEGREE OF

MASTER OF SCIENCE

GRADUATE PROGRAM IN CHEMISTRY
YORK UNIVERSITY
TORONTO, ONTARIO

APRIL 2022

Abstract

Herein is reported the synthesis and structure elucidation of three novel zinc complexes bearing neutral bidentate guanidine ligands. Ligand and complex structures were obtained computationally and leveraged against single-crystal studies to develop a method for predicting solid state structures of future complexes. Structure-activity relation was explored using computational chemistry. The catalysts were tested for ring opening polymerization of lactide to poly(lactic acid) in the melt, in the absence of any solvent, at 135 °C. The most active complex displayed a rate constant for propagation, k_p, of 26 $M^{-1}h^{-1}$. The catalyst showed some stereoselectivity with a heterotactic bias in the polymer (P_r = 0.60). The polymer number average molecular weight was determined to be ~4700 g mol^{-1}. MALDI-TOF mass spectrometry was used to elucidate the mechanism of the polymerization. The end groups suggested water activation, implying an activated monomer mechanism. The polydispersity index of the polymer was determined by gel permeation chromatography to be 1.10 indicating a well-behaved polymerization.

Acknowledgements

I would first like to thank Professor Gino G. Lavoie for giving me the opportunity to develop my skills as a researcher. Over the course of my academic career, Professor Lavoie has guided me to think critically and operate systematically, skills that I will carry with me in the future. I would like to thank my supervisorial committee; Professor Caputo and Professor Orellana for their guidance and advice, both in and out of the lab. I am also so thankful for Dr. Howard Hunter, who always went above and beyond when it came to lending his expertise in structure elucidation along with always offering a kind ear. I would like to highlight some of the amazing friends and colleagues I was fortunate enough to meet over my time at York University. Firstly, to past group members Mathew A. Wiebe and Juan E.R. Villanueva, the impact that your mentorships and friendships have had cannot be overstated. I am eternally grateful for everything you have taught me: fundamentals, practical lab skills, as well as your guidance outside of the lab. Thank you to current members Jesse LeBlanc and Victor Flores, our discourse about day-to-day chemistry helps cement my own understanding profoundly. To my friends of the Orellana Group, Nour, Hao, Anmol, and Brian, you have all played such an impactful role in my desire to pursue knowledge. Along with members from the Caputo Group, especially Jordan Bentley, you have never shied away from dropping everything to help me, thank you.

Lastly, to my family, this would not have been possible without you. Every sacrifice you made for me was not unnoticed. My success is attributed to you all. Thank you for everything you have done for me.

Table of Contents

List of Abbreviations

AMM	Activated Monomer Mechanism
BDI	β-diketiminate
CIM	Coordination Insertion Mechanism
COSY	Correlation Spectroscopy
DCIC	Diacyl Chloroimidazolium Chloride
DFT	Density Functional Theory
DIC	N,N′-Diisopropylcarbodiimide
DSC	Differential Scanning Calorimetry
EA	Elemental Analysis
GPC	Gel Permeation Chromatography
IPP	Inversely Polarized Phosphaalkene
IV	Intrinsic Viscosity
LA	Lactic Acid
NEt_3	Triethylamine
NHC	N-Heterocyclic Carbene
NHI	N-Heterocyclic Imine
NMR	Nuclear Magnetic Resonance
PDI	Polydispersity Index
PLA	Poly(lactic acid)
PLLA	Poly(L-lactic acid)
PDLA	Poly(D-lactic acid)
PLLA-b-PDLA	Stereoblock Poly(lactic acid)
PS	Polystyrene
QNMR	Quantitative Nuclear Magnetic Resonance
ROP	Ring Opening Polymerization
rt.	Room Temperature
RALS	Right Angle Light Scattering
RI	Refractory Index
SALEN	Salicylaldehyde Ethylenediamine
$Sn(Oct)_2$	Tin(II) 2-ethylhexanoate
TGA	Thermogravimetric Analysis
THF	Tetrahydrofuran
$TMSN_3$	Trimethylsilyl Azide
VT	Variable Temperature
XRD	X-ray Diffraction

List of Schemes

List of Figures

List of Tables

List of Equations

1 Introduction

1.1 Poly(lactic acid)

The Nobel prize-winning work of Ziegler and Natta in the 1960's has led to the mass production of polyolefins as commercially-useful polymers (**Figure 1**).Their work allowed for organo-polymeric materials to become the essential component in many everyday use items such as packaging, construction materials and medical devices.[1] As a result, an estimated 150 million metric tons of polyolefins are annually produced globally.[2] However, their continual and growing use in human life has led to the realization of some shortfalls. Polyolefins possess an inherent chemical inertness that causes them to accumulate in the environment for extended periods of time after being discarded.[3] In 2015, of 302 million metric tons of plastic waste generated, polyolefins (high and low density polyethylene, polypropylene, polystyrene) accounted for 56% (169 million metric tons).[4] Naturally-occurring weathering of debris results in formation of micro-particulate that finds its way into marine ecosystems whereby it is ingested by marine life. These micro-particulates can contain organic molecules, such as bisphenol A, that can accumulate and transfer the toxic substances up the food chain.[5]

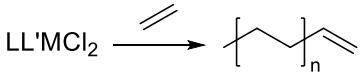

Where M = Ti, Zr, Hf

Figure 1. General form of the initial homogenous Ziegler–Natta catalyst (L = L' = Cp).

Effective strategies to mitigate the environmental effects of single-use plastics are to reduce their application and to design alternatives with end-of-life recyclability/reusability in mind. Given the declining reserves of fossil fuels coupled with the detrimental

environmental impact of non-compostable materials, interest has been generated for commercially-viable biodegradable alternatives. The ring-opening polymerization (ROP) of cyclic esters can be used to generate biodegradable polyesters in a controlled fashion from renewable inexpensive polysaccharide feedstocks, such as sugarcane, switchgrass and corn.[6] Annually, 150 billion tonnes of polysaccharides are produced naturally, with human consumption only accounting for approximately 1% by volume.[7]

Typically, the production of polymers from these feedstocks begins with separating the starch monomer precursor. These biopolymers are then depolymerized to produce monosaccharides such as sucrose, glucose and fructose. Transformation of these monosaccharides by biological enzymatic systems into building-block chemicals such as lactic acid or succinic acid then allows for polymerization of the monomers to commercially-useful polymers.[7]

Poly(lactic acid) (PLA) has emerged as a frontrunner in biodegradable plastics due to its synthesis from natural resource-derived precursors, its comparable mechanical properties to select polyolefins, and its ease of processability.[8] Owing to the stereogenic center of lactic, there exist two possible enantiomers; L-lactic acid and D-lactic acid (**Figure 2**).

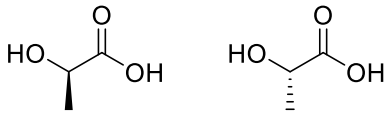

L-lactic acid D-lactic acid

Figure 2. Stereoisomers of lactic acid.

The industrial production of lactic acid is currently accomplished by microbial carbohydrate fermentation of starches into the optically-pure product.[6] Generation of racemic DL-lactic acid is accomplished synthetically by reacting acetaldehyde, generated from petrochemical sources, with HCN and a catalytic amount of base to produce lactonitrile. Hydrolysis by sulfuric acid generates lactic acid and an ammonium salt. The lactic acid is then esterified with methanol to produce methyl lactate, purified and then hydrolyzed to the racemic lactic acid product (**Figure 3**).

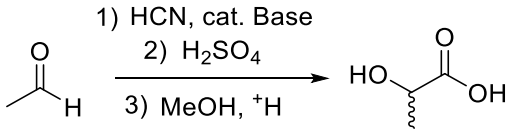

Figure 3. Synthetic route to *rac*-lactic acid

It is possible to separate the D- and L-enantiomers by high performance liquid chromatography (HPLC).[6] Owing to the stereogenic center of lactic acid, optical purity is of the utmost importance as the bulk material properties of the resulting PLA can be significantly influenced by enantiomeric impurities.[9]

Lactic acid is however not the monomer of choice in the production of PLA owing to the limitations of polycondensation. Rather, lactide, the cyclic dimer of lactic acid, is used preferentially as the monomer in the production of PLA. The chiral nature of lactic acid leads to three stereoisomers of lactide: L-lactide, D-lactide, and *meso*-lactide (**Figure 4**).

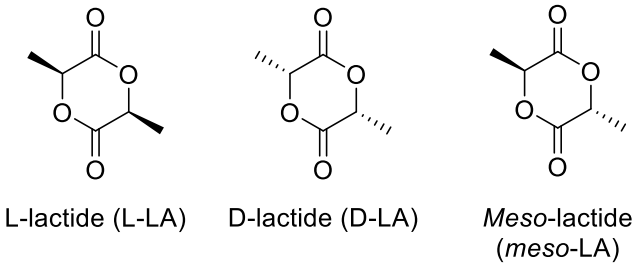

Figure 4. Stereoisomers of lactide.

Lactide is produced by the thermal degradation of low molecular weight oligomers of lactic acid, which are typically produced by step-growth polymerization.[6] The resulting lactide can then be polymerized to commercially-valuable PLA by ring opening polymerization (ROP). Once a commercial item consisting of PLA has served its purpose and is disposed of, naturally-occurring environmental degradation breaks down the PLA to LA. The relationship of lactic acid, lactide, and PLA is shown in **Figure 5**.

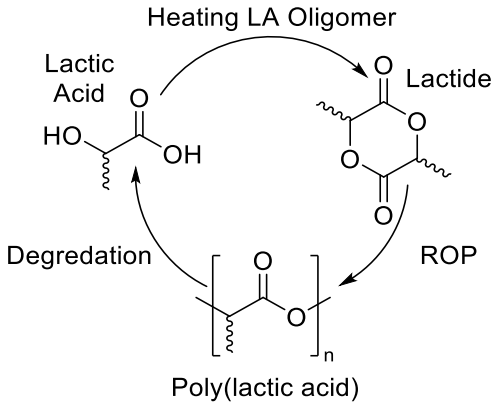

Figure 5. Relationship between lactic acid, lactide and poly(lactic acid).

The sequential arrangement of stereogenic centers in the polymer chain, or tacticity, greatly affects the bulk material properties (**Figure 6**). The irregular microstructure of atactic PLA results in an amorphous polymer and is typically not as useful in commercial products compared to polymers of other stereocomplexities.[10]

Heterotactic PLA has a repeat unit consisting of both D- and L-lactide and is amorphous as well. Syndiotactic PLA possesses repeating units with alternating relative stereogenic centers, affording a crystalline polymer with a melting temperature (T_m) of 152 °C.[11] Isotactic poly(L-lactic acid) (PLLA) and poly(D-lactic acid) (PDLA), which are enantiomers, have a T_m of 180 °C.[11] Most desirable is stereoblock PLA (PLLA-*b*-PDLA), which contains distinct "blocks" of PLLA and PDLA within a single strand of polymer. This polymer has a T_m of 200 °C and shows enhanced mechanical properties.[11] The production of stereoblock PLA can be accomplished by either the sequential addition of enantiopure D- and L-lactide or by the polymerization of a racemic mixture of D- and L-lactide by a stereoselective catalyst.[10]

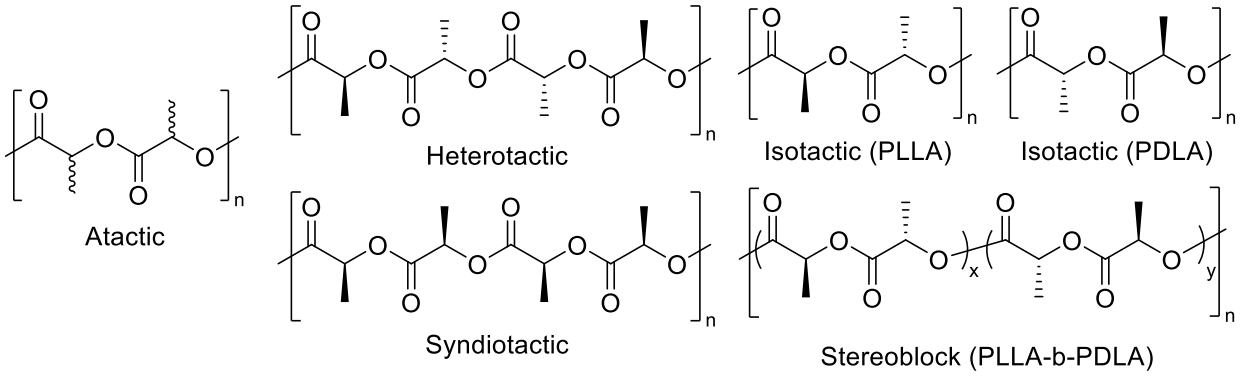

Figure 6. Various microstructures of PLA.

The tacticity of the polymer can be described in two manners. P_m is the probability of having two adjacent stereocenters with the same chirality between the linkage of the stereocenter of the growing polymer chain attached to the metal and the incoming monomer unit. Alternatively, P_r is the probability of having two adjacent stereocenters with the opposite chirality.[11] These probabilities are calculated by performing homonuclear decoupled $^1H\{^1H\}$ NMR experiments on the polymer to remove the scalar

coupling between the CH (methine) and CH_3 (methyl) fragments. This results in five unique resonances from tetrads, which represent the possible arrangements of four stereocenters. The relative integrations substituted into Bernoullian-derived equations generate for P_m and P_r values.[11]

There exist several degradation pathways of PLA, the principal one being environmental degradation or “weathering”. In environmental degradation, natural weathering processes break down water-insoluble long chain PLA into short water-soluble oligomers.[12] This is largely accomplished by water solvation of the polymer matrix hydrolysing the ester functionalities, cleaving the long polymer chains. The solvation of water molecules between polymer chains is facile for amorphous phases, but challenging for crystal phases as the highly order microstructure precludes the solvent molecules from permeating strands and hydrolysing them.[13] The hydrolysis products are carboxylic acid end group oligomers that act as catalysts in further ester hydrolysis.[13] As the degradation process continues, oligomers close to the surface of the matrix will leach out into the degradation medium, while those located deeper in the matrix will remain trapped and contribute to the acid-catalyzed ester hydrolysis. Many factors can affect the degradation rate of PLA, which include but are not limited to solubility of oligomers in the degradation medium, pH of the degradation medium, degradation temperature. Additionally, the number average molecular weight (M_n), the weight average molecular weight (M_w), the polydispersity index (PDI), which is the ratio of M_w to M_n, the morphology and the percentage crystallinity of the polymer all affect the rate of degradation.[14]

1.2 Step-Growth Polymerization of PLA

1.2.1 Polycondensation

The polycondensation mechanism for the production of PLA is subject to the typical limitations of step-growth polymerization. Ultra-pure conditions are required to achieve the very high conversions (>98%) needed to produce polymer chains with sufficiently large number average molecular weights that are commercially desirable. This, coupled with the polydispersity index (which is a measure of uniformity of polymer lengths in a given mixture) of two for step growth polymerizations, make polycondensation an unfavourable method in the production of PLA.[15]

There exist however methods to overcome the inherent shortcomings of PLA production by condensation of LA. Principally, these techniques aim to control the two equilibria that exist between the hydration and dehydration of carboxyl and hydroxyl terminals to produce PLA and the competing cyclization/de-cyclization of lactic acid to lactide (**Figure 7**).[6] High temperature, coupled with performing the condensation *in vacuo,* removes the condensed water from the system, driving the reaction towards the high conversions needed to produce PLA with appreciable length. This can be accomplished by Soxhlet extraction of water via molecular sieves over several days to accomplish high conversion to PLA.[15] The reaction conditions must be carefully monitored to ensure that the high evacuation does not result in the removal of the lactide monomer which can lead to lower molecular weight polymer.

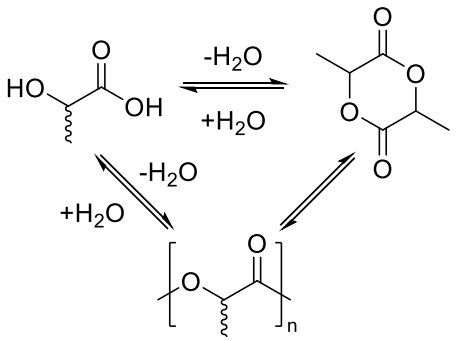

Figure 7. Relationship between lactic acid, lactide and PLA.

1.3 Chain Growth Polymerization of PLA

Alternatively, the chain-grown polymerization of lactide affords higher molecular weight PLA as a product of better control of the polymerization process.[11] In contrast to step growth polymerization of lactic acid to PLA, the chain-grown polymerization of PLA by lactide is the most prevalent synthetic methodology used in commercial manufacturing. As a product of better control of the polymerization process, chain growth polymerizations afford higher molecular weight polymers much faster than step growth polymerizations as monomers only react with already growing polymer chains to generate an overall lower PDI.[11] There are four principal chain growth polymerization mechanisms for the production of PLA: cationic, anionic, coordination-insertion mechanism, and activated monomer mechanism.

1.3.1 Cationic Polymerization

Cationic ROP of lactide to produce PLA are induced by strong Brønsted acids and alkylating agents, such as triflic acid or methyl triflate, respectively.[13,16] The initiation step sees the formation of an oxocarbenium of one of the carbonyl groups of the lactide by

protonation or alkylation. The delocalization of positive charge across the endocyclic oxygen and the oxocarbenium activates the adjacent O-CH bond allowing for a nucleophile, whether it be an externally added alcohol or the carbonyl group of another lactide monomer to attack (**Figure 8**).

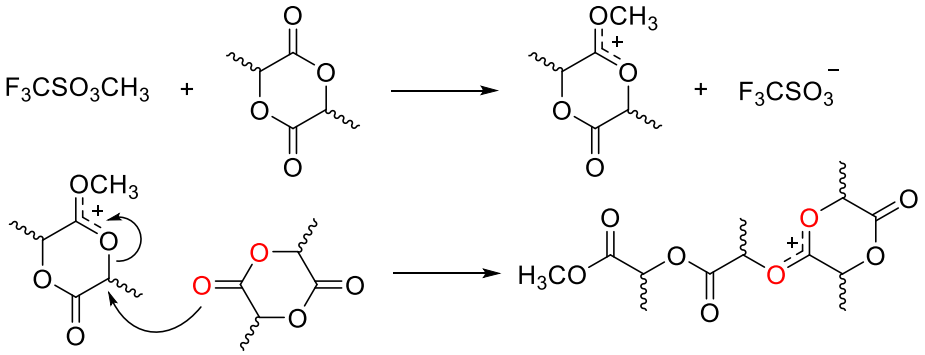

Figure 8. Cationic ROP of lactide in the absence of an alcohol initiator.

In the case where the carbonyl group of another lactide monomer performs the attack, the propagation step involves lactide monomers attacking the endocyclic O-CH bond of the activated monomer. The propagation continues until termination by a monofunctional nucleophile or chain transfer.[13,17]

1.3.2 Anionic Polymerization

Anionic ROP of lactide to produce PLA is induced by strongly nucleophilic anions, such as metal alkoxides. Nucleophiles attack the carbonyl carbon of the lactide monomer, producing a tetrahedral anionic oxygen intermediate that causes ring opening by breaking the endocyclic O-CO bond.[13,18] The resulting alkoxide acts the nucleophile in subsequent propagation steps (**Figure 9**).

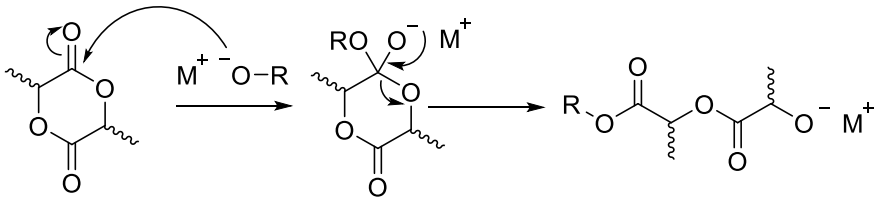

Figure 9. Initiating step of anionic ROP of lactide facilitated by a metal-alkoxide .

The chain growth is terminated by a quenching agent or by protic impurities present in the lactide feedstock, such as lactic acid or water. Strongly nucleophilic initiators or bases have been known to deprotonate the endocyclic CH-O in the monomer leading to racemization of the lactide and subsequently, poorly-defined microstructure of the resulting polymer.[13,19]

Initiators have also been known to promote transesterification, or backbiting reactions, in which the alkoxide end group of a growing polymer chain substitutes at the ester carbon of another polymer chain. Transesterification is often associated with a broadening of the PDI and the molecular weight of the polymers are often too low for common commercial applications.[13] There exist two types of transesterification reactions: intermolecular and intramolecular. In intermolecular transesterification, a growing polymer chain breaks the ester bond of an already-formed polymer chain, scrambling the polymer lengths and increasing the PDI (**Figure 10**).

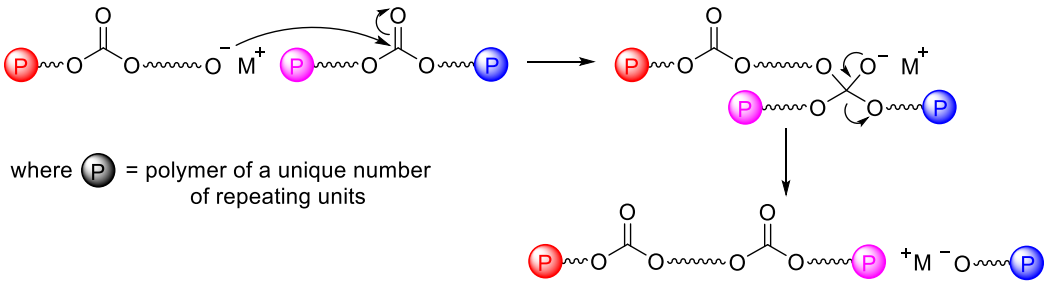

Figure 10. Intermolecular transesterification of PLA resulting in scrambling of polymer chains.

Alternatively, in the intramolecular reaction, the alkoxide end group of a growing polymer chain substitutes at an ester functionality found along the length of the same growing chain, leading to the cyclization of the PLA (**Figure 11**).

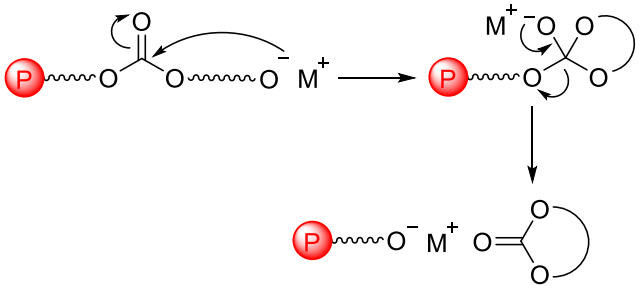

Figure 11. Intramolecular transesterification of PLA resulting in cyclized product.

1.3.3 Coordination-Insertion Mechanism and Active Monomer Mechanism

The coordination-insertion mechanism (CIM) is the most widely accepted mechanism of metal-catalyzed ROP of lactide (**Scheme 1**).[20] Typical catalytic systems that undergo CIM contain alkali earth, group 14, or transition metals (Mg, Sn, Ti, Zn) that are weakly Lewis acidic.[21] These catalytic systems, also known as initiators, are typically furnished with anionic or neutral spectator ligands, along with an alkoxide ligand that participate in the catalytic cycle. Alkoxides are preferentially used owing to their nucleophilicity. However, they often promote epimerization side reactions, which can greatly impact the microstructure and resulting bulk material properties of the polymer.[15] The alkoxide ligand can be generated from addition of the requisite alcohol to a precatalyst and plays a crucial role in the initiation step of the catalytic cycle. The mechanism begins with the coordination of a monomer to the metal center through the carbonyl group, thereby

activating the acyl carbon for a migratory insertion. This leads to the ring opening of the monomer with retention of the stereochemistry. The new metal alkoxide complex acts as the propagating species in the polymerization. Transesterification can occur during CIM resulting in shorter polymer chains and broadening of the PDI.

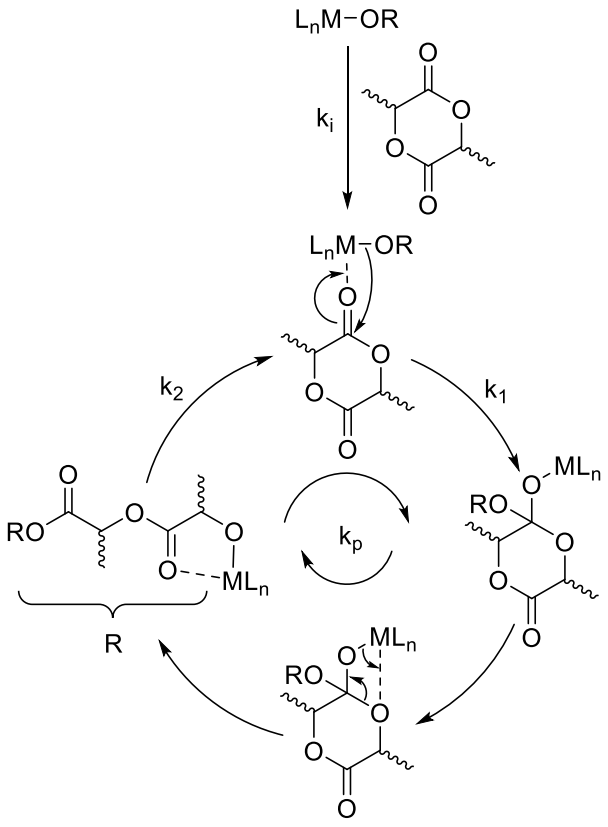

Scheme 1. CIM of lactide ROP.

The thermodynamics of DL-lactide ROP was determined by measuring the heat capacities and enthalpies of combustion. The enthalpies and entropies for ROP of lactide were determined to be –27 kJ mol^{-1} and –13 J mol^{-1} K^{-1} in the melt, indicative of an exothermic process.[15] The polymerization of lactide ROP is an overall second-order rate law with first order with respect to the monomer and initiator concentrations. Kinetic features of a successful polymerization include: a high rate of initiation to propagation

(k_i/k_p), and a high rate of propagation to transesterification (k_p/k_{tr}).[15] Catalytic activity is best represented by the rate of propagation (R_p) and is determined by equation 1:

$$R_p = -\frac{d[LA]}{dt} = k_p[I][LA] \quad (1)$$

wherein [LA] = lactide concentration, [I] = concentration of the initiator.

Given that both k_p and [I] are constant, equation 1 can be simplified to equation 2. The pseudo first-order rate constant, k_{obs}, is determined by monitoring the conversion of LA to PLA during the polymerization. By performing experiments at different concentrations of initiator, the k_p can be determined.

$$R_p = -\frac{d[LA]}{dt} = k_{obs}[LA] \quad (2)$$

In contrast to CIM, Lewis acidic metal salt catalysts and organocatalysts proceed through an activated monomer mechanism (AMM) for the ROP of lactide.[22,23] This mechanism begins similarly to the CIM as the initiation step sees the activation of the monomer by the Lewis acidic metal center upon coordination of the carbonyl group of lactide (**Scheme 2**). The lack of a metal–alkoxide bond to perform the migratory insertion and subsequent ring opening in AMM catalysts necessitates the addition of a polar protic cocatalyst, typically an alcohol. This external nucleophile attacks the electrophilic carbon of the carbonyl group and a subsequent proton migration to the endocyclic oxygen of lactide results in the ring opening of the monomer. In the absence of a cocatalyst, polar impurities in the monomer such as water or lactic acid, can serve as the nucleophile. The now ring-opened monomer capped with a hydroxyl group undergoes a chain transfer, whereby the ring-opened monomer dissociates from the catalyst and a new monomer coordinates.

These hydroxy-capped ring-opened monomer and oligomers act as the polar protic external nucleophile to ring-open an additional monomer, growing the chain length by one unit.

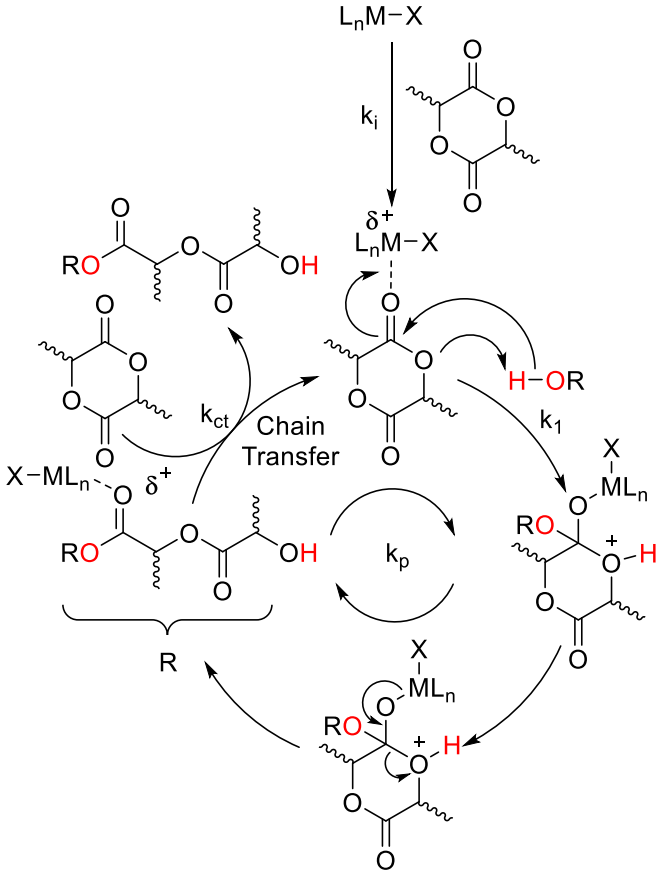

Scheme 2. ROP of lactide by the activated monomer mechanism.

The principal difference between AMM and CIM is that an AMM initiator necessitates an external cocatalyst (normally an alcohol). In CIM, the catalytic system is a two-in-one component, with the nucleophile (normally an alkoxide) σ-bonded to the metal. This distinction, coupled with the necessity of chain transfer for propagation of growing polymer chains in AMM make for the production of large molecular weight polymers more challenging compared to a catalytic system that proceeds through CIM. Production of

large molecular weight polymers with a narrow PDI through an AMM-based initiator is however possible. Given that hydroxy end-capped oligomers exhibit similar reactivity towards the activated monomer, all oligomers will progressively be transformed into large molecular weight polymers.[24] This would imply that the kinetics of the chain transfer equilibria are well behaved. Thus, both the rate constants for chain transfer and for initiation are much larger than the rate constant for propagation ($k_{ct} \gg k_p$ and $k_i \gg k_p$).[24]

1.4 Catalytic Systems for Lactide ROP

There exists a plethora of metal-based catalytic systems used for the ROP of lactide. The industrial standards are simple homoleptic catalysts such, zinc(II) lactate, aluminium isopropoxide and tin(II) octoate ($Sn(Oct)_2$), in conjunction with alcohol co-initiators. These catalyst are capable of lactide polymerization in both solution or in the melt (in the absence of any solvent), which itself requires a reaction temperature of at least 130 °C. Although desirable for their convenient synthesis, they have been known to promote transesterification, which lead to an increase in the PDI.[8]

1.4.1 Tin Octoate

Tin octoate ($Sn(Oct)_2$) serves as the industrially-preferred catalyst (**Figure 12**) owing to its high activity, its ability to produce high molecular weight polymers and its high solubility in organic solvents as well as in molten lactide.[13] The enthalpy and entropy for the polymerization of lactide by tin octoate was determined to be 23.3 ± 1.5 kJ mol^{-1} and 22.0 ± 3.2 J mol^{-1} K^{-1}, with an activation energy of 70.9 ± 1.5 kJ mol^{-1}.[25] The polymerization mechanism in which tin octoate proceeds through has long been contested. However, CIM is now the most widely accepted one with the caveat that the

initial 2-ethylhexanoate "ligand" does not act as the nucleophile in the migratory insertion. This conclusion was reached by end-group analysis of PLLA using ^{1}H NMR spectroscopy, which showed carboxylic acid, and hydroxyl groups and none of the ester end group that would be generated if the octanoate acted as the nucleophile.[26]

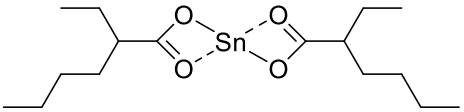

Figure 12. Industry standard $Sn(Oct)_2$ catalyst used in the ring-opening polymerization of lactide.

Commercial tin octoate regularly contains significant quantities of impurities such as water and octanoic acid.[26,27] The activity of tin octoate for lactide ROP was markedly improved by the addition of an alcohol cocatalyst such as 1-dodecanol. The actual active species in the polymerization was thus determined to be a tin alkoxide and the mechanism of polymerization in fact begins with the equilibrium reaction of the alcohol and tin octoate to produce either the monoalkoxide or bis(alkoxide) tin species along with octanoic acid (**Figure 13**).

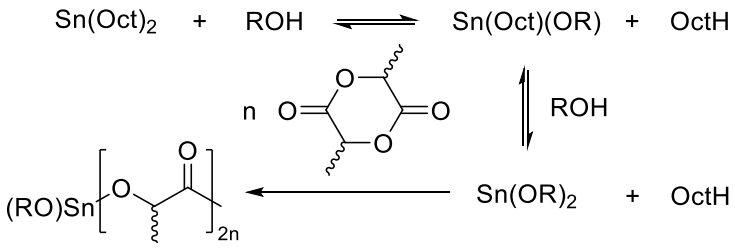

Figure 13. Mechanism of activation for tin octoate by an alcohol cocatalyst.

The tin alkoxide acts as the initiator in the CIM previously observed. Tin alkoxides produce PLLA in THF at 80 °C with molecular weights of up to 1,000,000 g/mol. There is

evidence, however, for the formation of metal aggregates that decrease activity for high monomer concentration polymerizations.

Although an industrially preferred catalyst, there are drawbacks to the use of tin octoate for the preparation of PLA. Tin octoate promotes depolymerization and transesterification reactions as the monomer concentration decreases.[16,28] This catalytic system also possesses no stereoselectivity. Nonetheless, the polymerization of >90% L-LA catalyzed by $Sn(Oct)_2$ produces PLLA that is 90% isotactic with a melting point of 165–170°C.[11] This material is well suited for many commercial applications. However, this material is not suitable as a replacement for polyolefins. This necessitates the stereoselective polymerization of racemic lactide to produce isotactic stereoblock PLA, a task unachievable by the tin catalyst.[11] An alternative catalyst capable of polymerizing lactide into a stereoregular polymer is thus warranted.

Despite reports of cytotoxicity, tin octoate has sporadically been approved for production of PLLA for application in food packaging and medical devices depending on the empirical safety data.[29] The use of tin octoate for the production of PLLA for food packaging require the complete removal of the metal from the resulting polymers, which adds cost to the overall production of the material. Furthermore, the removal can be challenging as the growing polymer chain is attached to tin through an alkoxide bond.[30] The metal alkoxides also affect the thermal properties of the final polymer, decreasing melt processability at high temperatures.[16]

1.4.2 Zinc Complexes Bearing Anionic Ligands

Zinc catalytic systems are an attractive initiator compared to tin as they exhibit high activity, relatively low toxicity, low cost and high tolerance to polar impurities found in lactide. The anionic ligands commonly coordinated to zinc complexes are phenoxy-amines, phenoxy-imines, and β-diiminates (BDI) (**Figure 14**). These ligands have attracted interest due to their ease of synthesis, ability to stabilize low coordinate metal alkoxides and the high catalytic performance of the corresponding transition metal. The BDI zinc isopropoxide complexes (**I**) of Coates have garnered considerable attention due to high activities and stereoselectivities (**Table 1**).[31] The group determined that initiating with an alkoxide produce PLLA with predictable M_n and narrow PDI, while metal amide, acetate and alkyl catalysts resulted in a loss of control in the polymerization as a product of the comparatively lower k_i values (relative to k_p). The rate of polymerization was also greatly improved by increasing the steric imposition of the substituents on the BDI aromatic rings.

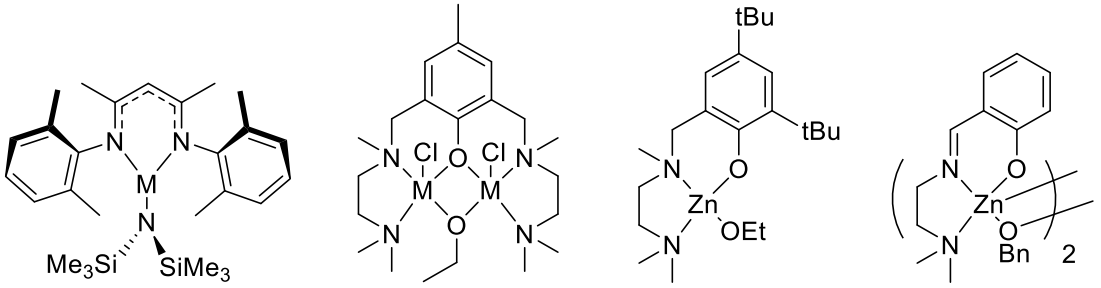

I where M = Mg, Zn

II where M = Mg, Zn

III

IV

Figure 14. Select highly active complexes bearing anionic ligands for the ROP of LA.

Table 1. Rate constants for the ROP of LA to PLA for select highly active complexes bearing anionics ligands.

Catalyst	[I]:[LA]	Rate constants
I	1:490	$k_{app} = 9 \times 10^{-4}$ s^{-1}
II	1:300	$k_p = 0.37$ M^{-1} s^{-1}
III	1:650	$k_p = 2.2$ M^{-1} s^{-1}
IV	1:50	$k_p = 0.68$ M^{-1} s^{-1}

[I] = equivalents of initiator, [LA] = equivalents of lactide. All polymerizations were done at room temperature in DCM.

The binuclear metal alkoxides complexes **II** where M = Zn were shown to have the highest activity and best control of the polymerization process. This is in stark contrast to BDI complexes **I** where M = Zn showed the lowest activity.[32] This was reasoned that the complexes had different rate determining steps (RDS) in the CIM. Two possible RDS exist for CIM, either the coordination of the lactide carbonyl group (k_2) or the migratory insertion of the alkoxide to the carbonyl group (k_1 in **Scheme 1**).[15] Due to the lower coordination number of BDI zinc complexes **I**, k_2 is much larger than k_1. Thus, the rate determining step is migratory insertion. The more polarized M-OR bond in the magnesium complex leads to activities greater than in the corresponding zinc complex. In contrast, the greater coordination number of the binuclear metal alkoxides complex **II** made the coordination and activation the rate determining step. Thus, the stronger Lewis-acidic zinc complex leads to greater activities than the corresponding magnesium complex. The phenoxy-amine complex **III** showed much higher activity than the phenoxy-imine/amine complex **IV** as **III** existed as a mononuclear complex in solution and thus has greater propensity to

coordinate the incoming monomer.[33] It becomes apparent that the coordination number of the complex plays a vital role with the activity decreasing from **III** > **IV** > **II**.

Despite the high activity and stereoselectivity observed in these complexes bearing anionic ligands, they all possess inherent sensitivity to air and moisture, along with potential acidic impurities in the monomer feedstock. This necessitates polymerizations being carried out under inert atmosphere and with ultra-purified lactide monomer (via sublimation). Moreover, the high polymerization activities are only observed for polymerization in solution rather than in the melt, the latter being preferred by the industry.[8] These limitations preclude their industrial application as these conditions would prove costlier than using the less performant tin octoate catalyst.[8]

1.4.3 Zinc Complexes Bearing Neutral Ligands

In the pursuit of a more robust catalyst, zinc complexes bearing *neutral* ligands have become of interest. In contrast to anionic ligands, neutral ligands are often more tolerant towards water, lactic acid, and alcohol cocatalysts. Research into zinc complexes of neutral ligands is still in its infancy. However, emerging ligand systems include phosphinimines, carbenes, and guanidines (**Figure 15** and **Table 2**).[34–36]

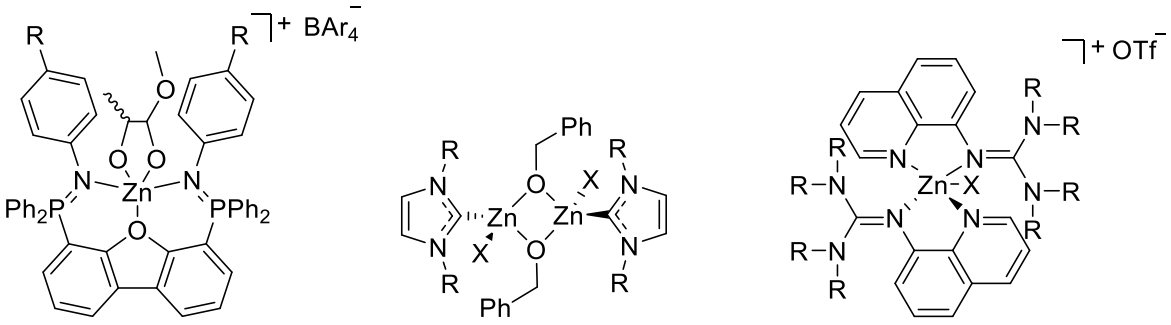

Figure 15. Select highly active complexes bearing neutral ligands for the ROP of LA.

Table 2: Rate constants (k_p) for the ROP of LA to PLA for select highly active complexes bearing neutral ligands.

Catalyst	Solvent	Temperature (°C)	k_p (M^{-1} s^{-1})
V	DCM	25	0.17
VI	DCM	25	0.9
VII	Neat	130	2.6×10^{-3}

[I] = equivalents of initiator, [LA] = equivalents of lactide. All polymerizations were done at room temperature, in DCM.

The phosphinimines catalyst (**V**) of Hayes are competitive with those of anionic counterparts, with the added benefit of air and moisture stability.[34] The phosphinimines catalyst was highly active in the ROP of lactide, reaching 90% conversion of 200 equivalents of *rac*-LA in less than an hour. The catalyst showed some stereoselectivity with the formation a slightly heterotactic polymer ($P_r = 0.63$). After the first 200 equivalents of monomer had completely polymerized, further addition of 200 equivalents of monomer and complete polymerization provided evidence of an immortal polymerization. Matrix-assisted laser desorption ionization-time of flight (MALDI-TOF) of the resulting polymer

showed mass peaks separated by 72 *m/z*, representative of intermolecular transesterification. The addition of a slight stoichiometric excess of lactide to the catalyst suggested a CIM. Observation of a new phosphorus resonance in the ^{31}P NMR spectrum (δ 29.4) downfield from that of the precatalyst (δ 28.9) along with a O-CH_3 singlet for the lactate end group in the ^{1}H NMR spectrum indicated a ring-opened monomer from a migratory insertion. Enthalpy and entropy for the polymerization of lactide was determined to be 47 ± 1 kJ mol^{-1} and 147 ± 4 J $mol^{-1}K^{-1}$.

The monodentate N-heterocyclic carbene zinc complexes **VI** of Tolman were one of the most successful early iterations of zinc-carbene catalyst for lactide polymerization.[35] Molecular weight dispersity indices as low as 1.2 were observed, characteristic of a large k_i relative to k_p with limited chain transfer or termination steps. MALDI-TOF mass spectroscopy of the resulting polymer indicated the presence of the benzyl-alkoxide fragment, with only minor degrees of transesterification. The complex boasts 96% lactide conversion in 20 min, generating PLLA with an M_n value of 17,000 g/mol, only slightly lower than the expected value of 18,600 g/mol. The high activity of the catalyst is partly attributed to the existence of a mononuclear species in solution at low concentrations (>20 mM) and dinuclear at either high concentrations or in the solid state. The catalyst also demonstrated modest stereoselectivity. The ^{1}H NMR spectrum of the polymer shows slight preference of heterotactic linkages, with a P_r value of 0.6, principally due to chain-end control as the systems contains no stereogenic centers.

Herres-Pawlis's work marks one the first-generation guanidine containing zinc complexes (**VII**) for lactide polymerization.[37] Initial work focused on zinc complexes bearing strongly Lewis-basic guanidine ligands, coupled with highly Lewis-acidic zinc

metal centers owing to strongly non-coordinating counteranions. The system displays a low PDI of 1.2, indicating that polymer chains were initiated rapidly and very few chain termination events occurred to produce large polymers with similar degree of polymerization. The enthalpy and entropy of polymerization were determined to be 79±4 kJ mol^{-1} and –33 J mol^{-1} K^{-1}. Interestingly, the polymerizations proceeded in the absence of both a coordinated alkoxide and an alcohol initiator. The kinetic analysis was consistent with a coordination insertion mechanism. UV-Vis and fluorescent spectroscopy of the polymer (isolated by precipitation of PLLA dissolved in DCM from EtOH) showed strong absorptions in regions common with the guanidine ligands. This suggests that the ligand was incorporated in the polymer chains. In order to support the coordination insertion mechanism, pure L-lactide was used as the monomer. The resulting polymer, analyzed by ^{1}H NMR spectroscopy, did not show any racemization. Herres-Pawlis proposed that the highly nucleophilic neutral ligand was the initiator in the CIM, modeling the mechanism with density functional theory (DFT) to corroborate their findings (**Figure 16**).

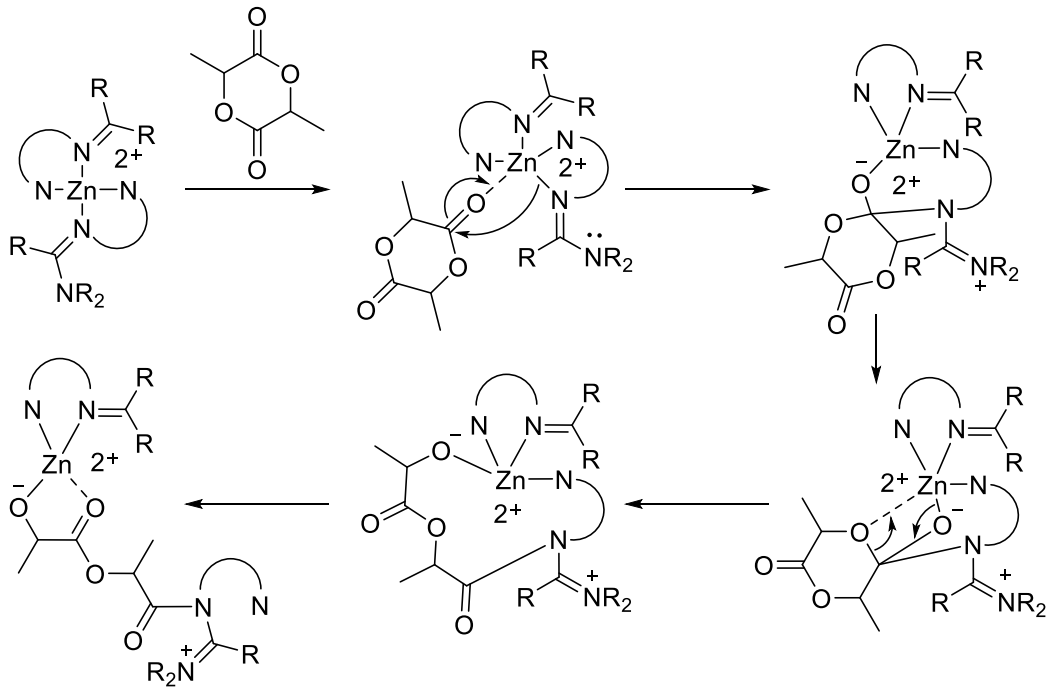

Figure 16. Proposed mechanism for the ROP of lactide by a nucleophilic guanidine ligand. The triflate counterions are omitted for simplicity.

1.5 N-Heterocyclic Imine

N-Heterocyclic imines (NHIs) are the cyclic analogues of guanidines (**Figure 17**, **i**) and can be described by two resonance forms (**Figure 17**, **ii** and **iii**).[38] The existence of these two mesomeric structures are the product of electron density from the endocyclic nitrogen atoms being delocalized though the π-system onto the exocyclic nitrogen. The extent of this delocalization (and thus basicity and nucleophilicity) can be fine-tuned by substitutions of the imidazole backbone as well as the substitutions of the R groups.[39]

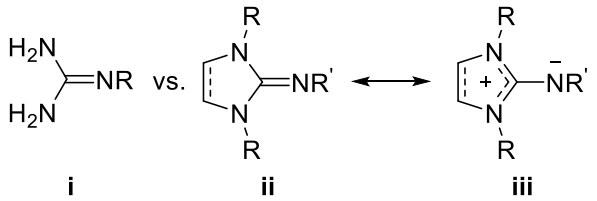

Figure 17. Structural relationship between acyclic guanidine (**i**) and the mesomeric structure of cyclic guanidine (**ii** and **iii**).

Acyclic and cyclic guanidines were first reported by Stearns and Rapoport in 1977.[40] They prepared alkyl-guanidines, owing to their prevalence in biologicals systems and in antihypertensive drugs, such as clonidine and guanethidine.[40] The synthetic methodology of the group tested whether guanidine moiety of acyl-guanidines were stable in the presence of a strong reducing agent such as $LiAlH_4$ (**Scheme 3**).[40]

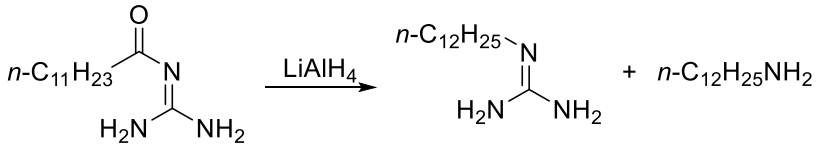

Scheme 3. Synthetic route employed by Stearns to synthesize acyclic guanidines.

Reduction of the acyl-guanidine to the alkyl-guanidine was successful and over-Reduction to the corresponding amine was minimized by careful control of the reaction temperature. The reduction of cyclic substrates to cyclic-guanidines was challenged by the presence of aluminum salts during the isolation procedure (**Figure 18**). The comprehensive workaround developed by Stearns included solubilizing the salts in a basic aqueous solution followed by addition of benzyl chloroformate to acylate the guanidines. Any excess benzyl chloroformate is quenched by addition of glycine and the resulting guanidine derivative is extracted with dichloromethane (DCM) and then subjected to hydrogenolysis to recover the target cyclic-guanidine in yields ranging from 28 – 53%.

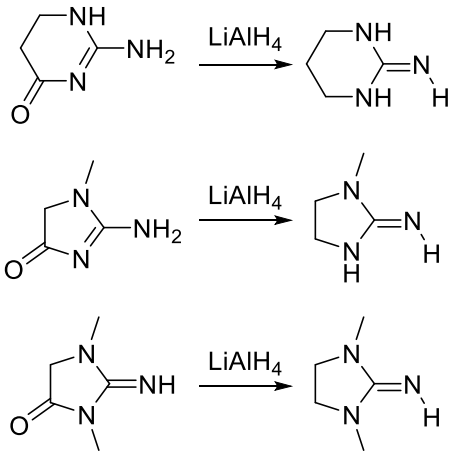

Figure 18. Cyclic acyl-guanidines targeted for reduction to their corresponding NHI.

It was not until Kuhn in 1995 that a high yielding synthetic procedure was developed that popularized cyclic-guanidine as ligands in coordination chemistry.[38] Kuhn began with the methylation of 2-amino-1-methylimidazole by methyl iodide to give the 2-amino- 1,3-dimethylimidazolium salt that was then deprotonated by potassium hydride to give the 1,3-dimethylimidazole-2-imine in a 94% yield (**Figure 19**).[41]

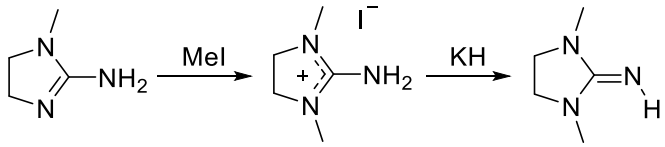

Figure 19. Kuhn synthetic route to accessing NHI ligands.

Kuhn demonstrated the heightened Lewis basicity of cyclic guanidines, with an ability to access an "additional lone pair" on the exocyclic nitrogen by donation of π-electron density from the endocyclic nitrogen atoms. Thus, addition of two equivalents of trimethylsilyl chloride (TMSCl) to the 1,3-dimethylimidazole-2-imine gives the exocyclic nitrogen with two trimethylsilyl (TMS) groups (**Figure 20**).[41] Kuhn's work sparked research into

applications of NHIs in mono- and polydentate N-donor ligands in coordination chemistry of homogeneous catalysis.[38]

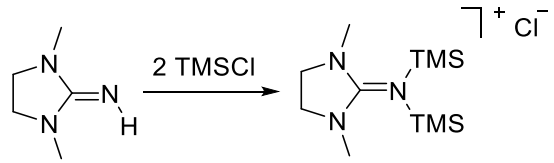

Figure 20. Bis(trimethylsilyl) guanidinum chloride accessed by Kuhn.

The work by Tamm in 2004 extended the library of existing NHIs by exploiting the numerous free carbenes and reacting them with trimethylsilyl azide ($TMSN_3$) in a Staudinger-type reaction to produce the corresponding N-silylated cyclic guanidine.[42] Desilylation of this intermediate by methanolysis yields the corresponding NHI (**Scheme 4**).

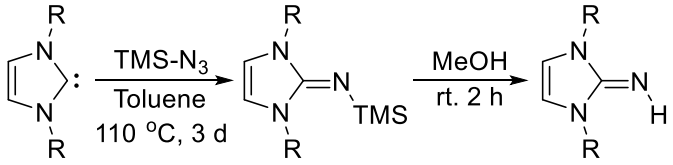

Scheme 4. Synthetic route employed by Tamm to synthesize cyclic guanidines.

Although the work done by Tamm expanded the available NHIs for studies as ligands in coordination chemistry, the synthetic route failed to accommodate electron-deficient carbenes. These carbenes were commonly unstable to the Tamm's reaction conditions. Recent work by Eisen has illustrated that chloroimidazolium chloride intermediates, which are readily prepared for electron-poor carbenes, are excellent

electrophiles and readily react with primary amines to produce the corresponding NHI (**Scheme 5)**. [43]

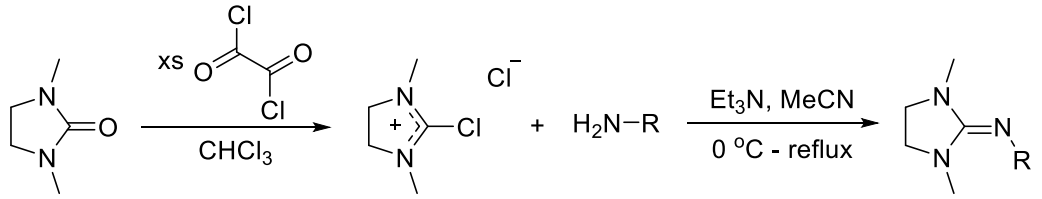

Scheme 5. Alternative synthetic route employed by Eisen to synthesize cyclic guanidines.

1.5.1 Coordination Chemistry of N-Heterocyclic Imines

The cyclic imidazolin-2-iminate anion and derivatives thereof are 2σ,4π-electron donor ligands and are therefore isolobal to the ubiquitous cyclopentadienyl (**Figure 21**).[38] Thus, these compounds possess great potential as both Cp^- and nitrogen-based donor ligands find many applications in coordination complexes of both early and late transition metals.

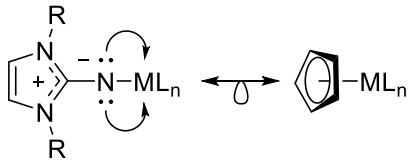

Figure 21. Isolobal relationship of imidazolin-2-iminate and cyclopentadienyl.

Tamm used these NHIs as monodentate ligands in a series of titanium complexes. Upon activation with methylaluminoxane (MAO), these precatalysts were tested as homogenous ethylene co-polymerization with monomers containing polar functional groups (**Figure 22**).[44] Tamm's work highlighted the strong electron-donating capability and high modularity of these ancillary ligands.

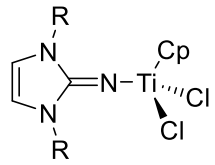

where R= *t*Bu

Figure 22. Complex bearing imidazolin-2-iminato fragment.

Tamm also prepared yttrium complexes containing NHI ligands that featured a short metal-nitrogen bond of 1.96 Å (**Figure 23**).[45] The short nitrogen-metal bonds serve as a testament to the ability of the azole ring in delocalizing positive charge and afford very Lewis basic ligands with strong affinities towards coordination of electropositive early transition metals. These complexes serve as analogues to the elusive rare-earth metal imido complexes. They catalyzed intramolecular hydroamination of alkenes and alkynes with moderate-to-high activity. The catalyst was capable of generating quantitative yields of the Markovnikov intramolecular hydroamination product with 5 mol % catalytic loading at room temperature.[45]

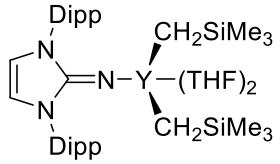

Where Dipp = 1,3-diisopropylphenyl

Figure 23. Yttrium complexes bearing an NHI ligand prepared by Tamm.

Nomura has also used NHI ligands in transition metal complexes for olefin copolymerization polymerization of ethylene and norbornene (NBE) (**Figure 24**, where x is the mole fraction of NBE repeating units in the polymer).[46] The group focused on isoelectric analogues of Tamm's earlier half-sandwich titanocene work by substituting titanium for a vanadium metal center.

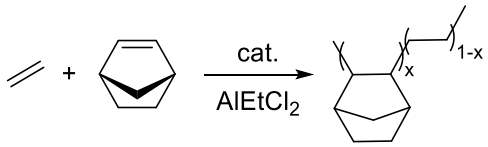

Figure 24. Copolymerization of ethylene and NBE.

The group reasoned that designing a catalytic system that combines the NHI ligand with the classical Ziegler-type vanadium catalyst would afford a complex that displayed exceptionally high activities towards olefin polymerization and copolymerization (**Figure 25**). These (arylimido)vanadium(V) dichloride complexes containing imidazolidin-2-iminato ligands showed superior catalytic performance to the copolymerization of ethylene and NBE after activation by an aluminum cocatalyst ($AlEt_2Cl$). This is desirable owing to the much lower price of $AlEt_2Cl$ over MAO and an overall lower amount coinitiator. These catalysts produced copolymers containing as much as 40 mol % of NBE with a turnover frequency (TOF) of 81 kg polymer mol cat^{-1} h^{-1}. Interestingly, the catalytic activity correlates with the ^{51}V NMR chemical shift. Nomura postulated that the increase in electron donation through the anionic ligands lead to a corresponding increase in stability of the active site and a subsequent increase in catalytic activity.[47]

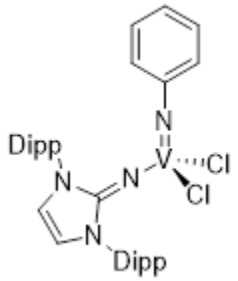

Figure 25. Catalytic systems proposed by Nomura.

Late transition metal complexes bearing imidazolin-2-iminato ligand are scarcer than the early transition metal counterparts. This is principally attributed to the inherent

electron richness of late *d*-block metals that can destabilize the metal-nitrogen bond.[38] Despite this, there are examples of NHI ligands on group 10 transition metals that perform interesting chemical transformations, such as the metal-induced rupture of the N−N bond. Severin prepared nickel(II) complexes bearing the imidazolin-2-iminato ligand by first reacting an N-heterocyclic carbene (NHC) with N_2O.[48] This covalent adduct was then reacted with a zerovalent nickel precursor, $Ni(COD)_2$, which then produced a bimetallic complex where the metal had inserted into the N−N bond of the N_2O group (**Figure 26**). Severin's work marks one of the earlier examples of metal mediated N-N cleavage as well as low coordination number nickel complexes.

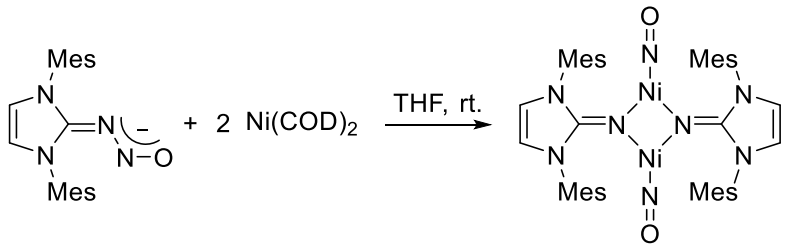

Figure 26. Complex proposed by Severin that boast metal-mediated N-N cleavage.

The Lavoie group has reported the first monoanionic bidentate ligand scaffolds bearing an imidazol-2-imine nitrogen donors and anionic oxygen donors.[49] The ligand

scaffold bears resemblance to the Shell Higher Olefin Polymerization (SHOP) ligand (**Figure 27**), with the addition of the highly modular/tuneable guanidine fragment.

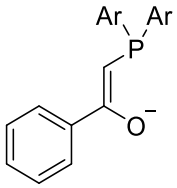

Figure 27. SHOP ligand.

This modularity provides control over the performance of the catalyst. This imidazol-2-imine ethenolate ligand was synthesized by reaction of the nucleophilic N-heterocyclic imine with a 2-haloacetophenone with subsequent deprotonation. Owing to the mesomeric structure of the NHI fragment, the resulting ligand also exhibits two canonical forms where additional electron density is positioned on the exocyclic nitrogen (**Figure 28**).

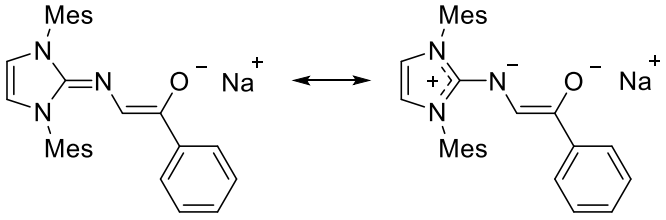

Figure 28. Mesomeric structure accessible by the guanidine-ethenolate ligand.

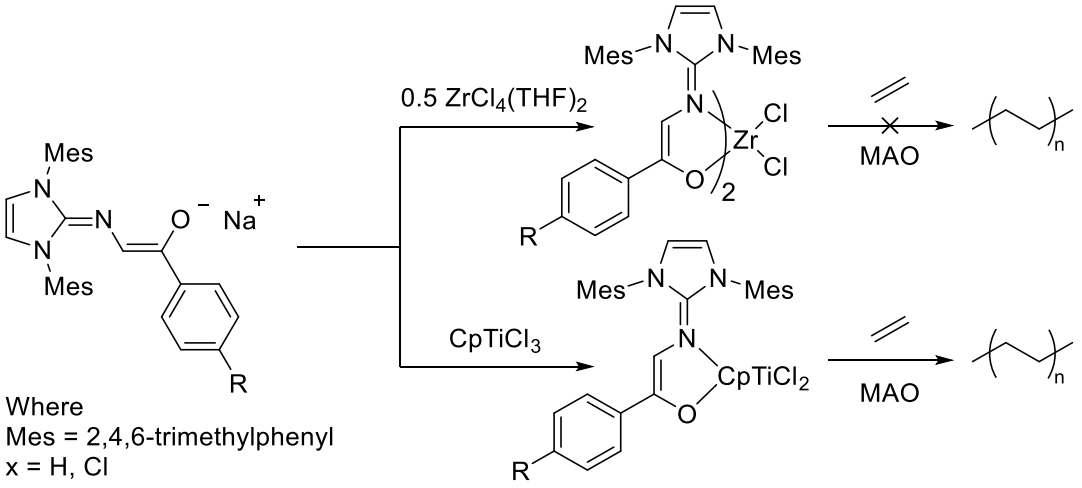

Scheme 6. Synthetic route used by the Lavoie group to access group 4 complexes for ethylene polymerization.

Group 4 complexes (Ti, Zr) were obtained by reaction of the ethenolate salt with either $ZrCl_4(THF)_2$ or $CpTiCl_3$ (**Scheme 6**). The zirconium complex only produced trace quantities of polyethylene. In contrast, the titanium complex showed promising catalytic activity and fine-tuning of the ligand structure by substituting a chlorine on the para position of the phenyl ring afforded slightly enhanced catalytic activity of 170 kg PE mol cat^{-1}.[49] Changes in the NHI building block would also lead to modification of the electronic and steric characteristics of the ligand, allowing for better understanding into the structure–activity correlation .

1.6 Proposed Work

The characteristics of the ideal catalyst for lactide polymerization are robustness towards air, moisture and acidic impurities of the monomer. Additionally, the catalytic system should be low cost, odourless, colourless, non-toxicity, thermally stable and be highly active in the ring-opening polymerization of lactide. The current industrial catalyst ($Sn(Oct)_2$) is an undesirable catalytic system with target applications for PLA in food

packaging and medical devices. Both applications have a strict requirement against contamination by heavy metals.[8] Purification processes to remove these metals exist but they are costly and time-consuming.[8] Thus, developing a zinc-based catalyst is attractive due to the inherent low toxicity and abundance of zinc. Moreover, the new catalysts would benefit from spectator ligands that are capable of imparting stereoselectivity to produce PLA with a well-defined microstructure and enhanced bulk material properties.

In this project, the Lavoie group aims to exploit the ability to tailor the electron density on the exocyclic nitrogen of cyclic guanidines to develop a new class of neutral bidentate ligands for a zinc-based catalyst for the ROP of lactide. The research presented herein is based on the synthesis and coordination of neutral bidentate ligands, which are derived from the diacyl chloroimidazolium chloride **1** (**Scheme 7**).

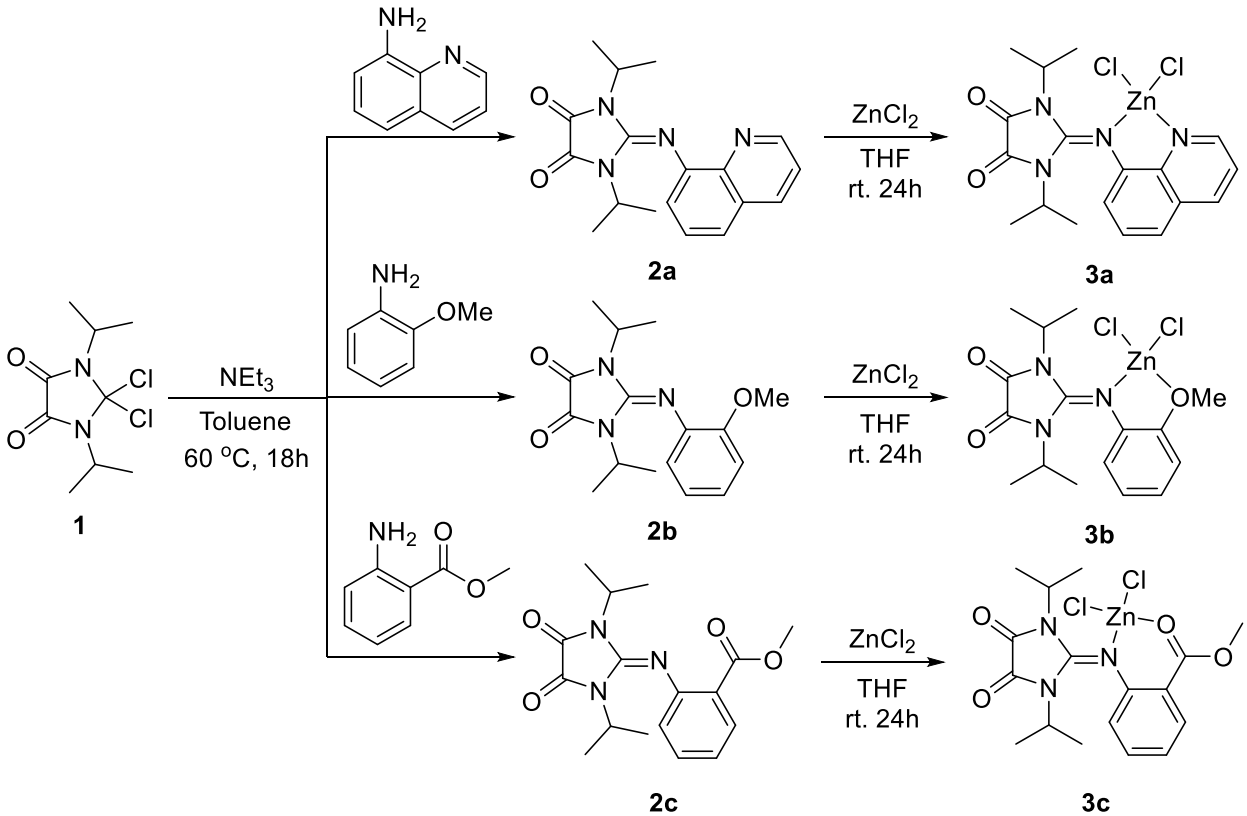

Scheme 7. Synthetic route used to access ligands **2** and complexes **3**.

As a product of the strong π-acidic diacylated NHC fragment, less electron density of the endocyclic nitrogens will be delocalized over the π system to the exocyclic nitrogen.[50] This will result in a relatively stronger $C=N_{exo}$ character compared to a corresponding imidazole containing no acyl groups. This will allow the complex to survive the harsh condition of bulk polymerization by preventing ligand dissociation or thermal decomposition at high temperatures (135 °C). The resulting metal complexes (**3a**, **3b, 3c**) possess a range of Lewis acidities in the zinc metal centre owing to the modular ligand fragment. This will allow for variation in electronic, sterics and size of the metallocycle to develop an understanding of the structure–activity relationship. The amines selected as second donor fragments include a strong electron donating methoxy group, a weak electron withdrawing ester group, and a weakly inductively withdrawing quinoline group. This selection provides a range of electronic properties and steric imposition of the coordination sphere of the complex. The heightened tunability to the mental centre through the ligand scaffold will allow for optimal Lewis acidity to facilitate rapid coordination of the monomer, but not so acidic as to shut down catalytic performance.[30]

2 Methods

2.1 General remarks

Unless otherwise specified, all reactions and manipulations were performed under an inert atmosphere of dry argon using standard Schlenk techniques or in a nitrogen filled glovebox. N,N′-Diisopropylcarbodiimide (DIC) was purchased from Sigma-Aldrich and stored on molecular sieves and under an inert atmosphere of argon. Diacyl chloroimidazolium chloride (DCIC) **1** was synthesized using reported literature procedures.[51] All flash column purification were carried out using 45–60 μm mesh silica. All other specified reagents were purchased from either Sigma-Aldrich or Alfa Aesar and used as received. All protio-solvents were dried over activated alumina columns, degassed, and stored on molecular sieves prior to use. Deuterated solvents C_6D_6 and toluene-d_8 were purchased from Sigma-Aldrich, stirred over sodium and benzophenone, degassed by freeze-pump-thaw cycles, vacuum transferred into dry ampules and stored on molecular sieves prior to use. $CDCl_3$ was purchased from Sigma-Aldrich, dried over CaH_2, degassed by freeze-pump-thaw cycles, vacuum transferred into dry ampules and stored on molecular sieves prior to use. All glassware was dried overnight in an oven at 160 °C, prior to use. Characterization by ^1H and ^{13}C NMR spectra were recorded on a Bruker 400 or Bruker UltraShield 300 MHz NMR spectrometer at room temperature unless otherwise stated. ^1H NMR spectra were referenced to the residual protio-solvent resonance (δ 7.27 ppm for $CDCl_3$, 7.15 ppm for C_6D_6 and 2.08 ppm for toluene-d_8). NMR multiplicities are abbreviated as follows: s = singlet, d =doublet, t = triplet, q = quadruplet, quint = quintet, sext = sextet, sept = septet, m = multiplet, br = broad. *J*-Couplings are

expressed in Hertz (Hz). Elemental analyses were performed at York University on a Vario EL cube instrument.

Computational Details

Geometry optimizations and NBO analyses were carried out using Gaussian 16. Molecular visualization and structural preoptimization were performed on Avogadro version 1.2.0. Values for Muliken charges and Wiberg bond indices were obtained directly from the output file. Unless otherwise stated, computations were performed using the M06 functional and the Def2TZVP basis set. For compounds **3a–c**, a split basis of Def2TZVP (for atoms C, H, N, O, Cl) and SDD (for Zn) was utilized. Computations were performed on the Shared Hierarchical Academic Research Computing Network (SHARCNET: www.sharcnet.ca) and made possible by Compute Canada (www.computecanada.ca).

X-ray Crystallography

Diffraction data was collected on a Bruker APEX-II CCD diffractometer with a MoK (λ = 0.71073) radiation source. Crystals were mounted under a stream of N_2 and kept at 173.0 K during data collection. The structure was solved in Olex 2.2 using the XS structure solution program and refined with SHELXL refinement package suite.[52,53].

MALDI-TOF Mass spectrometry

MALDI-TOF data was obtained at the AIMS laboratory of University of Toronto on a Bruker AutoFlex Speed MALDI-TOF instrument. The laser used for ionization was a 355 nm 3rd harmonic Nd YAG laser. The variable repetition was set to 2 kHz, the pulse energy ≥ 100 µJ. Samples were prepared in a dithranol THF matrix.

Gel Permeation Chromatography

Acquisition and analysis were graciously performed by Kathleen May and Rachele Carafa of the Foucher Lab from Ryerson University. Samples were dissolved in HPLC grade THF to a concentration of 30 mg/mL. The polymer solution was drawn into a syringe and pushed through a 0.45 μm filter. The instrument was set to a flow rate of HPLC grade THF of 1 mL/min and the column was washed with THF twice prior to sample injection. A polystyrene (PS) standard in THF was analyzed before the samples for proper calibration. The sample (100 μL) was injected and analyzed by right angle light scattering (RALS), intrinsic viscosity (IV) and refractive index (RI) to calculate M_n, M_w, PDI.

General Procedure for Polymerization

Unless specified, all polymerizations were carried out using unpurified reagent grade *rac*-lactide. In a nitrogen filled glovebox, a custom lactide polymerization flask was charged with catalyst. Next, the desired amount of *rac*-lactide was added to reach the desired stoichiometric ratio of initiator to monomer (ie. [I]/[M] = 1:100, 1:200, 1:1000 etc...). If co-initiator is required, 1 equiv. of BnOH is added to the mixture. A stir bar is added and the solid mixture is homogenized with stirring over a magnetic stir plate. The reaction vessel is capped, brought outside the glovebox and submerged into a preheated oil bath (135±2 °C). The polymerization is considered started when all monomer has melted and the mixture is homogenous. After the desired time, the flask is removed from the oil bath, cooled under running water until solidified and cool to the touch. The polymers are worked up by dissolving the solid in 3 mL DCM, sonicated for 5 min, then precipitated in cold absolute ethanol (ice bath). The supernatant is decanted off, the gummy precipitate is collected and dried in *vacuo* to a constant weight.

General Procedure for Polymerization Kinetic Studies

The polymerization procedure for kinetic studies is the same as above with the following exceptions. Under an inert flow of argon, aliquots of the reaction mixture are taken at predefined times from the start of the polymerization (1 h, 1.5 h, 2 h, 2.5 h, 3 h) and dispensed directly into pre-weighed NMR spectroscopy tubes. The reaction mixture solidifies immediately upon contact with the tubes, With the exact mass of reaction mixture dispensed, 700 µL of $CDCl_3$ is added and the mixtures shaken until homogenous. Samples are subjected to ^1H NMR spectroscopy, with a relaxation delay (d1) set to 60 s.

2.2 Synthesis of Compound 2a

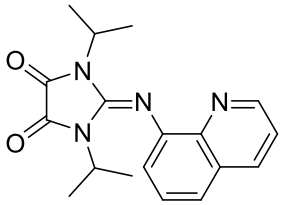

A 50-mL Schlenk tube was charged with DCIC (200 mg, 0.790 mmol) and toluene (3 mL). Under an inert atmosphere of argon, the off-white solution was treated with a solution of 8-aminoquinoline (114 mg, 0.790 mmol) and NEt_3 (330 µL, 2.37 mmol) in toluene (3 mL) at 0 °C. The resulting brown solution was then stirred at 60 °C for 18 h. The resulting orange slurry was filtered and the solid washed with toluene (3 × 1 mL). The combined toluene-soluble fractions were dried *in vacuo*, resulting in a yellow oil. The product was further purified by flash silica column chromatography (hexanes:ethyl acetate:triethylamine 80:15:5) (213 mg, 0.656 mmol, 83%). ^1H NMR (300 MHz, $CHCl_3$): δ 8.86 (dd, *J* = 4.2, 1.8 Hz, 1H, Ar), 8.16 (dd, *J* = 8.3, 1.8 Hz, 1H, Ar), 7.60–7.47 (m, 2H, Ar), 7.43 (dd, *J* = 8.3, 4.2 Hz, 1H, Ar), 7.23 (dd, *J* = 7.0, 1.8 Hz, 1H, Ar), 4.15 (sept, *J* = 6.9 Hz, 2H, $CH_3(C\underline{H})CH_3$), 1.35 ppm (br s, 6H, $C\underline{H_3}(CH)C\underline{H_3}$), 1.23 ppm (br s, 6H, $C\underline{H_3}(CH)C\underline{H_3}$). ^{13}C NMR (75 MHz, $CDCl_3$) δ 157.5 (C=O), 149.9 (Ar), 142.8 (Ar), 140.0 (Ar), 138.0 (C=N), 136.0 (Ar), 128.9 (Ar), 126.7 (Ar), 122.8 (Ar), 121.8 (Ar), 117.6 (Ar). 46.6 ($CH_3(\underline{C}H)CH_3$),

19.2 ppm ($\underline{C}H_3(CH)\underline{C}H_3$). Anal. Calc. for $C_{18}H_{20}N_4O_2$ (%): C, 66.65; H, 6.210; N, 17.27. Found (%): C, 66.72; H, 6.107; N, 17.36.

2.3 Synthesis of Compound 2b

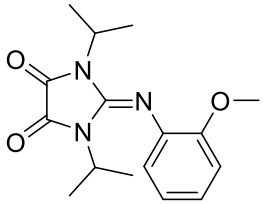

A 50-mL Schlenk tube was charged with DCIC (200 mg, 0.790 mmol) and toluene (3 mL). Under an inert atmosphere of argon, the off-white solution was treated with a solution of *o*-anisidine (89.1 µL, 0.794 mmol) and NEt_3 (330 µL, 2.37 mmol) in toluene (3 mL) at 0°C. The resulting dark brown solution was then heated at 60 °C for 18 h. The resulting yellow slurry was filtered and the residue washed with toluene (3 × 1 mL). The filtrate was dried *in vacuo*, resulting in a yellow oil. The product was further purified by flash column chromatography (hexanes:ethyl acetate:triethylamine 90:5:5) (204 mg, 0.672 mmol, 85%). ^{1}H NMR (300 Hz, $CDCl_3$): δ 7.07 (ddd, *J* = 8.1, 7.6, 1.8 Hz, 1H, Ar), 6.91 (m, 3H, Ar), 4.27 (br s, 2H, $CH_3(C\underline{H})CH_3$), 3.81 (s, 3H, $OC\underline{H}_3$), 1.38 ppm (d, *J* = 6.9 Hz, 12H, $C\underline{H}_3(CH)C\underline{H}_3$). Full characterization found in literature.[51]

2.4 Synthesis of Compound 2c

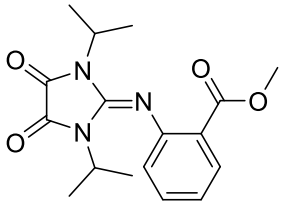

A 50-mL Schlenk tube was charged with DCIC (1.02 g, 4.04 mmol) and toluene (7 mL). Under an inert atmosphere of argon, the beige solution was treated with a solution of methyl anthranilate (525 µL, 4.04 mmol) and NEt_3 (1.7 mL, 12.1 mmol) in toluene (5 mL) at 0 °C. The resulting brown solution was then stirred at 60 C for 18 h. The resulting yellow slurry was filtered and the solid washed with toluene (3 × 1 mL). The combined toluene-soluble fractions were dried *in vacuo*, resulting in a yellow oil. The product was further purified by flash

column chromatography (hexanes:ethyl acetate:triethylamine 90:5:5) (1.15 g, 3.47 mmol, 86%). ^{1}H NMR (300 MHz, $CDCl_3$): 7.97 (d, *J* = 7.9, Hz, 1H, Ar), 7.49 (t, *J* = 7.9, Hz, 1H, Ar), 7.15 (t, *J* = 7.3, Hz, 1H, Ar), 6.88 (d, *J* = 8.0, Hz, 1H, Ar), 4.19 (sept, *J* = 7.1, Hz, 2H, $CH_3(C\underline{H})CH_3$), 3.84 (s, 3H, $OC\underline{H_3}$), 1.37 ppm (d, *J* = 6.75, Hz, 12H, $C\underline{H_3}(CH)C\underline{H_3}$). ^{13}C NMR (75 MHz, $CDCl_3$) δ 166.1 ($C{=}O_{Ar}$), 157.1 (C=O), 146.0 (Ar) 136.2 (C=N), 133.3 (Ar), 131.2 (Ar), 123.1 (Ar), 120.3 (Ar), 119.2 (Ar), 52.0 (OCH_3), 46.4 ($CH_3(\underline{C}H)CH_3$), 19.1 ppm ($\underline{C}H_3(CH)\underline{C}H_3$). Anal. Calc. for $C_{17}H_{21}N_3O_4$ (%): C, 61.62; H, 6.39; N, 12.68. Found (%): C, 61.24; H, 6.107; N, 13.14.

2.5 Synthesis of Compound 3a

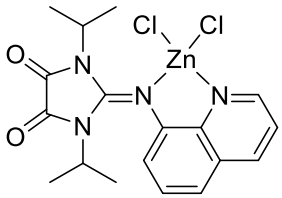

A 20-mL scintillation vial was charged with $ZnCl_2$ (21.0 mg, 0.154 mmol) and THF (1 mL). The colourless solution was then treated with a solution of compound **2a** (50.1 mg, 0.155 mmol) in THF (1 mL) with stirring. The resulting yellow reaction mixture was stirred at room temperature for 24 h. The reaction mixture was then dried *in vacuo* to produce a yellow solid that was washed with pentane (5 × 1 mL). The yellow insoluble solid were dried in vacuo (69.5 mg, 0.151 mmol, 98%). ^{1}H NMR (300 MHz, $CDCl_3$): δ 9.00 (dd, *J* = 4.8, 1.6 Hz, 1H, Ar), 8.61 (dd, *J* = 8.4, 1.6 Hz, 1H, Ar), 7.87 (dd, *J* = 8.4, 4.8 Hz, 2H, Ar), 7.75 (t, *J* = 7.9 Hz, 1H, Ar), 7.37 (dd, *J* = 7.9, 1.6 Hz, 1H, Ar), 4.40 (br s, 2H, $CH_3(C\underline{H})CH_3$), 1.57 (d, *J* = 6.9 Hz, 6H, $C\underline{H_3}(CH)C\underline{H_3}$), 1.44 ppm (d, *J* = 6.9 Hz, 6H, $C\underline{H_3}(CH)C\underline{H_3}$). ^{13}C NMR (75 MHz, $CDCl_3$) δ 157.5 (C=O), 156.2 (C=N), 150.1 (Ar), 140.9 (Ar), 139.1 (Ar,), 138.2 (Ar) 129.7 (Ar), 128.3 (Ar), 125.5 (Ar), 123.7 (Ar), 121.6 (Ar), 50.3 ($CH_3(\underline{C}H)CH_3$), 19.6 (CH_3), 18.8 ppm (CH_3). Anal. Calc. for $C_{18}H_{20}Cl_2N_4O_2Zn$ (%): C, 46.93; H, 4.38; N, 12.16. Found (%): C, 47.13; H, 4.42; N, 12.24.

2.6 Synthesis of Compound 3b ·THF

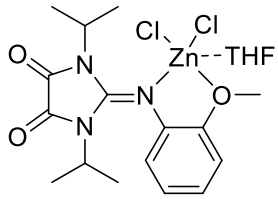

A 20-mL scintillation vial was charged with $ZnCl_2$ (22.5 mg, 0.165 mmol) and THF (1 mL). The colourless solution was then treated with a solution of compound **2b** (50 mg, 0.165 mmol) in THF (1 mL) with stirring. The resulting yellow reaction mixture was stirred at room temperature for 24 h. The reaction mixture was then dried *in vacuo* to produce an orange solid, which was then washed with pentane (5 × 1 mL) and then pentane insoluble fraction dried *in vacuo* (65.3 mg, 0.149 mmol, 90%). ^{1}H NMR (300 Hz, $CDCl_3$): δ 7.09 (ddd, *J* = 8.1, 7.4, 1.8 Hz, 1H, Ar), 7.00–6.84 (m, 3H, Ar), 4.27 (br s, 2H, $CH_3(CH)CH_3$), 4.11 (m, 4H, THF), 3.81 (s, 3H, OCH_3), 2.00 (m, 4H, THF), 1.39 ppm (d, *J* = 6.9 Hz, 12H, $CH_3(CH)CH_3$). ^{13}C NMR (75 MHz, $CDCl_3$): δ 158.4 (C=O), 148.5 (Ar), 136.5 (Ar), 133.4 (Ar), 124.9 (Ar), 121.2 (Ar), 120.2 (Ar), 111.1 (C=N), 70.3 (THF), 55.6 (OCH_3), 47.1 ($CH_3(CH)CH_3$), 25.4 (THF), 19.3 ppm ($CH_3(CH)CH_3$). Anal. Calc. for $C_{20}H_{29}Cl_2N_3O_4Zn$ (%): C, 46.94; H, 5.71; N, 8.21. Found (%): C, 46.94; H, 5.45; N, 8.42.

2.7 Synthesis of Compound 3c ·0.5 THF

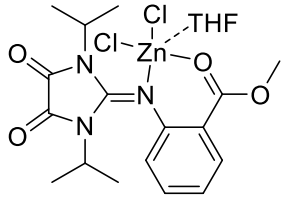

A 20-mL scintillation vial was charged with $ZnCl_2$ (20.4 mg, 0.150 mmol) and THF (1 mL). The colourless solution was then treated with a solution of compound **2c** (50 mg, 0.150 mmol) in THF (1 mL) with stirring. The resulting yellow reaction mixture was stirred at room temperature for 24 h. The reaction mixture was then dried *in vacuo* to produce an off white solid, which was then washed with pentane (5 × 1 mL). Drying in *vacuo* while heating (75 °C) results in a fine yellow powder, **3c·THF** (65.3 mg, 0.121 mmol, 81%). ^{1}H NMR (300 Hz, $CDCl_3$)

δ: 7.98 (d, *J* = 8.0 Hz, 1H, Ar), 7.50 (t, *J* = 8.0 Hz, 1H, Ar), 7.16 (t, *J* = 7.5 Hz, 1H, Ar), 6.87 (d, *J* = 8.0 Hz, 1H, Ar), 4.19 (sept, *J* = 7.1 Hz, 2H, $CH_3(C\underline{H})CH_3$), 4.01 (m, 2H, THF) 3.84 (s, 3H, $OC\underline{H_3}$), 1.98 (m, 2H, THF) 1.37 ppm (d, *J* = 6.75 Hz, 12H, $C\underline{H_3}(CH)C\underline{H_3}$)^{13}C NMR (75 MHz, $CDCl_3$): δ 166.2 ($C{=}O_{Ar}$), 158.1 (C=O), 145.4 (C=N), 135.5 (Ar), 133.5 (Ar), 131.3 (Ar), 123,6 (Ar), 120.2 (Ar), 119.2 (Ar), 70.4 (THF), 52.2 (OCH_3), 47.2 ($CH_3(\underline{C}H)CH_3$), 25.3 (THF), 19.2 ppm ($\underline{C}H_3(CH)\underline{C}H_3$). Anal. Calc. for $C_{21}H_{29}Cl_2N_3O_5Zn$ (%): C, 45.31; H, 5.42; N, 8.34. Found (%): C, 45.16; H, 5.36; N, 8.69.

3 Results and Discussion

The synthesis of NHIs from many different NHC building blocks has been well explored. The electronic features of the NHI ligand, which include σ-donation and π-withdrawing characteristics, are strongly influenced by the parent NHC fragment. The most π-acidic NHC fragment bears strongly electron withdrawing acyl groups on the backbone of the ring. The π-accepting ability of the NHC fragments can be inferred from the ^{31}P NMR spectrum chemical shifts of the corresponding phenylphosphaalkene derivatives (NHC=PPh) as demonstrated by Bertrand (**Figure 29**).[50]

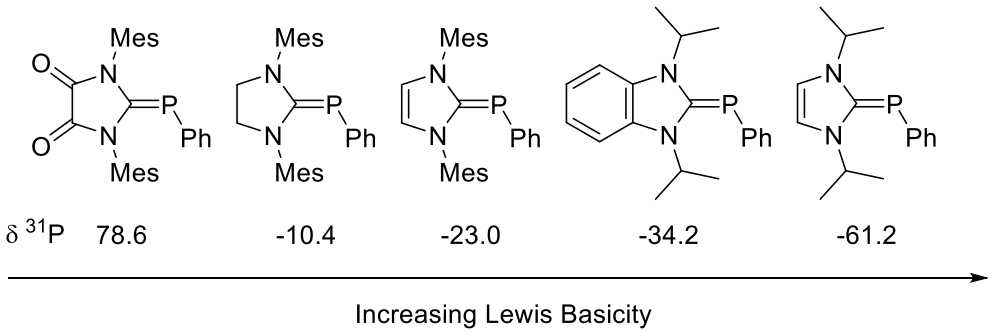

Figure 29. Phenylphosphaalkene adducts of various NHC fragments with varying π acidity.

Generally, an increase in π-acidity of the NHC results in a decrease in the Lewis basicity of the corresponding phosphaalkene. Thus, in the inversely polarized phosphaalkenes (IPPs) of more Lewis acidic carbenes, the phosphorus atom experiences less shielding corresponding to a more positive ^{31}P NMR chemical shift. In the case of an NHI generated from the acylated NHC, the corresponding NHI ligand would show strong σ-donation with an increased π-acidic character. Therefore, the coordinated NHI ligand should stabilize the resulting complex to the high temperatures often used in lactide polymerization. This is due to the strongly σ-donating and π-

withdrawing character of the ligand, resulting in short and strong metal-nitrogen bonds. This would prevent dissociation of the ligand from the complex during the polymerization by the lactide. The heightened π-acceptor character of the ligand would also result in a relatively more-electron poor metal center. This may heighten catalytic performance by facilitating rapid coordination of the lactide monomer.

A careful balance of Lewis acidity in the metal complex must however be achieved to prevent too much electron density being transferred to the metal centre, thereby decreasing its electroposivity and preventing coordination of the monomer. Alternatively too little electron density on the metal centre of complex would result in a low rate of migratory insertion (k_1) in the catalytic cycle (**Scheme 1**). Balancing the electron density of the metal centre of the catalyst plays a key role in developing a system with high catalytic performance.

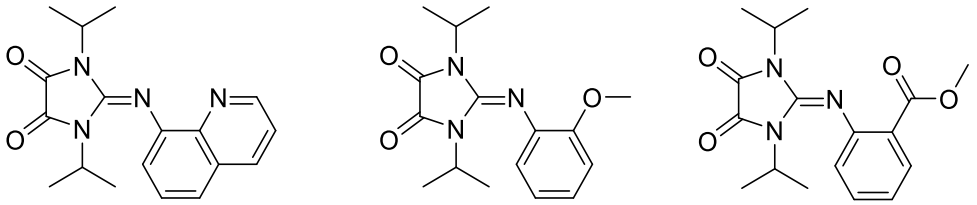

2a **2b** **2c**

Figure 30. Neutral bidentate ligands (**2a-c**) of interest, bearing different second donor fragments.

All ligands **2** bear the acylated NHC fragment that results in a strong π-acidic exocyclic nitrogen, while maintaining the characteristic strong σ-donor ability of NHIs (**Figure 30**). The modularity of the system is highlighted through the series with a “second donor” with varying Lewis basicity accessible to chelate to the zinc metal center. Compound **2a** bears

a guanidine donor and a strong quinoline σ-donor. To complement this bidentate ligand, compound **2b** was developed with a weaker methoxy σ-donor. The weak methoxy donor would allow for higher Lewis acidity of the zinc center in the corresponding complex and may result in higher polymerization activity.[1] Ligand **2c** represents a middle ground between the strongly σ-donor of **2a** and the weakly σ-donor of **2b**. The carbonyl oxygen of the methyl ester of **2c** should be more strongly σ-donating than the sp^3 hybridized oxygen of **2b**, while still being less strongly donating than the quinoline nitrogen of **2a**. A fine balance of electron density on the zinc metal center is required to achieve a highly active complex for ROP of LA to PLA. This must be achieved without compromising the stability of the complex to the polar impurities (such as lactoyl and lactic acid) found in the monomer, or the harsh conditions of bulk polymerization.

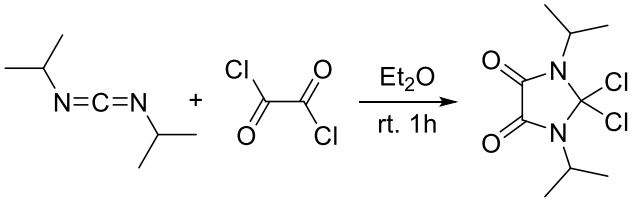

1

Scheme 8. Synthetic route to synthesize **1**.[50]

The synthesis of the NHI ligands **2** begins with the preparation of the key intermediate **1** from a dialkylcarboiimide and oxalyl chloride (**Scheme 8**). The modularity of the ligand is demonstrated in that any dialkylcarboiimide could be used to generate the corresponding intermediate **1**.[51] A library of ligands could thus be easily prepared by using the appropriately modified ligand precursor **1**. Diisopropylcarboiimide was chosen as the steric bulk of the corresponding ligand would possess neither a too large (as would be the case with *tert*-butyl or cyclohexyl) nor too small (as in a methyl group) alkyl group.

This serves as an appropriate starting point for generating a series of complexes for lactide polymerization. The synthesis of **1** was adapted from Xi and after 1 h in diethyl ether at room temperature, near quantitative yields were obtained.[51]

3.1 Synthesis of Compound 2a

Following the isolation of **1**, the synthesis of ligand **2a** was performed based on analogous literature reports that synthesized NHIs from dichloroimidazolium chlorides.[51] The ligand precursor **1** was treated with 8-aminoquinoline in the presence of a base. The amine undergoes a substitution reaction at the dichlorinated C_2 position of the diacylimidazole generating the target ligand **2a**. Reaction of **1** with 8-aminoquinoline and 2 equivalents of triethylamine were unsatisfactory. The 8-aminoquinoline competed with triethylamine as a base in the reaction and as a result, a theoretical maximum yield of 50% could be obtained. An isolated yield of 33% of the target molecule **2a** after 24 h was actually achieved (**Scheme 9**).

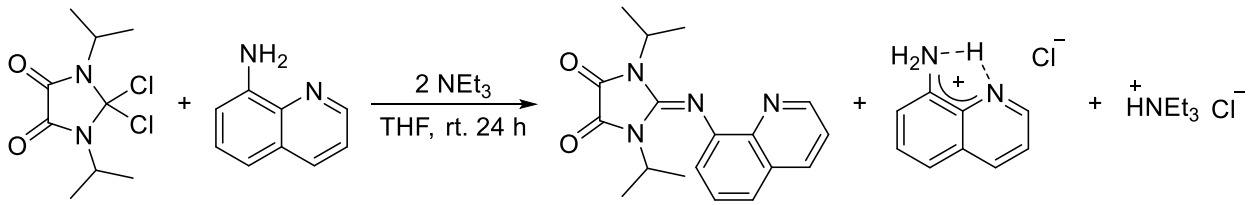

Scheme 9. Select observed products from reaction of **1** and 8-aminoquinoline.

The reactions conditions were optimized by increasing the quantity of triethylamine, using toluene as solvent to simplify isolation of compound **2a**, and increasing the reaction temperature to 60 °C. The desired product **2a** were isolated in 81% yield after 18 h (**Scheme 10**) by simple filtration and subsequent column

chromatography (hexanes:ethyl acetate:triethylamine 80:15:5), with NEt_3 used to de-acidify the silica and prevent protonation of the strongly basic **2a**.

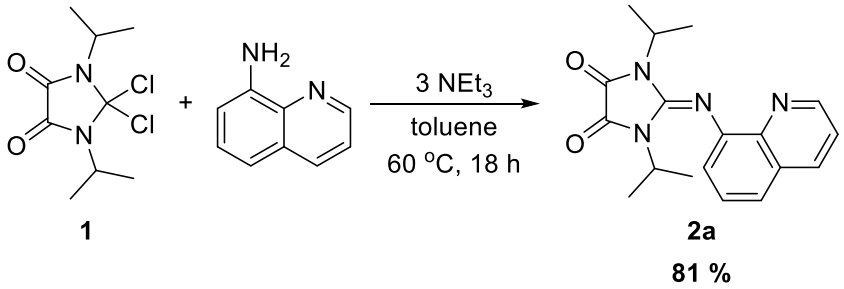

1 **2a**

81 %

Scheme 10. Synthetic route employed to synthesize ligand **2a**.

3.1.1 Variable-Temperature NMR Analysis

Characterization of **2a** by ^1H NMR spectroscopy revealed a broad resonance at 1.29 ppm for the methyl protons (**Figure A1**), likely due to restricted rotation of the azole ring about the formal carbon–nitrogen double bond. Variable-temperature (VT) NMR experiments were performed to measure the C=N bond rotational energy barrier (**Figure 31**).

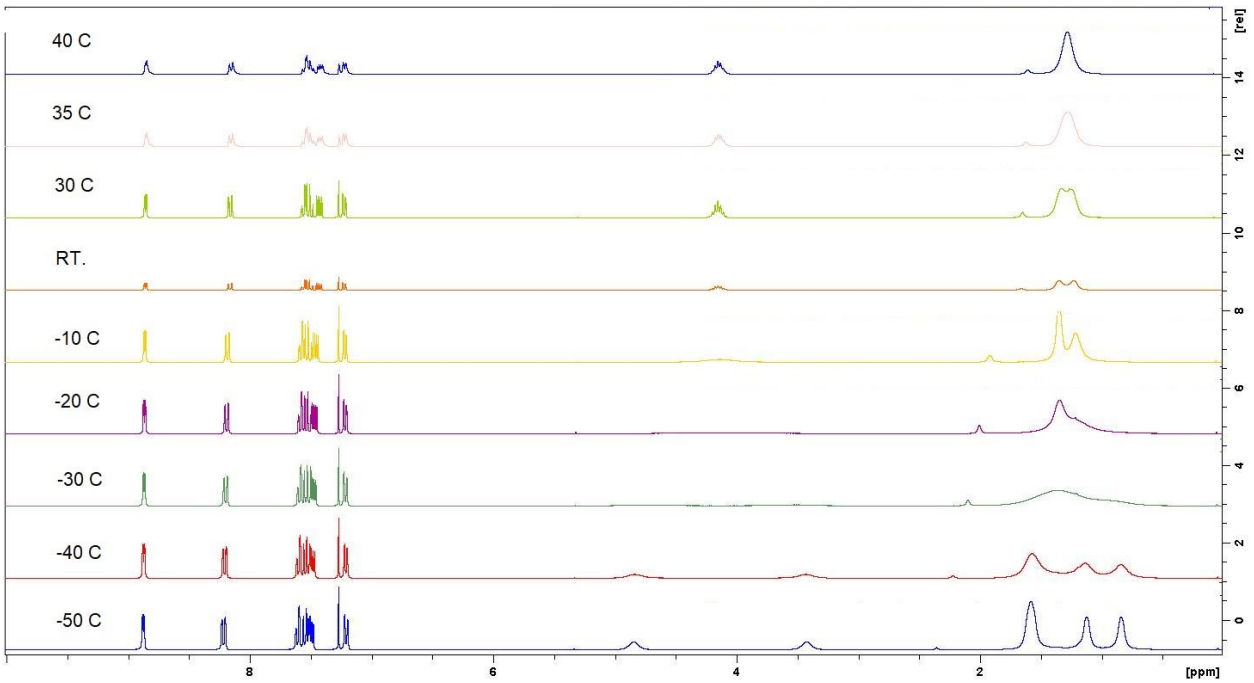

Figure 31. Variable temperature NMR spectrum of **2a** (300 Mz, $CDCl_3$).

Upon incremental cooling of the sample to –50 °C, the broad doublet observed for the methyl signals turned into three broad singlets. One of the three singlets integrated to 6 protons and the other two to 3 protons each. This suggested a secondary restricted rotation. The methyl signals on the isopropyl group close *(syn*) to the quinoline ring had become inequivalent, while the methyl signals for the isopropyl group across the azole ring remained equivalent. This resulted in the three broad singlets observed. This was attributed to the large quinoline moiety impeding the rotation of the isopropyl group at cold temperatures. This resulted in unique methyl signals for each CH_3 on the same isopropyl group, the large difference in chemical shifts being attributed to the ring current of the quinoline moiety deshielding one methyl group over another. Upon warming of the sample two coalescence points were observed for the methyl signals. The first coalescence point was at –35 °C corresponding to two singlets (δ 1.15 and 0.87 at –50 °C), each integrating to 3, coalescing. This indicated the isopropyl groups were both free to rotate and that

methyl group of a given isopropyl group were equivalent. The second coalescence point was at 33 °C, where both isopropyl groups become equivalent with no restricted rotation about the C=N bond.

The rate constant at the coalescence temperature (T_c) can be defined by the following equation (equation 3):

$$k = \frac{\pi|\nu_A - \nu_B|}{\sqrt{2}} \quad (3)$$

wherein ν_A and ν_B are the chemical shifts of resonances prior to coalescence. The Gibbs free energy of rotation $\Delta G^{\ddagger}$ (equation 5) can be derived from the Eyring equation (equation 4) and the rate constant at the coalescence temperature (equation 3).

$$k = \frac{k_B T}{h} e^{-\frac{\Delta G^{\ddagger}}{RT}} \quad (4)$$

$$\Delta G^{\ddagger} = RT_c ln \frac{k_B T_c \sqrt{2}}{\pi h|\nu_A - \nu_B|} \quad (5)$$

wherein R is the gas constant, k_B is the Boltzmann constant, T_c is the coalescence temperature and h is Planks constant

The coalescence temperature of –35 °C for the methyl resonances on the same isopropyl group indicated free rotation about the N_{endo}–$C_{isopropyl}$ bond. Substitution into eq. 3 resulted in a $\Delta G^{\ddagger}$ of 47.5 ± 1.0 kJ mol^{-1}. A coalescence temperature of 33 °C for the isopropyl resonances indicates free rotation about the formally C=N double bond, with a $\Delta G^{\ddagger}$ value of 59.6 ± 1.0 kJ mol^{-1}. The difference in the two $\Delta G^{\ddagger}$ values is reasonable as the C–N_{exo} bond possesses double bond character and should thus require more energy to overcome a greater rotational energy barrier than the N_{endo}–$C_{isopropyl}$ single bond.

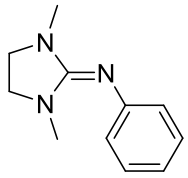

Figure 32. Cyclic imidazolidine phenyl-guanidine.

Bond rotational energies for the C=N have been reported for some guanidine-type systems. A cyclic imidazolidine phenyl-guanidine was reported to have a $\Delta G^{\ddagger}$ of 33.5 kJ/mol in $CDCl_3$ (**Figure 32**).[54,55] The higher value in Gibbs free rotational energy for the acylated ligand compared to the analogous imidazolidine-based guanidine confirms the pronounced impact the NHC "building block" has on the electronics of the resulting NHI. This difference in $\Delta G^{\ddagger}$ was as expected and the difference in magnitude between the two values confirms the electron-withdrawing acyl groups on the backbone of the azole ring increase exocyclic C–N bond order. This is done by reducing the availability of the endocyclic nitrogen lone pairs to delocalize electron density through the π system of the azole ring. This delocalization would otherwise increase the single bond character of the exocyclic C–N bond and thus decreasing the $\Delta G^{\ddagger}$.

This is supported by the data from Bertrand on phosphaalkene adducts of NHCs, the acyl groups withdraws electron density from the endocyclic nitrogen atom that would otherwise be delocalized over the π system onto the exocyclic phosphorus resulting in a significant downfield shift.[50] For the analogous guanidine systems, this results in a greater C=N double bond character compared to the corresponding imidazole or imidazoline derivative containing no acyl groups. The difference in the two $\Delta G^{\ddagger}$ values is 26.1 kJ/mol, indicating that **2a** does in fact have a higher C–N_{exo} bond order than that of the corresponding saturated imidazoline-based guanidine.

In comparison, the $\Delta G^{\ddagger}$ value for the C(O)–NH_2 bond in nicotinamide in $CDCl_3$ is 60.0 kJ/mol (**Figure 33**).[56] The C(O)–NH_2 $\Delta G^{\ddagger}$ value of nicotinamide is equivalent to **2a** (59.6 ± 1.0 kJ mol^{-1}) and show that the carbon exocyclic nitrogen bond order of **2a** is comparable to that of an amide. These comparisons highlight the balanced Lewis basicity achieved in **2a**: it shows more double bond character than the imidazoline analogue, closer resembling the electronic arrangement found in an amide. This characteristic is valuable when implemented in catalytic design as minor changes in the electronics of the ligand reflect directly to the metal center. Reducing the Lewis basicity of the ligand too much would result in an overly Lewis acidic metal center. This could result in lower lactide polymerization activity as the catalyst could be more prone to deactivation by polar impurities in the lactide, such as lactic acid or reduce the rate of the migratory insertion (k_2) in the catalytic cycle (**Scheme 1**), shutting down catalytic activity.[57]

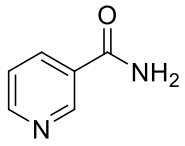

Figure 33. Structure of nicotinamide.

3.2 Synthesis of Compound 2b

Compound **2b** was synthesized with the same synthetic methodology of compound **2a**. Implementation of identical conditions resulted in the successful synthesis of the target ligand **2b** (**Scheme 11).**

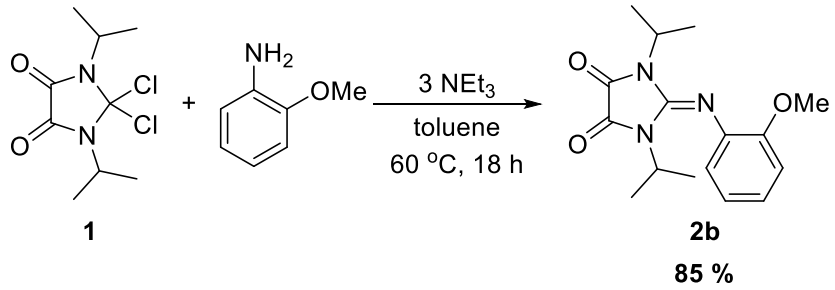

Scheme 11. Synthetic route employed to synthesize ligand **2b**.

The ^{1}H NMR spectrum of **2b** shows a sharp doublet representing all 12 methyl protons at room temperature compared to the broad doublet in **2b** (**Figure A5**) indicating that that the methyl protons across the azole ring are in magnetically equivalent environments. This further suggests that the C–N_{exo} bond is not in fact a true C=N bond but has significant single bond character, allowing for rotation about this bond even at room temperature, leading to equivalent isopropyl groups. To better understand the bond rotational energy about the carbon–nitrogen exocyclic bond, VT-NMR experiments were performed (**Figure 34**).

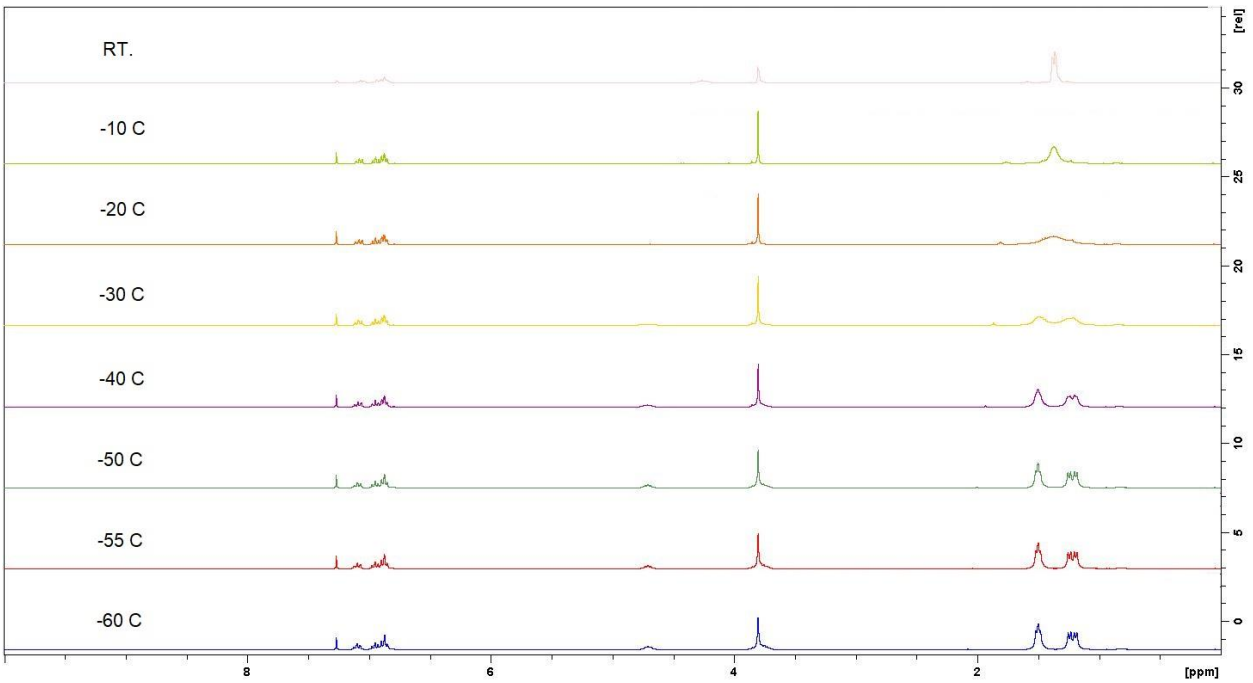

Figure 34. Variable temperature NMR spectrum of **2b** (300 Mz, $CDCl_3$).

Cooling the sample down to –60 °C resulted in the appearance of two signals (δ 1.50 and 1.25 ppm), each integrating to 6 and representing all 12 methyl protons. At this low temperature, the restricted rotation about the C–N_{exo} bond is such that the methyl protons across the azole ring become inequivalent. One signal (1.25 ppm) is a broad overlapping set of doublets, which indicates restricted rotation of one of the two isopropyl groups. The other signal appears to be two overlapping doublets of with peak separation that makes it appear as a 1:2:1 triplet. The difference in frequency between these two signals ($\Delta\nu_{A\text{-}B}$) is 86.4 Hz. The two resonances (δ 1.50 and 1.25 ppm) individually coalesce at –30 °C. This indicates no more restricted rotation about the N_{endo}–$C_{isopropyl}$. Further increasing the temperature to –20 °C leads to the two signals coalescing into the signal at δ1.38 ppm. This indicates free rotation about the C–N_{exo} bond.

Substituting these temperatures into eq. 3 yields a Gibbs free energy for the N_{endo}–$C_{isopropyl}$ and C–N_{exo} bond rotation of 51.9 ± 1.0 kJ mol^{-1} and 50.6 ± 1.1 kJ mol^{-1}, respectively. The observation of the N_{endo}–$C_{isopropyl}$ bond rotational energy barrier being higher than the C–N_{exo} bond is counter intuitive owing to the C–N_{exo} bond possessing more double bond character. This result can be attributed to the sensitivity of the methodology. VT NMR spectroscopy for the purpose of measuring bond rotational energy only provides information on the overall trend and not absolutely values as the results can be subject to bias based on the increment of temperature increase. Regardless, this energy barrier for the N_{endo}–$C_{isopropyl}$ bond rotational energy barrier of **2b** is statistically equivalent to that for **2a**. However, the C=N bond rotational energy barrier significantly higher in **2a** than **2b** owing to the less extensive conjugated π-system of the second donor fragment in **2b**.

3.3 Synthesis of Compound 2c

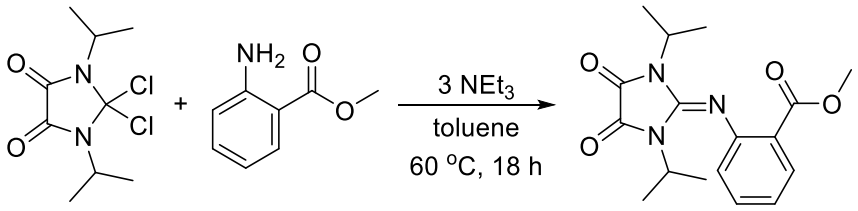

1 **2c**

Scheme 12. Synthetic route employed to synthesize ligand **2c**.

The synthesis of the ligand **2c** follows the same synthetic methodology for **2a** and **2b** (**Scheme 12**). The ligand was isolated by filtration to remove residual NEt_3•HCl and subsequently purified by flash column chromatography (hexanes:ethyl acetate:triethylamine 90:5:5), with NEt_3 used to de-acidify the silica and prevent

protonation of the strongly basic **2c**. Ligand **2c** was isolated in a 86% yield, with the impurity isolated from the column being mostly the imidazolone decomposition product of **1** (**Scheme 13**).

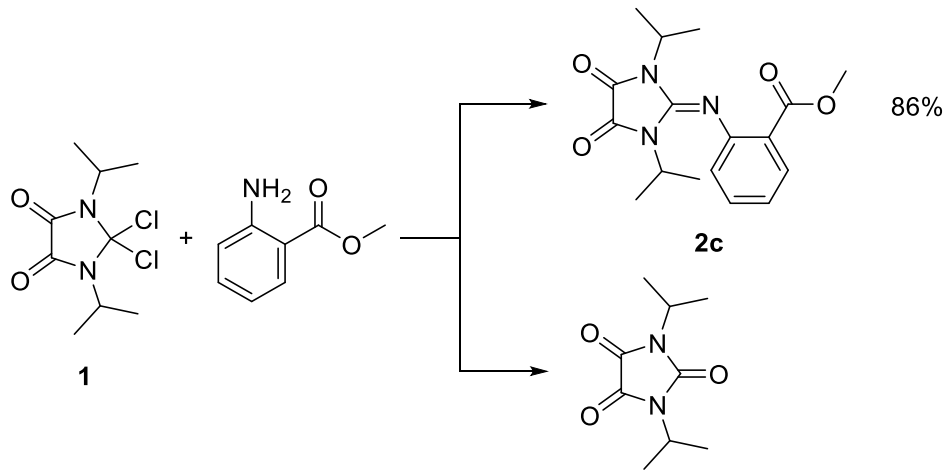

Scheme 13. Products from the synthesis of ligand **2c**.

Characterization by ^{1}H NMR spectroscopy suggests a $\Delta G^{\ddagger}$ different to what was observed for **2a** and more akin to **2b**. Like **2a** and **2b**, all four methyl groups were observed as one single doublet at room temperature. The doublet of the methyl protons, however, was sharp like what was observed for **2b**. This is in contrast to the broad doublet observed for **2a**. This indicates free rotation about the C=N bond at room temperature for **2c**.

A VT-NMR spectroscopy experiment was performed to determine the bond rotational energy of the C1–N_{exo} and N_{endo}–$C_{isopropyl}$ bonds (**Figure 35**).

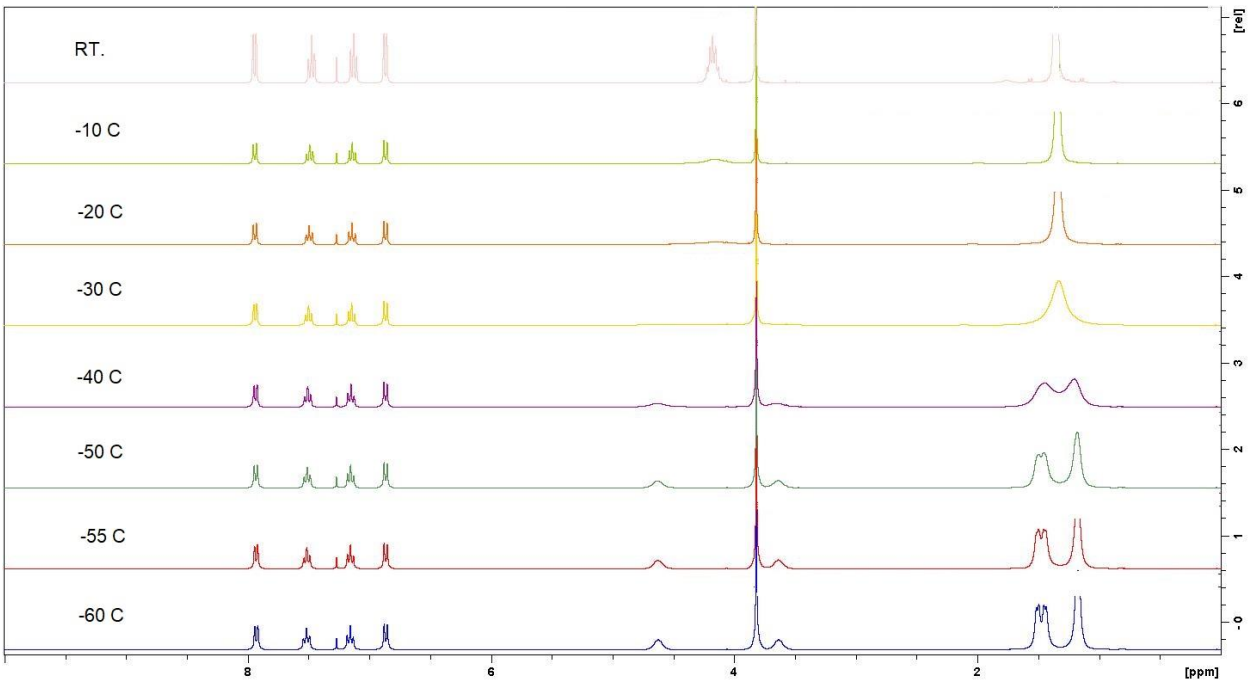

Figure 35. Variable temperature NMR spectrum of **2c** (300 Mz, $CDCl_3$).

Similar to **2b**, complete de-coalescence to produce two unique signals for the methyl protons across the azole ring was observed at –60 °C with similar coupling in the doublet at 1.50 ppm, indicating restricted rotation about the N_{endo}–$C_{isopropyl}$ bond. The doublet for the methyl signal at 1.50 ppm coalesced at approximately –45 °C indicating no more restricted rotation about the N_{endo}–$C_{isopropyl}$ bond. Both methyl signals coalesce into each other at approximately –35 °C into a broad singlet, indicating free rotation about the C1–N_{exo} bond.

Based on these temperatures the bond rotational energy was calculated to be 48.3 ± 1.0 kJ mol^{-1} and 47.4 ± 1.1 kJ mol^{-1} for the N_{endo}–$C_{isopropyl}$ and C1–N_{exo} bond respectively. The N_{endo}–$C_{isopropyl}$ bond rotational energy barrier for **2c** is statistically equivalent to those for both **2b** and **2a**. As expected, compound **2c** resembles **2b** in terms of C=N_{exo} bond character with both compounds having sharp doublets at room

temperature for the methyl signals, indicating free rotation about this C=N_{exo} bond. The C=N_{exo} bond rotation energy barrier for **2c** is smaller than for **2a** as the anthranilate functional group is sterically smaller that the large planar aromatic quinoline ring, which interferes with the bond rotation.

3.4 Synthesis of Compound 3a

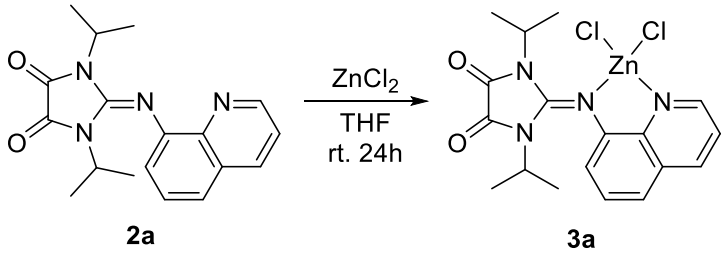

Scheme 14. Synthetic route employed to synthesize complex **3a**.

Compound **3a** was prepared by simple addition of **2a** to $ZnCl_2$ in THF (**Scheme 14**).[36] The ^{1}H NMR spectrum of **3a** reveals all chemical shifts of the resulting species are shifted downfield, relative to the free ligand. This is consistent with electron density donation to the metal center. In contrast to the broad doublet for the methyl signals in ligand **2a**, the methyl signals of **3a** are now two unique sharp doublets (**Figure A3**). This is due to the coordination of the Lewis acidic metal center to the nitrogen donor of the ligand. The electron withdrawing effect of the metal centre decreases the electron density of the C=N_{exo} bond and as a result, decreases the bond order. There is less restricted rotation about this exocyclic bond and the previously broad doublet is now two sharper doublets.

3.4.1 Crystal Structure

The solid-state structure of complex **3a** was determined by single-crystal X-ray diffraction crystallography (XRD). Suitable crystals were grown by vapour diffusion of pentane into a saturated solution of **3a** in THF at room temperature. Complex **3a** possesses a four-coordinate zinc atom that is coordinated to two chlorides and chelated to ligand **2a**, resulting in a five-membered metallocycle (**Figure 36**).

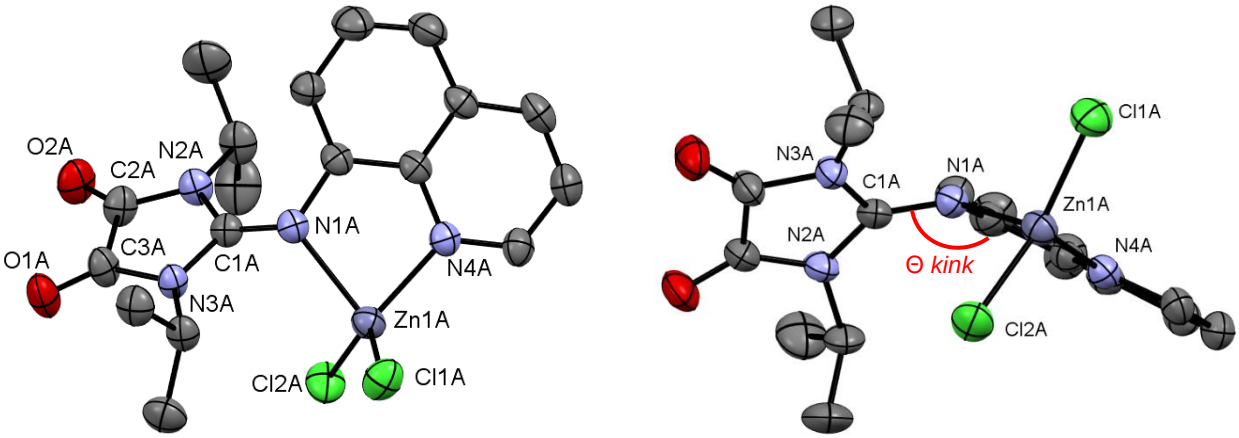

Figure 36. Solid-state structure of **3a**, ORTEP drawn at 50% probability.

Table 3 Select averaged bond lengths(Å), bond angles and structural parameters for complex **3a**.

Zn1–N4	2.032(4)
Zn1–N1	2.164(4)
Zn1–Cl1	2.2160 (15)
Zn1–Cl2	2.191(15)
C1–N1	1.284(6)
C1–N2	1.401(6)
C1–N3	1.380(6)
O1–C3	1.203(6)
O2–C2	1.206(6)
N1–Zn1–N4	81.03(6)
Cl1–Zn1–Cl2	122.45(7)
N2–C1–N3	108.96(4)
θ ZnN_2, $ZnCl_2$	82.54(11)
Twist	43.98(17)
θ Kink	125.107 (12)
ρ	0.92
τ_4	0.87

Selected averaged bond lengths and angles for complex **3a** are shown in **Table 3**. The Zn1–N4 bond length of 2.032(4) Å is similar to that of the related dimethylimidazolidine-based derivative (**Figure 37**, right) (2.045(1) Å), indicating that the strong donor character of the quinoline nitrogen is maintained within ligand **2a**.[36] The Zn1–N1 (2.164(4) Å) bond length compared to the non-acylated guanidine counterpart is notably longer (2.039(1) Å) indicating that the acyl groups of the azole ring play a part in tuning the donor capability of the guanidine nitrogen.[36] The C1–N1 bond length was observed to be 1.284(6) Å, shorter than the comparable non-acylated guanidine reported in literature (1.327(2) Å).[36] This is indicative that the strongly electron-withdrawing acyl groups of the carbene building block influence the exocyclic nitrogen. This is evidenced by the C1–N1 bond showing more double bond character than single bond. The influence of the acyl groups of the NHC fragment is further illustrated by the C1–N2 and C1–N3 bond lengths of the azole ring (1.401(6) and 1.380(6) Å, respectively). These bonds are

longer than the non-acylated guanidine reported in literature (1.355(2) and 1.352(2) Å). The longer C1–N2 and C1–N3 bonds of **3a** indicate more single bond character as there is less electron donation from the endocyclic nitrogen atoms through the azole π-system. This is due to the electron-withdrawing acyl groups of the backbone.[36] The N2–C2 and C3–N3 bonds of the azole backbone were determined to be 1.378(7) and 1.376(6) Å, respectively. The average of these bonds are statistically equivalent to the average of the C1–N2 and C1–N3 bonds, indicating that the lone pair of the endocyclic nitrogen is evenly distributed across the π system of the NHC fragment.

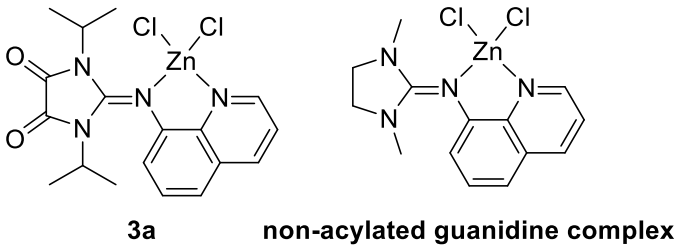

3a **non-acylated guanidine complex**

Figure 37. Comparison of **3a** to an acyclic guanidine-containing complex.

The azole bond lengths can be related directly to the extent of delocalisation of the charge around the NHC fragment. Increased electron delocalization across the NHC fragment results in uniformity in the bonds associated to the extended π-system, which includes the guanidine functional group. This extent of charge distribution can be expressed as the structural parameter ρ, where a value of 1 is indicative of completely uniform distribution of the charge across the entire guanidine unit.[36] The ρ value is calculated by the following equation 6:

$$\rho = \frac{2a}{b+c} \quad (6)$$

wherein *a*, *b* and *c* represent the bond lengths shown in **Figure 38**.

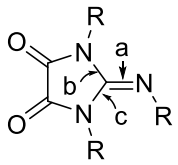

Figure 38. Required bond lengths for calculation of ρ.

The structural parameter ρ in **3a** was determined to be 0.92, indicative of lower distribution of electron density throughout the azole ring unit, compared to the non-acylated guanidine complex (0.98). This can be rationalized by the higher bond order of the C1–N1 bond compared to the C1–N2 and C1–N3 bonds. The strongly electron-withdrawing acyl groups of the azole ring reduce the electron density that the endocyclic nitrogen atoms contribute to the π-system of the guanidine functional group. Consequently the exocyclic nitrogen receives less electron density and the resulting C1–N1 bond is relatively shorter, decreasing the ρ value. The N2–C1–N3 bond angle of 108.96(4)° is a standard bond angle for the azole ring of an NHC slightly distorted by the hybridization of an exocyclic nitrogen.[58] The C=O bond lengths (1.203(6) and 1.206(6) Å) are comparable to most ketone C=O bond lengths of 1.22 Å.[59] The slightly shorter C=O bond lengths in **3a** compared to formamide indicate that the endocyclic nitrogen lone pair of **3a** is in fact not significantly channeling electron density towards the acyl group as this would result in lengthening of the C=O bond. The observation suggests that the endocyclic nitrogen lone pair is mostly localized on the nitrogen and there exists no appreciable delocalisation towards either the exocyclic nitrogen of the guanidine or the acyl groups.

The distorted tetrahedral coordination geometry of the zinc atom is well represented in the angle of 82.54(11)° formed between the plane of the 5-membered metallocycle and the $ZnCl_2$ plane. The τ_4 of **3a** was calculated to be 0.87. This distorted geometry can be attributed to the bite angle of the guanidine-quinoline ligand **2a** that was observed to be 81.08(6)°. This τ_4 parameter indicates the coordination about the metal center, with values ranging from 0 to 1 for a perfectly square planar and tetrahedral complex. It is calculated using the following equation 7:[60]

$$\tau_4 = \frac{360-(\alpha+\beta)}{141} \quad (7)$$

wherein α and β are the two greatest angles of coordination center.

There is a kink between the C1–N1 bond and the plane of the 5-membered metallocycle (**Figure 36**), with C1 of the azole ring positioned off the plane of the 5-membered metallocycle. The C1–N1 bond and the plane of the metallocycle are related by a *kink* angle θ value of 125.07°, possibly due to the mesomeric structure of cyclic guanidines. The partial sp^2 hybridization of the exocyclic nitrogen atoms in guanidines may leave slight sp^3 character on the exocyclic nitrogen, resulting in the pyramidalization of N1 and account for the observed kink. The pyramidalization of N1 is also reflected in the angles around this atom which are measured to be 111°, deviating from the expected 180° for a perfectly sp^2-hybridized atom.

Furthermore, the azole ring and the plane of the 5-membered metallocycle are twisted with respect to each other by 43.98(17)°. The twisting can be rationalized by the isopropyl group of the azole ring sterically clashing with the aromatic quinoline donor fragment. In order to reduce this steric congestion, the azole ring twists thereby alleviating

the unfavourable interaction. However, by twisting, the extended conjugation of the guanidine-quinoline ring is broken. The solid state structure is consistent with inequivalent methyl resonances observed in the ^{1}H NMR spectrum at room temperature (**Figure A9**). The presence of the kink in the ligand unit results in one pair of methyl groups across the azole ring in the inductive field generated by the aromatic ring current, thus making the methyl protons across the azole ring inequivalent at room temperature.

3.5 Synthesis of Compound 3b

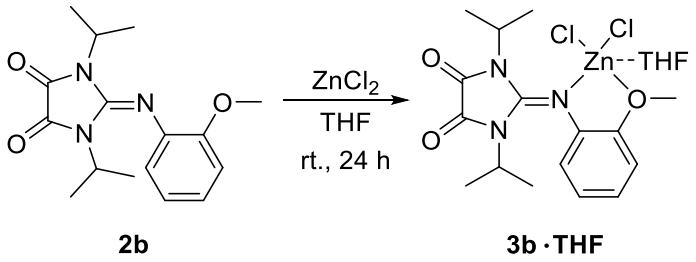

2b **3b·THF**

Scheme 15. Synthetic route employed to synthesize complex **3b**.

The synthesis of **3b** follows the identical protocol used for **3a**. Reaction of **2b** with $ZnCl_2$ in THF gave **3b** as a red oil (**Scheme 15**).The NMR spectroscopic data is in agreement with the structure of **3b** (**Figure A8**), with one THF molecule coordinated to the zinc metal center. This observation of the THF adduct of **3b**, **3b·THF**, is consistent with the weakly electron donating methoxy group and thus more Lewis acid zinc metal, allowing for coordination of THF. This observation supports the earlier predictions of the Lewis basicity of the second donor fragments in the ligand series **2a–c**. The presence of coordinated THF alludes to the lactide monomer readily binding to the enhanced Lewis acidic metal centre of **3b** compared to **3a**.

3.6 Synthesis of Compound 3c

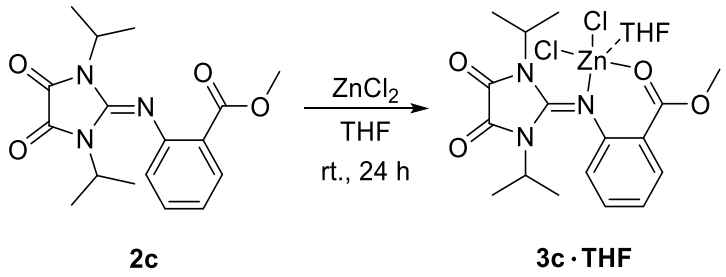

2c **3c · THF**

Scheme 16. Synthetic route employed to synthesize complex **3c·THF**.

The complex **3c** is generated from the same reaction conditions for **3a** and **3b**. Reaction of ligand **2c** with $ZnCl_2$ in THF affords the THF adduct of complex **3c** (**3c·THF**) in a 93% yield (**Scheme 16**). As observed for **3b**, the ^{1}H NMR spectrum of **3c** shows the presence of one equivalent of THF in the first coordination sphere of the complex. In contrast to **3b**, some of the THF coordinated in **3c** can be removed by drying the complex in vacuo (500 mtorr) at 70 °C. After 1 hour, the ^{1}H NMR spectrum of the solid shows the presence of only 0.5 equivalent of coordinated THF relative to the metal. The lability of this coordinating solvent to the metal is promising as the lactide monomer should be more Lewis basic than THF. As a result, coordination of the monomer should readily occur during the polymerization, assuring a rapid initiation step that would lead to all polymer chains beginning to grow at the same time (assuming no chain transfer events). This rapid initiation would thus lead to a low PDI.

3.7 Computational Analysis

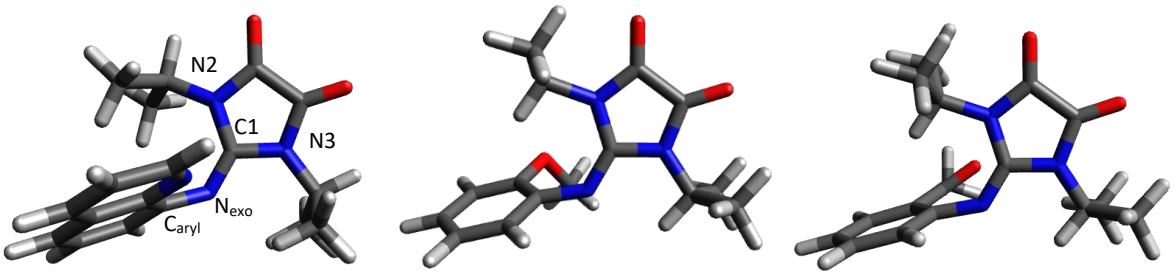

Figure 39. Structure of **2a** (left) **2b** (centre) **2c** (right) generated by DFT calculations.

Computational studies were performed on ligands **2a–c** to gain further insight into the structural differences resulting from coordination to zinc to generate complexes **3a–c (Figure 39**). The calculations were performed with the computational package Gaussian 16 on SHARCNET (Shared Hierarchy Academic Research Computing Network) using the M06 functional and the def2-TZVP basis set.[61] This level of theory was chosen as it is a highly versatile general use theory that was developed for organometallic and transition metal compounds.[62] def2-TZVP was chosen as it is an electron core potential (ECP) basis set, which simplifies the computational cost of the calculation without sacrificing accuracy. ECPs are commonly used for transition metal compounds as they simplify the modeling of the valence electrons by combining all core electrons into a single parameter. This approximation is important as it reduces computational cost as the core electrons do not play a critical role in chemical reactivity.[63] The optimized structures were first generated from preoptimization in the freeware Avogadro using the MMF94 force field. The MMF94 force field is a classical force field developed by Merck used to generate a starting three-dimensional structure that takes into account the forces between atoms.[64] The MMF94 force field is a general purpose force field that is relatively accurate in

preoptimizing the structures of many simply organic small molecules. Preoptimization simplifies subsequent calculations as key parameters such as the potential energy of atomic interactions is predicted in this step. This provides a more accurate starting point for calculating the potential energy when using higher level theory. The preoptimized structure was then refined by a geometry optimization using the more accurate but computationally-expensive M06/def2-TZVP calculations. Key geometric data are shown in **Table 4** based on the structures predicted by DFT from **Figure 39**.

Table 4. Comparison of key geometric data of ligands **2a–c** (Å)

	2a	**2b**	**2c**
C1–N_{exo}	1.258	1.272	1.255
C1–N2/3 (avg)	1.399	1.410	1.394
N_{exo}–C_{aryl}	1.373	1.400	1.377
θ Kink	128.5°	129.0°	131.1°

The calculated C1–N_{exo} bond lengths of **2a–c** were all consistent with a typical C=N bond (1.25 Å).[65] The C1–N_{exo} bond of **2b** was slightly longer at 1.272 Å. This trend was also observed in analysis of the C1–N2/3 bonds of **2a–c** were found to be 1.399, 1.410, 1.394 Å, respectively. Typical single C–N bond lengths are 1.47 Å, indicating that the lone pairs on the endocyclic nitrogen atoms of the azole ring are delocalized across the guanidine group.[65] Similarly, the calculated N_{exo}–C_{aryl} bond lengths of **2a** (1.373 Å), **2b** (1.400 Å) and **2c** (1.377 Å) also indicate conjugation throughout the quinoline aryl ring of **2a** and the anthranilate aryl ring of **2c**. The N_{exo}–C_{aryl} bond of **2b** showed significant lengthening and can be explained by the strong donating character of the ortho methoxy-ether group. Donation through the π-system localizes electron density on the aryl carbon

(C_{aryl}) attached to the exocyclic nitrogen. This results in electronic repulsion between the lone pair on the exocyclic nitrogen and the aryl carbon, thus lengthening the bond (**Figure 40**).

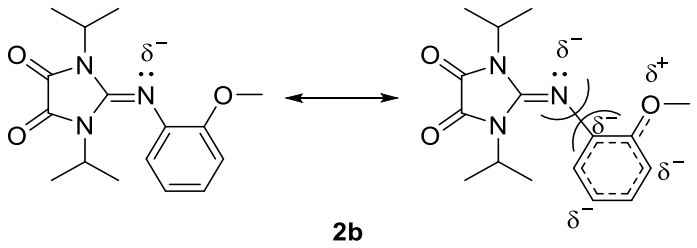

2b

Figure 40. Resonance structure of **3b** resulting in lengthening of N_{exo}–C_{aryl}.

To confirm this, a full natural bonding orbital (NBO) analysis and Wiberg Bond index (WBI) analysis were performed. NBO analysis is a method to localize wave functions into either one center and two center elements, which represent either a lone pair or a bond respectively. This is accomplished by manipulating the input atomic orbital basis set with the natural atomic orbitals (NAOs) and the natural hybrid orbitals (NHOs) to the corresponding NBOs.[66] Once the NBOs are obtained, the WBI is calculated from a series of orthogonal NAOs that are generated from the NBO calculation.[67] WBI are directly proportional to the bond order. Thus, for a purely single bond the WBI will be 1 and for a pure double bond, the value will be 2. The results of the WBI analysis are shown in **Table 5**. The C1–N_{exo} bonds of ligands **2a**–**c** showed a slightly greater double bond character (WBI of 1.67, 1.70, 1.68 for **2a**, **2b**, **2c** respectively) over imidazole-based guanidines (1.6) due to the acyl groups reducing delocalisation of the electron density from the endocyclic nitrogen atoms to the exocyclic nitrogen. This minimizes the contribution of the zwitterionic resonance structure that are accessible to NHIs and results in increased C1–N_{exo} double bond character. The WBI of the C1–N_{endo} bonds are entirely

consistent with single bond character demonstrating the efficacy of the acyl groups to reduce the delocalization of the endocyclic nitrogen lone pairs. Any delocalization of this lone pair would result in an increase of that bond order. The N2/3–C(O) WBI are higher than those for the C1–N2/N3 bonds, illustrating the electron-withdrawing effect of the acyl group to draw electron density from the endocyclic nitrogen lone pair.

Table 5. Comparison of WBI's and associated NPA charges of select NHI ligands.

Ligand	C1–N_{exo} WBI	C1–N2/N3 WBI	N2/3–C(O) WBI	C=O WBI	NPA charge (N_{exo})
2a	1.67	1.05	1.10	1.75	-0.506
2b	1.70	1.04	1.11	1.75	-0.508
2c	1.68	1.04	1.10	1.75	-0.501
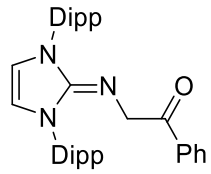	1.60	1.21	N/A	N/A	N/A

Another parameter of interest for this ligand series is the natural population analysis (NPA) charge of the exocyclic nitrogen atoms. The NPA charge is a description of the electron density on an atom as a function of the contributions of the NAO's from an atom-centered basis function. NPA have been often found to be a satisfactory qualitative description of the electronic effects of functional groups on substituted aromatic rings.[68] The NPA charges show a very slight increase in electron density on the exocyclic nitrogen

of **2a** and **2b** compared to that of **2c**. In **2b**, this can be attributed to the strong resonance effect of the methoxy functional group, pushing electron density towards the exocyclic nitrogen. This increase in electron density is accompanied with the complimentary lengthening of the N–C_{Aryl} bond previously observed. In **2a**, the weakly electron-withdrawing inductive effect of the quinoline ring does not account for the slight increase in exocyclic nitrogen NPA charge. The increase may be a result in the extensive π system of the quinoline ring providing electron density in which the exocyclic nitrogen can draw from. In the case of **2c**, the electron-withdrawing ester shifts electron density away from the exocyclic nitrogen. This accounts for **3c** having the lowest NPA charge of the ligand series.

Ligand **2a** was chosen to gain insight into the effect of coordinating these ligands to zinc and to compare to metrics with those of the solid-state structure of **3a**. Density functional theory (DFT) calculations were thus performed on **3a**. The calculations were performed with the computational package Gaussian 16 on SHARCNET using the M06 functional and a split basis set consisting def2-TZVP (H, C, N, O, Cl) and SDD (Zn) with an MF10 pseudopotential in order to minimize the computational cost and yet using an adequate basis set for the heavier transition metal.[69] As before, the optimized structure was first generated from preoptimization in Avogadro using the UFF force field. The preoptimized structure was then geometry optimized using the B3LYP functional and a split basis set consisting of 6-311+G(d,p) (H, C, N, O, Cl) and LANL2DZ (Zn). This DFT-optimized structure was then further optimized with the def2T-ZVP and SDD basis sets to give an optimized structure with computed metrics in good agreement with the crystal

structure. DFT predicted bond lengths within 1.1%, on average, of the observed values (**Table 6**).

Table 6. Comparison of DFT predicted bond lengths and angles compared to experimentally observed results from XRD.

3a	**Calculated (Å)**	**Observed (Å)**	***% Diff***
*Zn*1–*N*4 *Zn*1–*N*1	2.076 2.208	2.032 2.164	2.1 2.0
*Zn*1–*Cl*$_{(avg)}$	2.215	2.2035	0.5
C1–N1	1.288	1.284	0.3
C1–N2/N3 $_{(avg)}$	1.383	1.391	0.9
O–C$_{(avg)}$	1.192	1.204	1.0
θ N4-Zn1–*N1*	77.20	81.08	4.9
θ Cl1–Zn1–Cl2	132.30	122.45	7.7
θ N2–C1–N3	109.10	108.69	0.3

The deviation in bond angles is higher than the bond lengths as this requires high level theory to accurately predict the electron density across the azole ring. This would come at significant computational cost compared to the general purpose level of theory that accurately predicted the other structural parameters of **3a**.The largest differences between calculated and observed bond lengths were in metal-nitrogen bonds. The O–C bonds were predicted to be shorter than what was observed as the computation minimized the delocalization of electron density between the endocyclic nitrogens (N2/N3) and the acyl C=O bond.

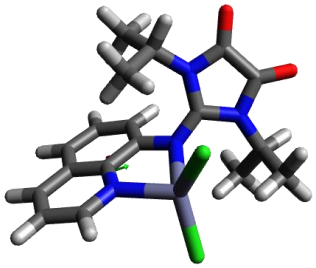

Figure 41. Structure generated by geometry optimization of **3a**.

The kink between the C1–N1 bond and the plane of the metallocycle ring is also predicted in the computational analysis (**Figure 41**).The pyramidalization of the exocyclic nitrogen was initially rationalized by an approximately sp^3 orbital, energetically lower than the HOMO. Full NBO and WBI computational analysis was performed to explain the observed geometry. From the NBO analysis, a series of molecular frontier orbitals were calculated (**Figure 42)**.

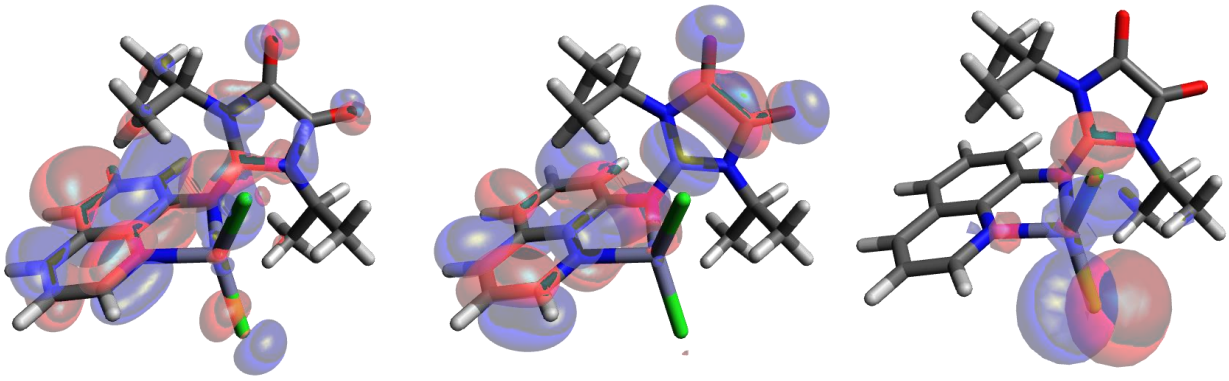

Figure 42. Series of frontier orbitals of **3a** generated from the NBO's (left: HOMO, centre: LUMO, right: HOMO-1)

The energy of the LUMO, HOMO, and HOMO-1 was determined to be –2.91 eV, –7.08 eV, –7.42 eV, respectively. This represents a HOMO-LUMO gap (Δε) in **3a** of 4.17 eV (–402 kJ/mol). Computations performed on benzene using the same level of theory resulted in, LUMO, HOMO and Δε energy of –0.95 eV, –6.44 eV, Δε of 5.49 eV (528

kJ/mol), respectively.[70] The large band gap of **3a** indicates high stability to redox reactions. The HOMO predominately resides on the exocyclic nitrogen and the aromatic ring of the quinoline second donor. The LUMO is distributed over the extensive π-system of the azole and aromatic rings. The HOMO-1 however does not show appreciable nitrogen character, but rather predominantly residing on the chlorine atoms.

The WBI's and select bond lengths are shown in **Table 7**. The C1–N_{exo} was determined to be 1.29 Å computationally and as such, this bond retains predominant double bond character as an average C=N bond is 1.28 Å.[65] This is corroborated by the C1–N2/N3 bond lengths of the azole ring itself (average 1.38) which are between a C=N bond (1.28 Å) and a C–N bond (1.46 Å), indicative of electron delocalisation in NHIs.[65] The WBI however represents a more complete representation of the molecular bonding than the C–N bond lengths. The WBI for the C1–N_{exo} bond of **3a** was determined to be 1.49, indicating the bond order is directly between a C1–N and C=N bond. This contrasts with the earlier conclusion that the C1–N_{exo} bond was predominately a double bond based on the calculated bond length. This WBI value requires the two atoms to have significantly sp^3 character, thus explaining the pyramidalization of the exocyclic nitrogen resulting in the observed kink angle.

Table 7. Selected WBI and bond lengths of complexes **3a–c**.

	C1–N_{exo} WBI	C1–N2/N3 (avg) WBI	N2/3–C(O) WBI	C=O WBI	C1–N_{exo} (Å)	C1–N2/3 (avg) (Å)
3a	1.49	1.10	1.05	1.80	1.29	1.38
3b	1.50	1.10	1.05	1.80	1.29	1.37
3c	1.48	1.12	1.05	1.80	1.29	1.38

DFT calculations were performed on complexes **3b** and **3c** at the same level of theory used for **3a** as this generated a computed structure that significantly resembles its solid state structure (**Figure 43**). All C1–N_{exo} bond lengths are statistically equivalent for complexes **3a–c**. This is a testament to the significant influence the parent NHC fragment plays in the main structural elements of the corresponding NHI and the minor role the second donor fragment plays. This result shows that the second donor functional group does not affect the electronic features of the exocyclic nitrogen inductively or through resonance of the aromatic ring. As the two fragments are independent of each other, new fragments would easily be incorporated. This ability to mix and match building blocks serves as a powerful tool in catalysis. Minor changes in steric and electronic features of the ligand often result in significant changes in catalytic performance. The weakly electron-withdrawing methyl ester functional group of **3c**, nor the strongly electron-donating methyl ether group of **3b** affect the C1–N_{exo} bond length.

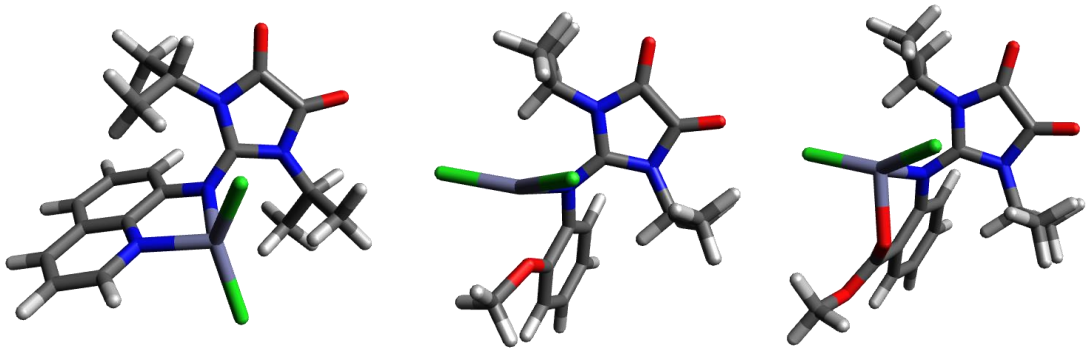

Figure 43. Structures of complexes **3a–c** generated from computational studies.

NHIs that are not substituted with electron-withdrawing acyl groups have a WBI of 1.2–1.4. The observed value of 1.49 is thus again most likely attributed to the influence of the acylated NHC fragment. Through resonance, the acyl group increase the double bond character of the C–N_{exo} bond. This is confirmed by the WBI of C1–N2/N3 and N2/3–C(O), 1.10 and 1.05, respectively. The WBI values of both bonds indicate that the electron density of the endocyclic nitrogen lone pair is slightly delocalized towards the metal centre, and the electron withdrawing effects of the acyl groups are slightly outcompeted by the withdrawing effects of the Zn metal. All complexes demonstrate the same pyramidalization of the exocyclic nitrogen that results in a kink angle ranging from 118 to 124° due to the partial sp^3 hybridization of the exocyclic nitrogen.

In comparison of the ligands **2a–c** to the corresponding complexes **3a–c**, the bond order for C–N_{exo} is significantly decreased from 1.7 to 1.5. This decrease in bond order is attributed to the Lewis acidity of the $ZnCl_2$ moiety drawing electron density away from the exocyclic bond. This is accompanied with a minor increase in bond order of the endocyclic C1–N2/N3 bonds. This change in bond order is anticipated as the zinc metal center is increasing the amount of electron density delocalization from the endocyclic nitrogen

atoms, thereby decreasing the C–N_{exo} bond order while increasing the C1–N2/N3 bond order.

The coordination of the metal centre also brings the anticipated corresponding change in the NPA charges of the exocyclic nitrogen atoms, from –0.51 in the ligands to in the –0.62 complexes. The change in N2/3–C(O) and C=O bond lengths from ligand to complex also supports the observation of the zinc metal centre drawing out electron density from the azole ring. The N2/3–C(O) WBI decreases from 1.10 to 1.05 upon coordination of the ligand to the metal. This change is reflected in the C=O bond order, increasing from 1.75 in the ligand to 1.80. This complementary decrease in WBI of the N2/3–C(O) bond and increase in C=O bond order is in line with the observation of the Lewis acidic metal centre drawing electron density form the endocyclic nitrogen lone pair and away from the conjugation of the azole backbone. While the metal centre is drawing the endocyclic nitrogen lone pair towards it through resonance, the effect is complemented by the electron-withdrawing effect of the acyl groups. They modulate the electron richness of the metal centre just enough to permit coordination of Lewis basic solvents such as THF in the coordination sphere of **3b** and **3c**. This observation suggests facile coordination of the more Lewis basic lactide to the metal, a requirement for the ring-opening polymerization of the monomer. The θ *kink* observed in complex **3a** was also present in the ligands **2** indicating that the pyramidalization of N_1 is not a product of coordination to a metal center drawing out electron density from the endocyclic nitrogen atoms but from the partial sp^3 hybridization of the exocyclic nitrogen.

3.8 Polymerization Studies

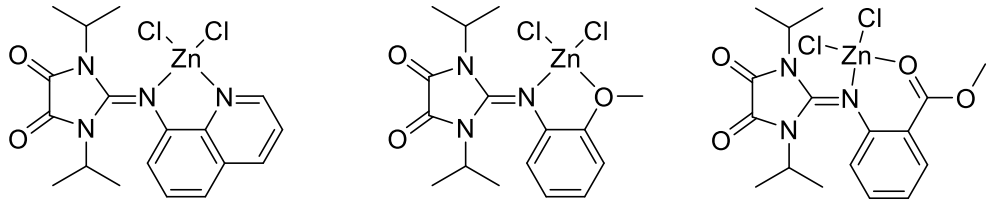

3a **3b** **3c**

Figure 44. Complexes tested for ROP of lactide to PLA.

Polymerization studies were carried out on complexes **3a**–**c** (**Figure 44**) using reagent grade *rac*-lactide, which had not been purified by sublimation, in the absence of any solvent. These bulk polymerizations were performed at 135 °C, using an initiator to monomer ([I]/[M]) ratio of 1:100 unless otherwise specified. The use of non purified *rac*-lactide reflects the industrial application of the catalysts **3a**–**c**. Polymerizations mediated by catalysts bearing anionic ligands often necessitate costly and time consuming purifications of *rac*-lactide to remove polar impurities which would otherwise poison the catalyst.[71] The purification of the monomer serves as an additional barrier for the large-scale implementation of PLA as a plastic substitute. "Time zero" during the polymerization experiments was chosen as the moment when all the monomer had melted and the mixture containing the catalyst was homogenous. Notably, all complexes **3a**–**c** were completely soluble in the molten lactide. The polymerization studies were also performed with purified *rac*-lactide where the conversions decreased on average by 10%. The complexes showed lower catalytic activity owing to the absence of acidic impurities or water, which likely act as the nucleophile in the first step of the ring opening of lactide. The ability of all complexes to polymerize lactide with non-purified *rac*-lactide is a testament to the stability of the catalytic systems to the polar and acidic impurities (lactic

and lactoyl acid) found in lactide. The catalytic performance of the catalyst **3a–c** in ROP of *rac*-lactide with and without the presence of a benzyl alcohol co-initiator (1 equiv.) are shown in **Table 8**.

Table 8. Molecular weight data of poly(DL-lactide) isolated using **3a–c** ,

Complex	Co-initiator	$M_{n\ NMR}$ (g/mol)
3a	none/	1300
	BnOH	770
3b	none/	1200
	BnOH	900
3c	none/	4700
	BnOH	3400
$Sn(Oct)_2$	none/	5100
	BnOH	5600

Polymerizations conditions: neat, 1 equiv. BnOH added where applicable, 135 °C, 24 h; all conversions were quantitative.

3.8.1 Molecular weight determination

The molecular weight determination by ^{1}H NMR spectroscopy was accomplished by end group analysis of the resulting polymer.[6] Lactide that is ring opened by a water molecule results in a polymer chain “capped” with a carboxylic acid (**Figure 45**).

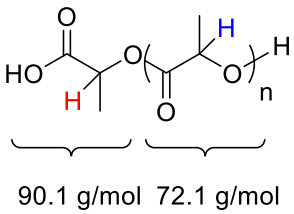

Figure 45. Structure of PLA generated from water performing the initial ring opening.

The methine of this resulting carboxylic acid end group resonates at δ = 4.37–4.35 ppm (**Figure 46**. red proton), while the methine proton of the PLA repeat unit resonates at δ = 5.17 ppm (**Figure 46**. blue proton).

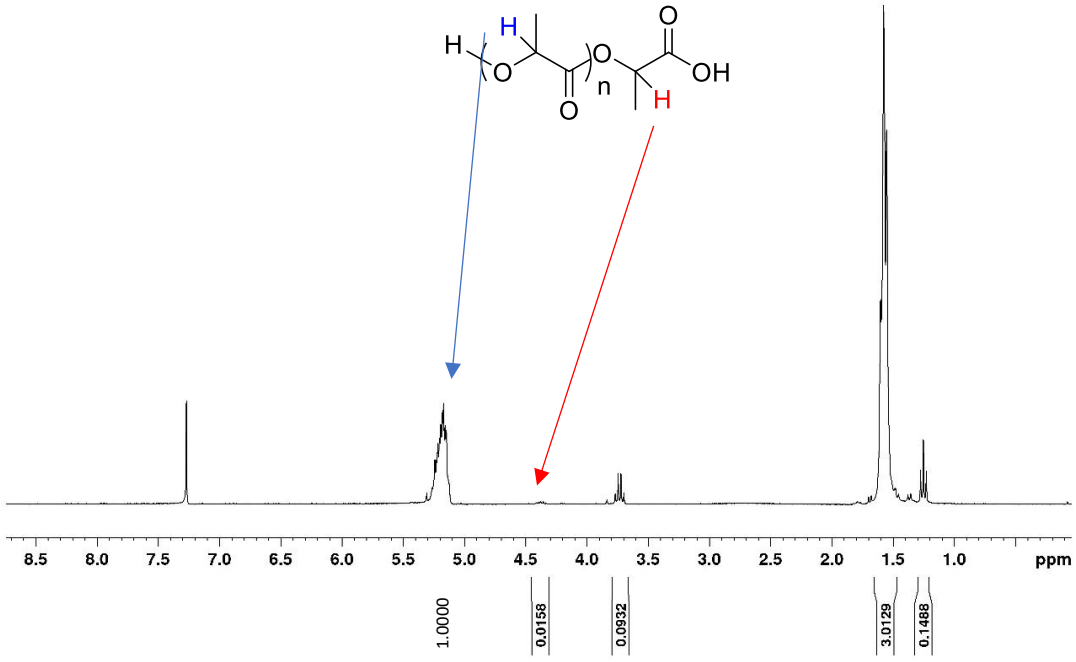

Figure 46. ^{1}H NMR spectrum of polymer generated by **3c** with resonances labeled to end group and repeat unit.

The relative integration of these two signals gives the amount of end groups per repeat unit. With the number of repeat units known, the M_n can be calculated based on the molecular weight of the repeat units and the end group.[6]

$$n = number\ of\ repeating\ monomers$$

$$n = 1/0.0158$$

$$n = 64.3$$

The relative integration of these two signals gives the amount of end groups per repeat unit. With the number of repeat units known, the M_n can be calculated based on the molecular weight of the repeat units and the end group.

$$M_n = (MW\ end\ groups) + (MW\ repeat\ unit) \times n$$

$$M_n = (90.1\ g\ mol^{-1}) + (72.1) \times (64.3)$$

$$M_n = 4700\ g\ mol^{-1}$$

GPC was performed on the polymers generated by complexes **3a–c** to validate the molecular weights observed by NMR spectroscopy and determine the PDI of the polymers. GPC characterizes polymers by separating the polymer mixture based on the hydrodynamic volume of the polymers. The hydrodynamic volume represents the volume a polymer chain occupies in solution. The polymer sample is dissolved in an organic solvent (mobile phase), then injected in a continuously flowing mobile phase that passes through a column. The column is packed with a porous crosslinked gel (polystyrene crosslinked with divinylbenzene) as the stationary phase. These pores are of variable size and separate the analyte based on the hydrodynamic volume that the polymer chain

occupies when in a solution. Smaller polymers will easily enter the pores of the column, resulting in the polymers having a high retention time. Larger polymers will not enter the pores as easily and will thus have a short retention time. The mobile phase containing the polymer is analyzed by a series of concentration sensitive detectors. In triple detection GPC, the polymer sample is analyzed by a concentration detector, viscosity meter, and light scattering detector. The differential refractometer gives the difference in refractive index, a colligative property, between the pure solvent and the solution of the analyte. The viscometer measures the viscosity of a solution containing a polymer sample in a solvent relative to viscosity of the solvent alone. The viscosity is related to the molecular weight of the polymer by the hydrodynamic volume and the Mark-Houwink constants (*K* and *a*). A universal calibration curve can be generated by plotting log(intrinsic viscosity × molecular weight) by retention time. When analysing the eluent of the GPC, the viscosity at a given retention time can then be used to determine an exact molecular weight. The light angle scattering detector involves irradiating the eluent with a beam and measuring the intensity of the resulting scattered light which is directly proportional to the molecular weight. A distribution of molecular weights of polymers can be observed and thus the PDI can be determined. The results of the GPC analysis on polymers generated by complexes **3a–c** are shown in **Table 9**.

Table 9. Results NMR spectroscopy analysis of polymers generated by complexes **3a–c** compared to the corresponding GPC analysis.

	$M_{n\ NMR}$ (g mol^{-1})	$M_{n\ GPC}$ (g mol^{-1})	$M_{w\ GPC}$ (g mol^{-1})	PDI (Đ)
3a	1300	1087	1171	1.08
3b	1200	1307	1358	1.04
3c	4700	2140	2347	1.10

All polymerizations carried out at 24h, 130 °C, neat. The conditions used led to 100% conversion of the monomer. Expected M_n = 14400 g mol^{-1}.

PDI's for polymers generated by initiators containing neutral guanidine ligand fragments range from 1.10-1.70.[1,8,36,57,71] These larger PDI's can be attributed in part to polymerizations where multiple initiators or active species are present. Neutral guanidines ligands have been observed to act as initiators, even in the case of the most active catalyst from Herres-Pawlis (**Figure 47**, right).

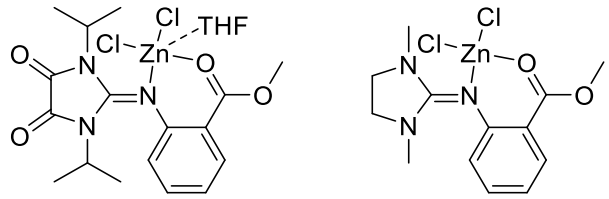

3c

Figure 47. Comparison of catalyst **3c** (left) compared to Herres-Pawlis's most active catalyst for the ring opening of *rac*-lactide (right).

The presence of multiple initiation mechanisms inevitably increases PDI as the k_i for each initiator will be different resulting in polymers beginning to grow at different initial rates. This difference in initial rate of polymer growth results in broadening of the PDI. The low PDI observed for polymers generated by complexes **3a–c** can be attributed to the enhanced π-acidity of the ligand fragment. Increased π-acidity of the ligand allows for more π back-donation from the metal center to the ligand. This results in strong metal-

ligand bonds, which are less likely to undergo ligand dissociation through thermodecomposition pathways. Shutting down this pathway prevents the ligand from becoming free of the metal complex and acting as a new initiator in the ROP of lactide. This would otherwise increase the PDI as the rate constant (k_1 and k_2) for this mechanism of polymerization will be different from that for catalyst **3c**.

In comparison to the two analytical techniques (NMR and GPC) used to determine molecular weight, GPC stands as the preferred method. GPC utilizes three different detectors to measure a variety of properties of the polymer to accurately depict the molecular weight distribution. The three detectors (low light scattering, viscometry and refractory index) work in unison describe different properties of the polymer to give an accurate representation of the polymers molecular weight. This is significantly more rigorous than NMR spectroscopy as the sensitivity of this analytical method is highly dependent on the ratio between the end group and repeat unit resonances. The ratio between the resonances is low (1.6%) and well below the desired ratio of 5% that would ensure an accurate description of the molecular weights. Despite a lower sensitivity, both methods agree in predicting molecular weights below 10,000 g/mol.

3.8.2 Kinetic Studies

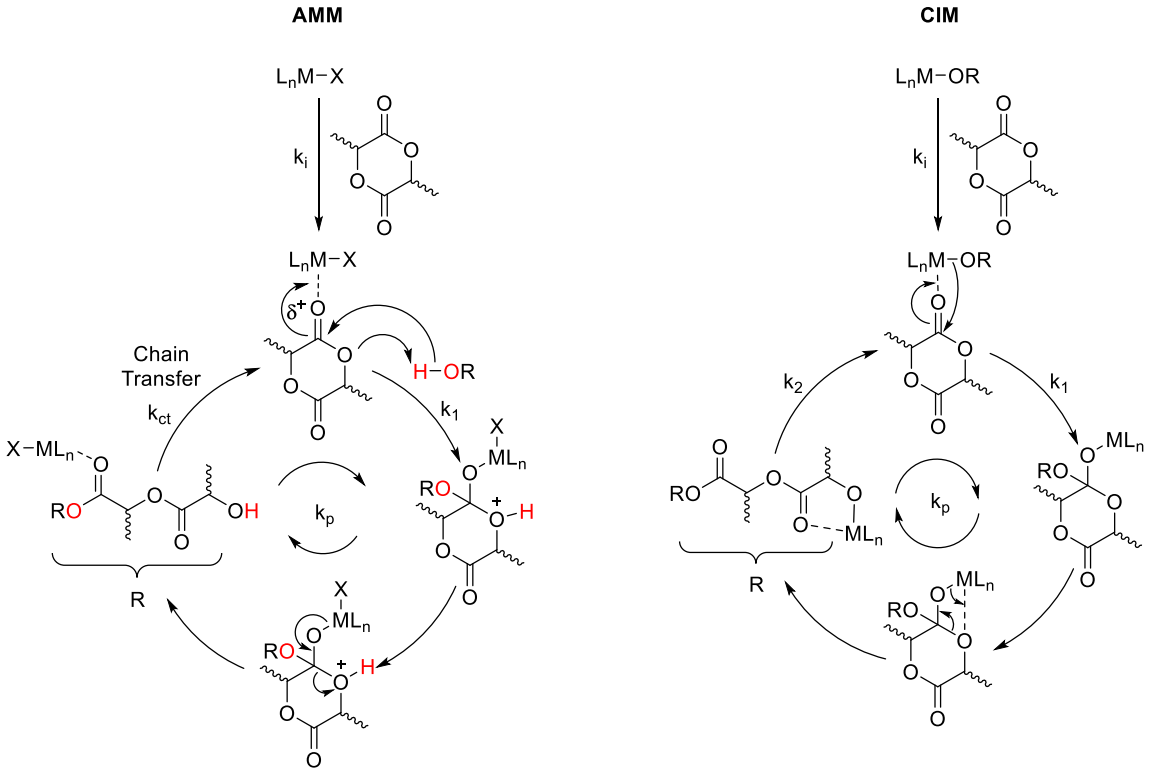

Figure 48. Comparison of AMM vs. CIM for the ROP of LA to PLA.

As the catalysts bear no alkoxide ligand, the assumed mechanism for the ROP of lactide by **3a–c** is AMM (activated monomer mechanism) and not CIM (coordination insertion mechanism) (**Figure 48)**. Catalytic performance is best described by the rate of propagation of the catalytic cycle, k_p. This rate constant can be described by the rate law previously defined in equation 1 and the simplified rate law from equation 2.

The rate of propagation (k_p) is obtained by first determining the observed rate (k_{obs}) as a function of initiator concentrations. The k_{obs} value is calculated from the slope of the semi-logarithmic plot $\ln[LA]_o/[LA]_t$ as a function of time (t) derived from the integration of the differential rate expression (equation 8), giving k_{obs} as the slope.

$$\ln [LA]_t = \ln[LA]_o - k_{obs}t \quad (8)$$

The k_{obs} values for **3c** were measured at various $[LA]_o/[I]$ (100, 200, 300, 500, 1000). The amount of lactide converted $[LA]_t$ was determined by ^{1}H NMR spectroscopy, based on integration of the methine region. As all LA is converted to PLA and no mass is lost, $[LA]_o$ was determined by the sum of the integration of the methine region of the PLA formed and the remaining LA at any given time ($[LA]_o = [PLA]_t + [LA]_t$). Plotting $\ln[LA]_o/[LA]_t$ as a function of time (t) yielded a linear relationship with k_{obs} given by the slope (**Figure. 49**).

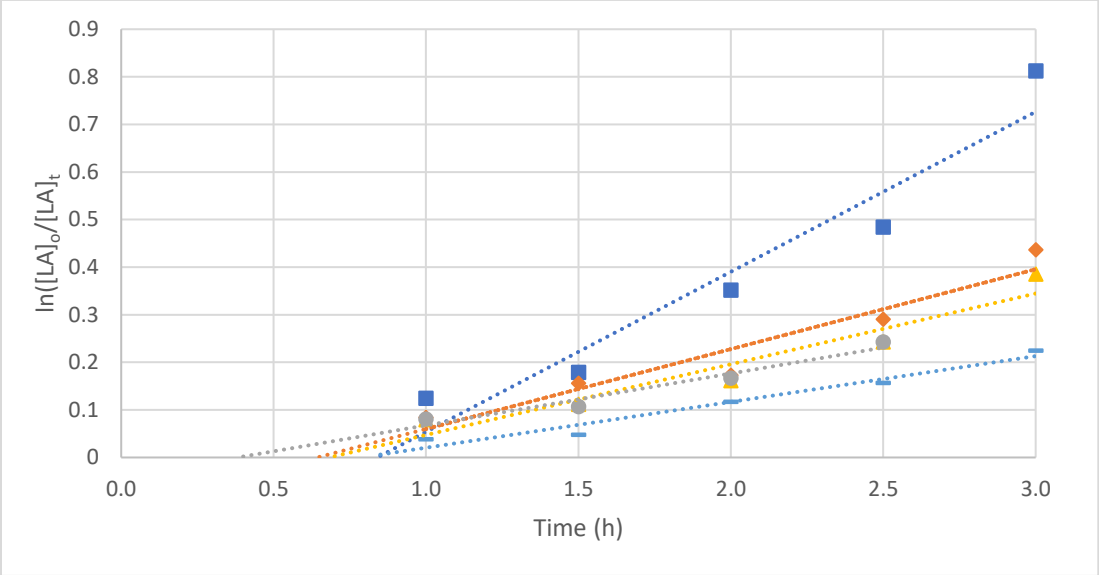

Figure 49. Plot of $\ln([LA]_o/[LA]_t)$vs. time for ROP of LA to PLA for complex **3c**·THF, ■ = 100[LA]/[I] (y = 0.33x - 0.28 and R^2= 0.93), ◊ = 200[LA]/[I] (y = 0.17x - 0.11 and R^2= 0.92), ▲ = 300[LA]/[I] (y = 0.15x - 0.10 and R^2= 0.92), ● = 500[LA]/[I] (y = 0.11x - 0.04 and R^2= 0.96), and ▬ = 1000[LA]/[I] (y = 0.10x - 0.08 and R^2= 0.96).

Table 10. Rate constants obtained from polymerization studies of **3c·THF** at various initiator to monomer ratios.

[LA]/[I]	k_{obs} (h^{-1})
100	0.330
200	0.168
300	0.148
500	0.109
1000	0.0960

Conditions: 3 h, 135 °C, solvent free, *rac*-lactide (no purification).

The k_{obs} values were obtained from the plot of $\ln[LA]_o/[LA]_t$ vs time (**Table 10**). These k_{obs} values are comparable to those for catalysts bearing related neutral guanidine bidentate ligands. The k_{obs} observed for a related system at [LA]:[I] = 500, 150 °C is slightly greater (4.54×10^{-1} h^{-1}) than what was observed for **3c•THF** (1.09×10^{-1} h^{-1}).[1] This effort represents a first-generation catalyst that possesses comparable activity (k_{obs}) to the well-established systems from Herres-Pawlis (**Figure 47**).

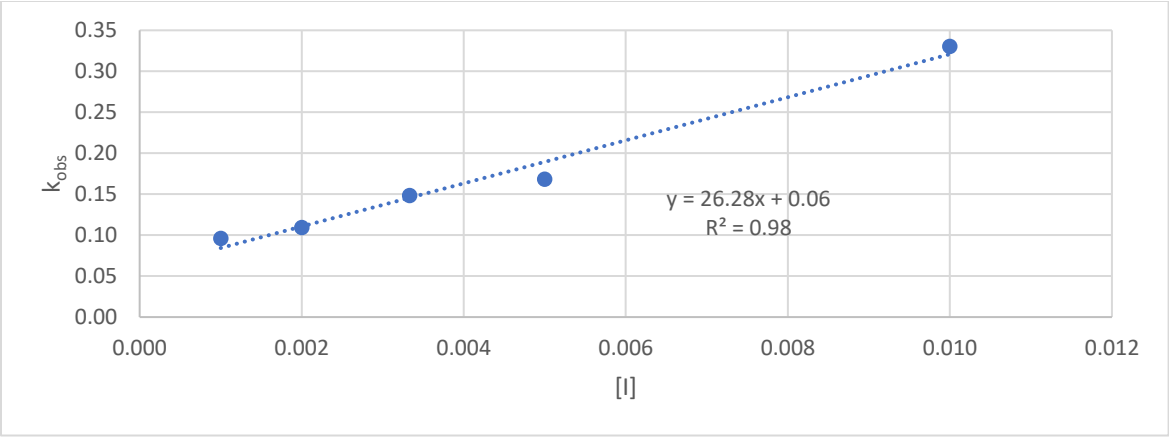

Figure 50. Plot of k_{obs} as a function of initiator concentration [I].

By plotting the k_{obs} as a function of [I], the slope of the resulting plot yields the k_p (**Figure 50**).The polymerizations are caried out in molten monomer, in the absence of any co-initiator. The activity or effective concentration of the monomer is 1 and the ratio of the [I]/[LA] is known, the activity of the initiator can be determined. Thus, k_{obs} was plotted against the activity of the initiator ([I]) and k_p was determined to be 26.2 M^{-1} h^{-1}. In comparison, Herres-Pawlis reported a k_p of 342 M^{-1} h^{-1} for their most active zinc initiators, which also incorporates a neutral donor ligand (**Figure 47**).[1] The difference in catalytic performance can be partly attributed to the steric congestion in **3c** compared to the system from Herres-Pawlis. The isopropyl groups of the NHI shield the metal center from the incoming monomer. This result has been previously observed in similar phenoxy-imine catalyst where performance begins to suffer as steric bulk near the nitrogen donor is increased.[72]

The lower activity with the increased steric congestion around the metal center implies that the rate limiting step of the polymerization (R_p) mediated by **3c** is the coordination (k_2) and not the migratory insertion (k_1) (**Scheme 1**). For an AMM system, if the electronics of the ligand were driving the reaction then the k_p of **3c**·THF would be higher than that of Herres-Pawlis as the coordination of the monomer (k_2) would be faster for a less electron rich metal centre. The steric influence of the ligand on the activity of the corresponding complex was underestimated based on the comparison of k_p.

The ROP of LA to PLA mediated by transition metal catalysts typically proceeds through a “living” polymerization, with the rate of chain termination significantly lower than the rate of propagation. This results in one growing polymer per active site on the catalyst. There however exist pitfalls to the classical living polymerization, as there is higher

propensity of catalyst contamination in the resulting polymer, along with lower catalytic productivity.[24] The alternative to this methodology is the “immortal” ROP of LA to PLA. The immortal polymerizations are two-component systems, consisting of the catalyst and a co-initiator which acts as a chain transfer agent (water, acidic impurity, external alcohol). As a result, the number of growing polymers is greater than the number of catalyst molecules and actually proportional to the ratio of co-initiator to catalyst.[24] Polymerizations that are living show a linear correlation between the M_n and the conversion. A plot of M_n values, both theoretical and measured by NMR spectroscopy, vs. monomer conversion can be shown in **Figure 51.**

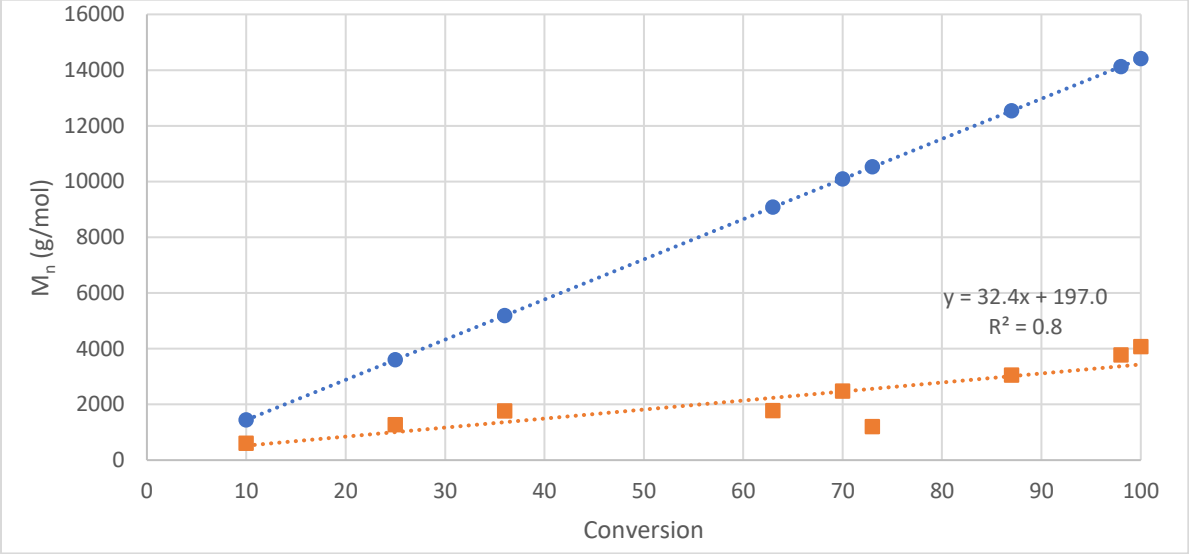

Figure 51. Graph of M_n as a function of conversion. The orange line is the $M_{n\ NMR}$ of PLA generated by **3c·THF**. The blue line represents the theoretical M_n at any given conversion.

A linear correlation between the two, where the given conversion has an $M_{n\ exp}$ in close agreement with the $M_{n\ calc}$, supports that the polymerization is well behaved and living. While the M_n vs. conversion did support the living nature of the polymerization, the

significant difference between the $M_{n\ exp}$ and the $M_{n\ calc}$ indicated significant transesterification events.

While there is a linear trend between M_n and conversion using **3c** (**Figure 51**; orange squares), the M_n values are significantly lower than the predicted theoretical M_n values (blue circles). This suggests significant transesterification events that result in cleavage of existing polymers by growing polymer chains. This results in a broad distribution polymer molecular weights with a high PDI. The addition of benzyl alcohol to the polymerization resulted in a lower M_n, indicating that the benzyl alcohol acts as a chain transfer reagent.

The structure of the active species was investigated by heating **3c·THF** with 10 equivalents of lactide in $CDCl_3$ to 65 °C and monitoring any changes by ^{1}H NMR spectroscopy. No change in the ^{1}H NMR spectrum was observed after several days of heating. There was no significant change in the chemical shift of the lactide to indicate coordination to the catalyst under these conditions. The signal associated with the coordinated lactide may have been buried under the free lactide signal. The lack of generation of active species is possibly attributed to the relatively low temperature the sample was heated to.

To promote generation of an active species, 2.5 equivalents of benzyl alcohol, a common co-initiator, was added. The larger amount of alcohol co-initiator compared to the trace amounts of water present could aid in generating an alkoxide active species. The alkoxide active species would be generated from the entropically driven metathesis of HCl from reaction of **3c·THF** and the BnOH at elevated temperatures. The addition of alcohol co-initiator and heating for 4 days resulted in the formation of multiple species. A

well-defined structure could not be determined owing to the multitude of chemical species present in the reaction mixture.

Of the multiple species formed, two were benzyl-alkoxide containing species, based on the integration of the associated methylene protons. Based on the integration of the methine proton of lactide (5.07 ppm), 3 equivalents of the monomer had been consumed. The integration of the methylene proton of benzyl alcohol (4.69 ppm) indicated that 2 equivalents have been consumed. In addition, signals appeared at 4.35 ppm for a methine proton associated with an end group of ring-opened lactide, as well as signals at 5.15 ppm for a methine proton associated with a low molecular weight PLA oligomer (**Figure 52**).

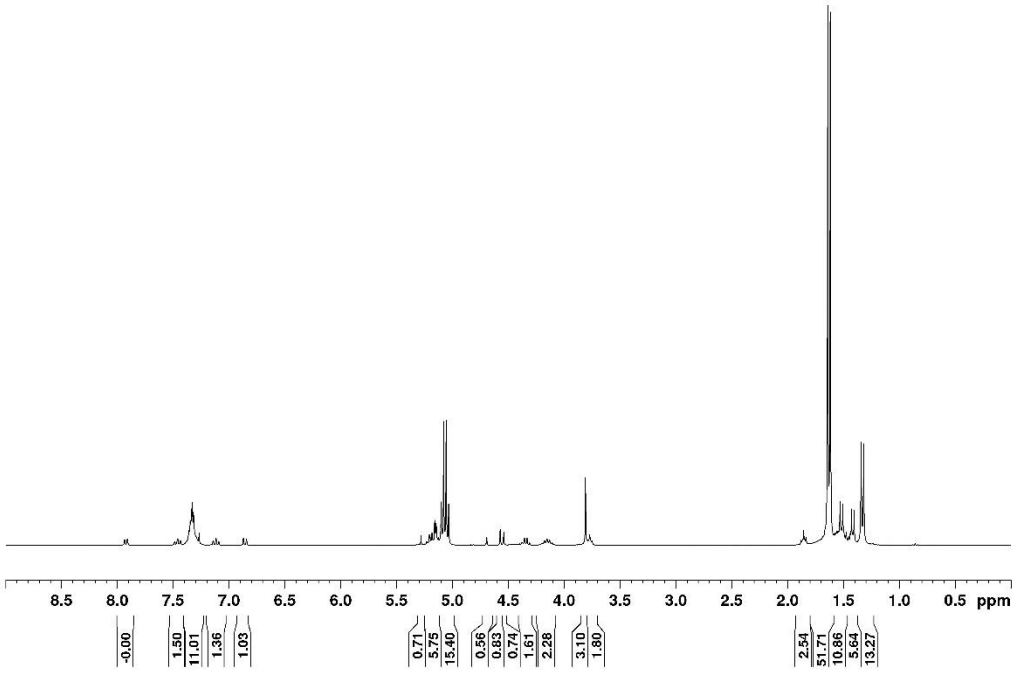

Figure 52. ^{1}H NMR (300 MHz, $CDCl_3$) spectrum of heating **3c·THF** with BnOH and excess LA for 4 days at 70°C.

A proposed structure for these two species **3c'-Cl** and **3c'-OBn** is shown in **Figure 53**. Both proposed compounds are generated by exchanging at least one of the two chloride ligands on **3c·THF** with a benzyloxide ligand. The active species **3c'-Cl** and **3c'-OBn** both exclude the presence of the coordinated THF indicating that the zinc metal center of **3c** requires stabilizing substrates, whether that be a donor solvent or the lactide monomer itself. This is due to the electron-withdrawing chlorine ligands, heightening the Lewis acidity of the metal centre. The electropositive metal centre now needs stabilization by a Lewis base. The coordination of an alkoxide, OR (where R = Bn or a propagating polymer/oligomer chain) provides the metal center with either sufficient electron density or steric congestion to favour the dissociation of the coordinated THF molecule .

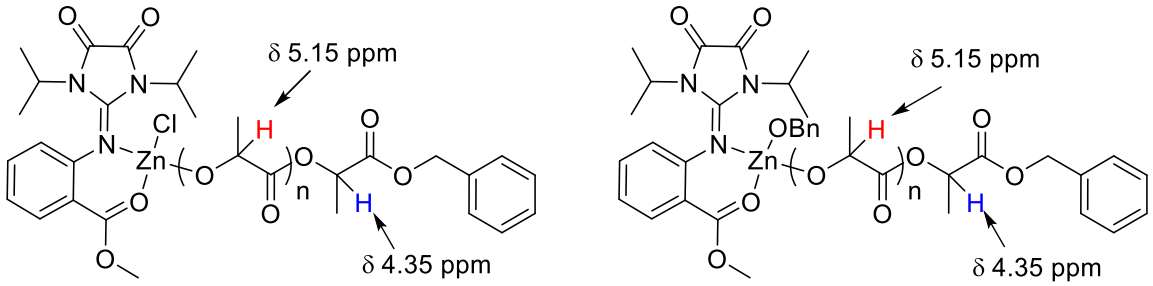

3c'-Cl **3c'-OBn**

Figure 53. Proposed structure of active species generated from addition of benzyl alcohol to complex **3c·THF** and excess lactide.

3.8.1 Mass Spectrometry

Mass spectrometry was used to elucidate the mechanism of the polymerization. Matrix-assisted laser desorption/ionization time-of-flight (MALDI-TOF) mass spectrometry is a common analytical method used to perform end-group analysis on PLA. This method gives an indication of what activated the monomer and thus the mechanism of polymerization. In MALDI-TOF mass spectrometry, the neutral polymer chains of PLA

undergo ionization through the addition of cationizing agents such as H^+, NH_4^+, Na^+, K^+, or Ag^+. The site of cationization is usually within the end group but can also occur along the length of the polymer.[73] The dithranol matrix used in the sample preparation also serves as a source of protons and facilitates ionization of the polymer sample. Assuming no fragmentation in the polymer chain has occurred by the ionization, MALDI-TOF spectrometry provides insight into the structure of the macromolecule.

Traces of polymers containing end groups associated to different methods of monomer activation can be observed in MALDI-TOF spectrometry. This is contrary to end group analysis from ^{1}H NMR spectrum where only the most prevalent method of activation of the monomer will be present in the spectrum. In the case of polymers generated by complexes **3a–c**, end groups associated with water activation were observed in the MALDI-TOF spectrum (**Figures 54–56**).This was determined by subtracting the predicted m/z of a polymer with n repeat units without any end groups from the m/z values observed in the MALDI-TOF spectra. This difference in mass represents the mass of both end groups and of the cation combined. The dithranol matrix used supplied certain cations (H^+, NH_4^+, Na^+, K^+) and so subtraction of the cation m/z led to the determination of end groups only possible by initiation of the polymerization by water. The multimodal distribution observed in these spectra is attributed to different cations associated with hydroxy end capped polymer chains, which include H^+, NH_4^+, Na^+, K^+. This was found by subtracting the predicted water end capped polymer m/z with n

repeat units from the observed spectra to determine which cation was associated with that modal distribution.

There was no evidence to suggest the ligand acted as the nucleophile in the ring opening polymerization. This would have become apparent by the end groups of the polymer chains having an m/z of 331.37, which is the molecular weight of the ligand. Ligand incorporation into the polymer has previously been observed with other zinc-based catalysts containing related neutral ligands. Owing to the lower nucleophilicity of ligand **2** compared to analogous non acylated guanidines, this type of initiation did not occur. Additionally, ethanol end groups were observed in the spectrum, suggesting esterification events during precipitation of the crude polymer from ethanol in the work-up procedures.

While polymers containing different end groups (OH and EtO) were present in the MALDI-TOF spectrum, the exact amounts of each type of polymer cannot be quantitatively determined. There was no evidence suggesting the formation of cyclic oligomers of PLA which has been observed in some initiators. The signal intensity in the MALDI-TOF spectrum is highly dependent on the end groups affinity to either a H^+ or

metal cation. As a result, estimating the fraction of polymer associated to each end group was not possible.[73]

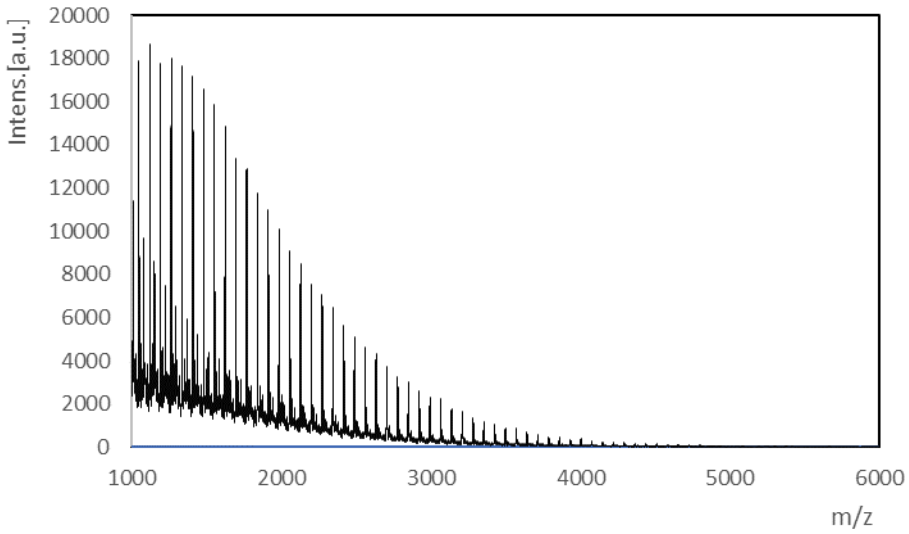

Figure 54. MALDI-TOF mass spectrum of PLA generated from **3a**.

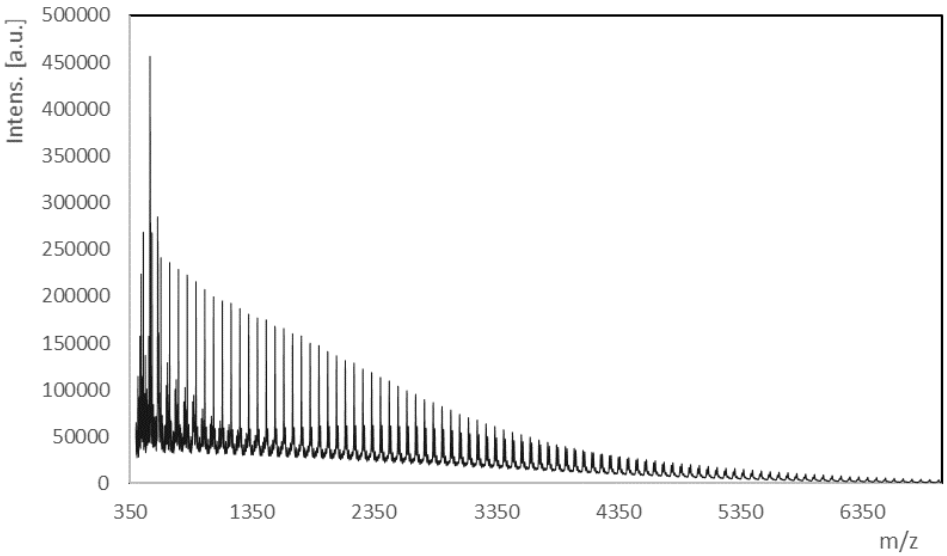

Figure 55. MALDI-TOF mass spectrum of PLA generated by **3b**.

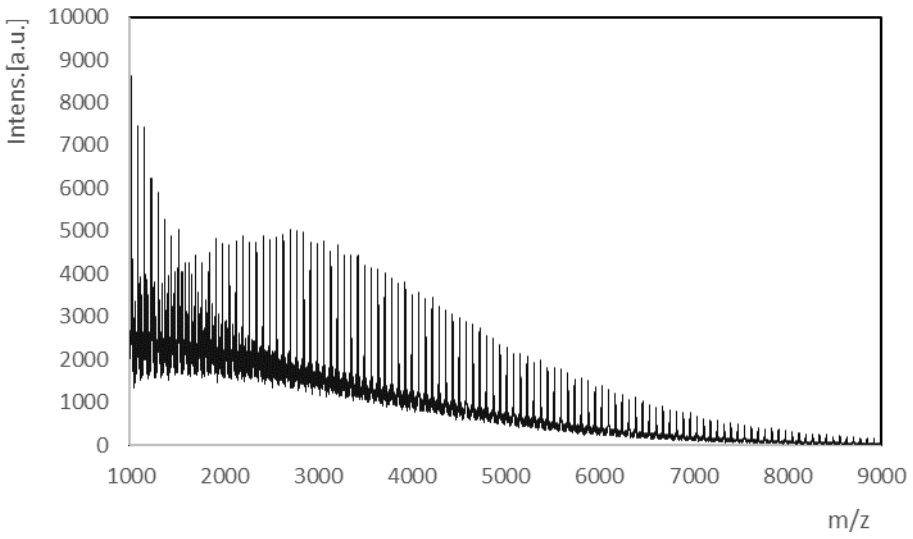

Figure 56. MALDI-TOF mass spectrum of PLA generated from **3c**.

MALDI-TOF mass spectrometry can be used to identify the presence of transesterification. In a ring opening polymerization of lactide devoid of transesterification, each catalytic turnover result in an increase in the polymer's molecular weight by 144 g/mol (the molar mass of lactide). The MALDI-TOF spectrum should therefore only contain polymers with m/z signal increments of 144. Transesterification causes cleavage of an ester linkage along the chain. Cleavages between monomer linkages will result in polymers with molecular weights of multiples of 144. If cleavage occurs between the ester linkage in the repeat unit, the molecular weight of the polymer will now be half the molecular weight of the monomer plus 144n (where n = number of repeat units). Transesterification results in polymers with molecular weights that are separated by 144n + 72 m/z compared to a polymer where transesterification did not occur whose molecular weight will be 144n. (**Figure 57**).

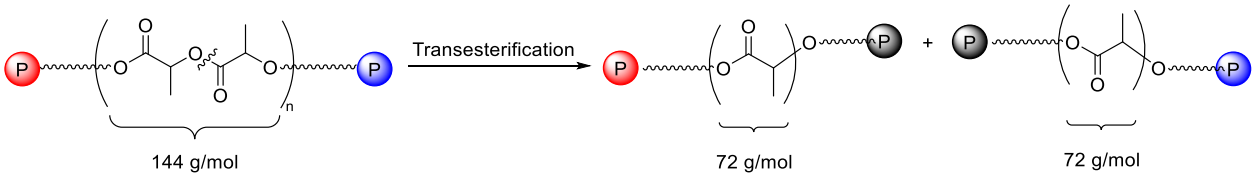

Figure 57. Transesterification of polylactide.

The MALDI-TOF mass spectrum showed polymers with peak separation of m/z 72, indicating the presence of transesterification however the low PDI observed from the GPC analysis suggests that the occurrence of this event was low .This can be attributed to a small amount of ionization polymer sample in MALDI-TOF resulting in fragmentation of the polymer chains. This occurrence shortens the overall polymer lengths observed and accounts for the discrepancy in number average molecular weights and would also lead to an inaccurate PDI. This fragmentation can be misattributed to transesterification, as both events would lead to polymer peaks separated by m/z 72 in the mass spectrum.

3.8.3 Tacticity

The tacticity of the polymers generated by **3c** were analyzed by ^{1}H NMR spectroscopy to gauge the stereoselectivity of the complex. The stereocontrolled ROP of *rac*-lactide can lead to different polymer microstructures. *rac*-Lactide consists of an equimolar mixture of *L*-LA and *D*-LA. The homopolymerization of either enantiopure *L*-LA or *D*-LA results in the generation of isotactic PLLA or PDLA, respectively. In the case of the generation of PLA from *rac*-lactide by a highly stereoselective catalyst, all *L*-LA will be polymerized, then all *D*-LA to generate the isotactic block copolymer PLLA-b-PDLA. Heterotactic PLA can be generated by alternating incorporation of *L*-LA and *D*-LA. In contrast, *meso*-lactide can generate either heterotactic or syndiotactic polymers. This depends on the orientation of the monomer relative to the growing end of the polymer

chain. For meso-lactide the stereogenic configurations is S and R. If monomers are consistently joined by an -*SR*-*SR*- linkage then the growing polymer will be syndiotactic. Alternatively if the two meso-lactide monomers are consistently joined by an -*SR*-*RS*- linkage then the resulting polymer will be heterotactic.

The simplest repeat unit used to describe the tacticity of PLA is defined as a tetrad, which represents two linked ring-opened lactide monomers. As lactide possesses two stereocenters, tetrads contain a total of four stereogenic centers. The relative arrangement of adjacent stereocenters can be described in two possible ways: *rac* or *meso*. When two adjacent stereocenters are of the opposite chirality, their relationship is defined as *rac* (*r*). Alternatively, if the two adjacent stereocenters have the same chirality, the relationship is described as *meso* (*m*). As every tetrad consists of four stereogenic centers, tetrads can be defined by a three letter arrangements that describes the microstructure of that small section in the polymer. For a tetrad consisting of two *L*-LA(SS) monomers, the relative configuration of the stereogenic centers would be -*SS*-*SS*- and the three-letter arrangement would be *mmm*. For a tetrad consisting of one *L*-LA (SS) and one D-LA (RR), the relative configuration of the stereogenic centers would be -*SS*-*RR*- and three-letter arrangement would be *mrm*. For a tetrad containing a *meso*-lactide, which can be present in *rac*-lactide or generated during the polymerization by epimerization, the microstructure becomes more complex. For a tetrad consisting of one *L*-LA (SS) and one *meso*-LA (SR), there are two possible arrangements of the stereocenters: -SS-SR- and -SS-RS-, which correspond to an *mmr* and an *mrr* tetrad, respectively. From the polymerization of *rac*-lactide, five possible tetrads can be generated (**Figure 58**).

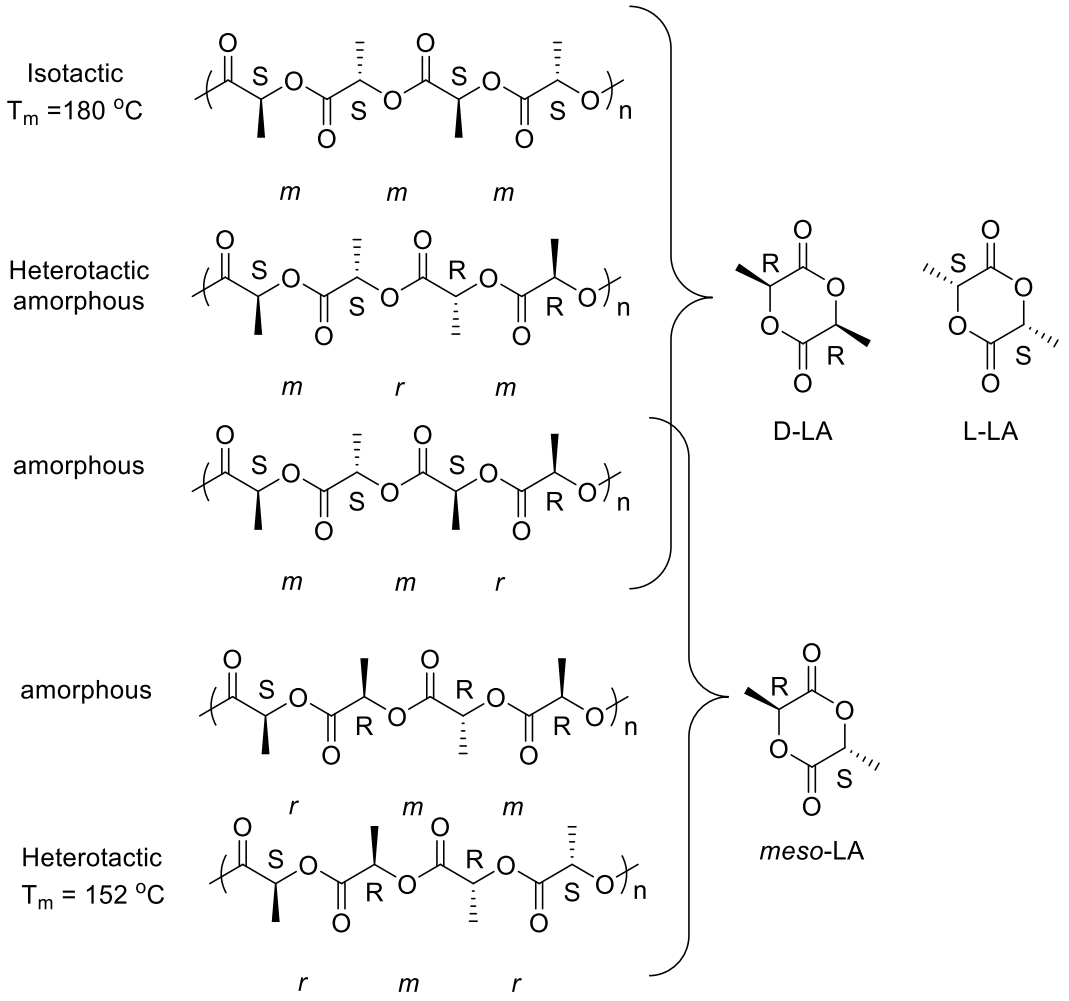

Figure 58. Select possible tetrads that exist from ROP of *rac*-lactide and *meso*-lactide .

Each specific tetrad results in unique mechanical properties of the resulting polymer. The melting temperature is significantly influenced by the microstructure of the polymer. Thus, a catalyst that imparts control over the microstructure is highly desirable.

Each tetrad can be distinguished from each other by performing a homodecoupled ^{1}H NMR experiment to remove the scalar coupling between the methyl and methine protons.[10] Saturation of the methyl signal of *rac*-PLA at δ = 1.50 ppm ($CDCl_3$) results in

singlets for the methine protons at δ = 5.17 ppm. Each singlet represents a methine from one of the unique possible tetrads: *mmm*, *mmr*, *mrm* and *rmr* (**Figure 59**) .

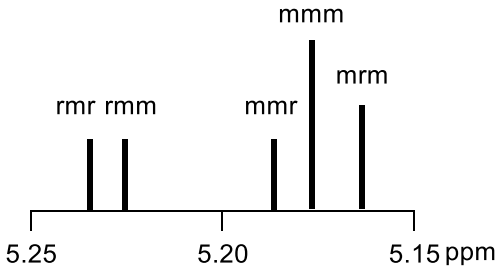

Figure 59. ^{1}H NMR spectrum (in $CDCl_3$) of the methine region of unique *rac*-PLA tetrads.[10]

The degree of stereoregularity in PLA can be described by either P_r or P_m, wherein $P_m = 1 - P_r$. These values represent the probability that two adjacent stereocenters are either *rac* or *meso*, respectively. For perfectly isotactic PLLA, where all tetrads are *mmm*, the P_m value is 1 and the P_r value is thus 0. For perfectly heterotactic PLA made from *rac*-LA, P_r is 1 and P_m is 0. Substitution of the relative integrations of the methine resonance attributed to a tetrad into Bernoullian-derived equations returns either a P_r or P_m value as described below (equation 9 and equation 10).[74]

$$P_m = 1 - 2\,I_1/(I_1 + I_2) \tag{9}$$

$$P_r = 2\,I_1/(I_1 + I_2) \tag{10}$$

wherein I_1 is the integration between 5.20 **–** 5.25 (in $CDCl_3$), for the *rmr*, *mmr* tetrads and I_2 is the integration between 5.13 **–** 5.20(in $CDCl_3$) for the *mmr mmm*, *mrm* tetrads.[74]

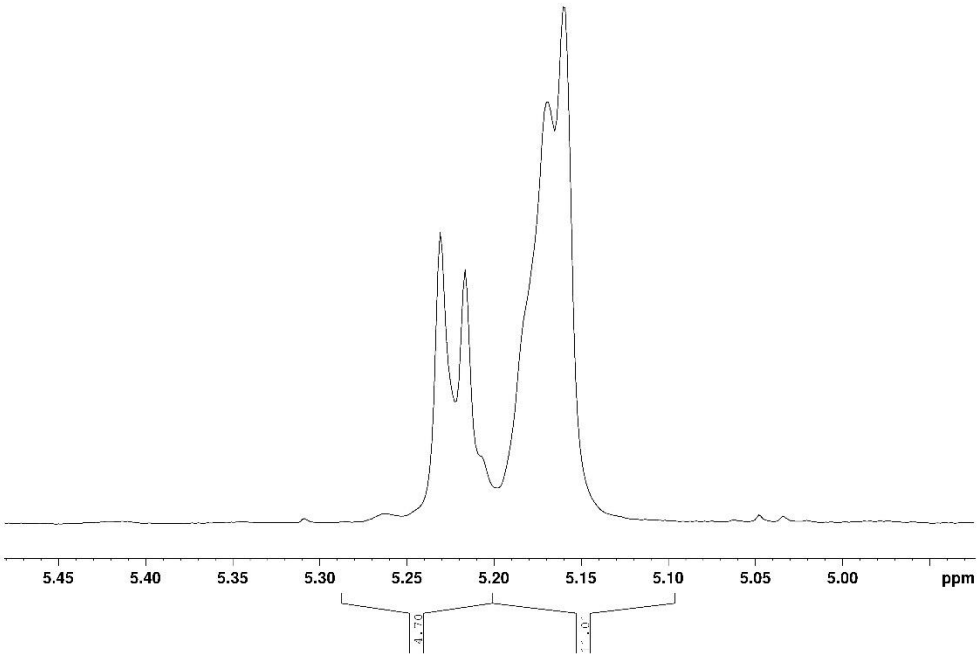

Figure 60. $^{1}H\{^{1}H\}$ NMR partial spectrum of the polymer generated from **3c**.

A $^{1}H\{^{1}H\}$ NMR experiment was performed on the polymer generated from **3c·THF** (**Figure 60**). The homodecoupled spectrum showed prominent methine signals from *rmr*, *rmm*, *mmm* and *mrm* tetrads. The P_r of the resulting polymer was calculated to determine if **3c** imparted any stereocontrol on the polymerization. Using equation 9 and 10 above and the I_1 and I_2 values from **Figure 60**, a P_r value of 0.60 was calculated. The value indicates that the PLA produced by **3c** was mostly atactic with a slight heterotactic bias. This result is similar to what is observed for many catalytic systems bearing neutral ligands that do not contain any stereogenic centers.

3.9 Thermostability Studies

Thermostability studies were performed on all three complexes **3** to gauge longevity in the harsh conditions required for lactide polymerization. The complexes were

dissolved in toluene-d_8 and heated to 130 °C in a J. Young tube and monitored by ^{1}H quantitative nuclear magnetic resonance (QNMR) spectroscopy over 96 h (**Figure A16A-F**). Complex **3a** and **3c** did not show any appreciable decomposition upon heating (<3% for both **3a** and **3c**). Heating of **3b** however produced two new unidentified species with doublets at 1.06 and 0.80 ppm. Assuming that these doublets represented the methyl protons from the decomposition products, 5% of **3b** decomposed after 5 h. This increased to approximately 7% and 10% over 22 h and 96 h, respectively (**Figure 61)**.

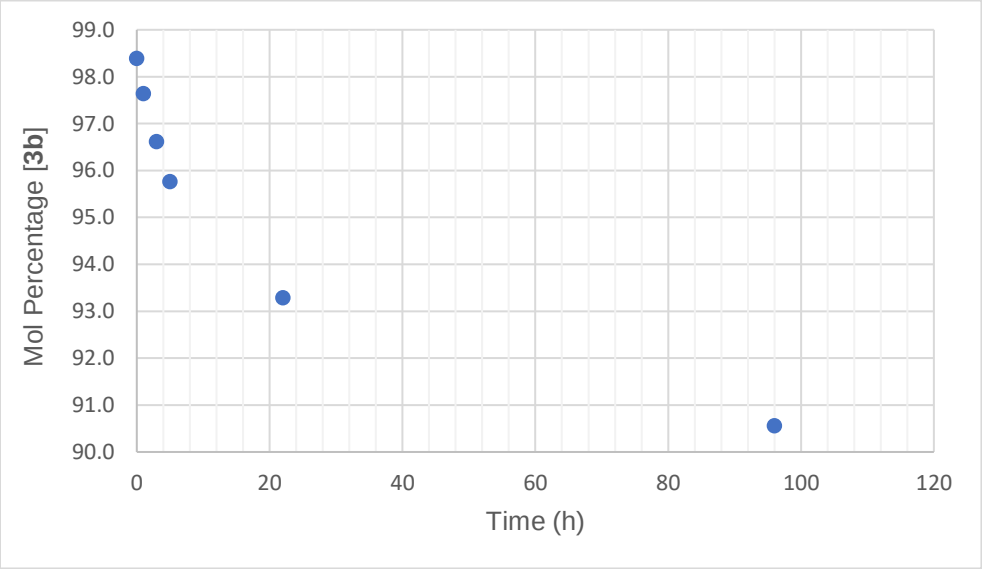

Figure 61. Mole percentage as a function of time of **3b** in a toluene solution held at 110 °C.

Calculation of the half-life of the complex was not possible as the rate of decomposition did not fit a first- or second-order rate law. The timescale of decomposition however is much longer than that for lactide polymerization (24 h). The decomposition slows down after 22 h and begins to plateau near 96 h. This may be attributed to an impurity in the catalyst that mediates the decomposition, possibly stoichiometrically. As

all the impurity is fully consumed within 96 h, the decomposition of **3b** slows down. The decomposition may be mitigated by the stabilizing effects of the lactide monomer or even polar impurities during the bulk polymerization.

Lactide polymerization, when performed “neat” (in the absence of any solvent), requires thermostability of the catalyst at 130 °C for 24 h. This decomposition product does not impact the polymerization mechanism as the MALDI-TOF of polymer generated by complex **3b** did not show any polymers being generated by initiators other than water. The low generation of high molecular weight polymers by **3b** implies that the decomposition product may be behaving as a chain transfer reagent, lowering the catalytic activity or turnover rate (k_p) of the catalyst **3b**.

4 Conclusions

Three new neutral bidentate NHI ligands bearing different second donor fragments were prepared. All three ligands were synthesized from a strongly electron-withdrawing acylated NHC scaffold. This represents the Lavoie group's first endeavour in developing a library of neutral bidentate NHI ligands for the ring opening polymerization of lactide. Variable temperature NMR spectroscopy was performed on all ligands to better understand the nature of the C=N bond in NHI ligands decorated with strongly electron withdrawing acyl groups. It was determined that the second donor fragment played a role in the bond rotational energy about the C=N bond, increasing proportionally with steric bulk of the organic fragment (**2a** > **2b** ≈ **2c**).

Computational studies were performed on the ligands and complexes to gain a better understanding of the bond order and electronic features of the ligand. The WBI and bond lengths shows that the acyl groups of the backbone exert a withdrawing effect equal to that of the withdrawing effect of the exocyclic nitrogen on the endocyclic nitrogen lone pair. Upon complexation to zinc, the withdrawing effect of the zinc metal center and exocyclic nitrogen outcompetes the acyl groups withdrawing effect resulting in a shift of electron density towards the Lewis acidic metal centre.

A single crystal of **3a** was analyzed by XRD. The solid-state structure shows a prominent kink between the plane of the azole ring and the metallocycle. This is attributed to pyramidalization of the exocyclic nitrogen atom due to incomplete hybridization to sp^2 because of electron delocalization from the endocyclic nitrogen. The crystal structure showed a ρ value of 0.92 indicating less electron density delocalization across the azole ring compared to unity where ρ would equal 1. The τ_4 value was determined to be 0.87

indicating a deviation of from the perfectly tetrahedral geometry (where τ_4 =1) due to the bite angle of the bidentate ligand.

The catalysts were generated from coordination to group 12 (Zn) and their thermal stability tested to determine suitability as initiators in the harsh conditions of bulk polymerization of lactide (neat, 135 °C). Complexes **3a** and **3c** showed to be thermally stable in toluene-d_8 at 110 °C for 96 h (decomposition less than 3%). Complex **3b** showed a decomposition of 10% after the same time period.

All complexes **3a–c** were tested as initiators for the ROP of LA to PLA. Catalyst **3c** showed competitive rates of polymerization with the industry catalyst ($Sn(Oct)_2$) under the same reaction conditions. The rate constant of propagation for **3c** was determined to be 26.2 $M^{-1}h^{-1}$. The polymer generated had an M_n = 4700 (by ^1H NMR spectroscopy end group analysis) and PDI was determined by GPC to be 1.10 indicating a well-controlled polymerization. Analysis by MALDI-TOF mass spectrometry of the polymer generated by **3c** showed OH end groups with varying counterions (Na^+, K^+, Li^+), indicating that the polymerization proceeds through an activated monomer activation by adventitious water. The polymer was determined to be atactic with a slight heterotactic bias (P_r of 0.6) by homodecoupled ^1H NMR spectroscopy experiments.

This class of highly modular ligand scaffolds allows for iterative testing to structure-activity relationship. With the modulation in the second donor fragment explored here, future work should expand on how the steric bulk of the alkyl groups on the endocyclic nitrogens play a role in catalytic performance. This will lead to a library of group 12 catalyst bearing neutral bidentate ligands for the effective ring opening polymerization of lactide to generate biodegradable PLA plastics.

5 References

(1) Schäfer, P. M.; Fuchs, M.; Ohligschläger, A.; Rittinghaus, R.; McKeown, P.; Akin, E.; Schmidt, M.; Hoffmann, A.; Liauw, M. A.; Jones, M. D.; Herres-Pawlis, S. Highly Active N,O Zinc Guanidine Catalysts for the Ring-Opening Polymerization of Lactide. *ChemSusChem* **2017**, *10* (18), 3547–3556. https://doi.org/10.1002/cssc.201701237.

(2) Kaminsky, W. Trends in Polyolefin Chemistry. *Macromol. Chem. Phys*. **2008**, *209* (5), 459–466. https://doi.org/10.1002/macp.200700575.

(3) Scott, G. *J. Polym. Environ*. **1999**. https://doi.org/10.1039/9781847551726.

(4) Geyer, R.; Jambeck, J. R.; Law, K. L. Production, Use, and Fate of All Plastics Ever Made. *Sci. Adv.* **2017**. *347*, 768-771. https://doi.org/10.1126/sciadv.1700782.

(5) Thompson, R. C.; Moore, C. J.; vom Saal, F. S.; Swan, S. H. Plastics, the Environment and Human Health: Current Consensus and Future Trends. *Philos Trans R Soc Lond B Biol Sci* **2009**, *364* (1526), 2153–2166. https://doi.org/10.1098/rstb.2009.0053.

(6) Inkinen, S.; Hakkarainen, M.; Albertsson, A.-C.; Södergård, A. From Lactic Acid to Poly(Lactic Acid) (PLA): Characterization and Analysis of PLA and Its Precursors. *Biomacromolecules* **2011**, *12* (3), 523–532. https://doi.org/10.1021/bm101302t.

(7) Zhu, Y.; Romain, C.; Williams, C. K. Sustainable Polymers from Renewable Resources. *Nature* **2016**, *540* (7633), 354–362. https://doi.org/10.1038/nature21001.

(8) dos Santos Vieira, I.; Herres-Pawlis, S. Lactide Polymerisation with Complexes of Neutral N-Donors - New Strategies for Robust Catalysts. *Eur. J. Inorg. Chem.* **2012**, *2012* (5), 765–774. https://doi.org/10.1002/ejic.201101131.

(9) Othman, N.; Jazrawi, B.; Mehrkhodavandi, P.; Hatzikiriakos, S. Rheology and Melt Fracture of Poly(Lactides). *Annual Technical Conference - ANTEC, Conference Proceedings* **2012**, *2*, 1170–1174.

(10) Stanford, M. J.; Dove, A. P. Stereocontrolled Ring-Opening Polymerisation of Lactide. *Chem. Soc. Rev.* **2010**, *39* (2), 486–494. https://doi.org/10.1039/B815104K.

(11) *Ligand Design in Metal Chemistry: Reactivity and Catalysis*; Stradiotto, M., Lundgren, R., Eds.; John Wiley & Sons: Chichester, West Sussex, UK, **2016**.

(12) Middleton, J. C.; Tipton, A. J. Synthetic Biodegradable Polymers as Orthopedic Devices. *Biomaterials* **2000**, *21* (23), 2335–2346. https://doi.org/10.1016/S0142-9612(00)00101-0.

(13) Gupta, A. P.; Kumar, V. New Emerging Trends in Synthetic Biodegradable Polymers – Polylactide: A Critique. *Eur. Polym. J.* **2007**, *43* (10), 4053–4074. https://doi.org/10.1016/j.eurpolymj.2007.06.045.

(14) Singh, R. Poly (Lactic Acid) as Degradable Resorbable Polymer Matrices in Biomedical Engineering: An Overview. *Int. J. Eng. Res. Adv. Tech.* **2018**, *4* (5), 56.

(15) Platel, R.; Hodgson, L.; Williams, C. Biocompatible Initiators for Lactide Polymerization. *Polymer Revs.* **2008**, *48* (1), 11–63. https://doi.org/10.1080/15583720701834166.

(16) Masutani, K.; Kimura, Y. *Chapter 1 PLA Synthesis. From the Monomer to the Polymer*. **2014**, 1–36. https://doi.org/10.1039/9781782624806-00001.

(17) Bero, M.; Dobrzyński, P.; Kasperczyk, J. Synthesis of Disyndiotactic Polylactide. *Journal of Polymer Science Part A: Poly. Chem.* **1999**, *37* (22), 4038–4042. https://doi.org/10.1002/(SICI)1099-0518(19991115)37:22<4038::AID-POLA2>3.0.CO;2-F.

(18) Kricheldorf, H. R.; Kreiser-Saunders, I. Polylactones, 19. Anionic Polymerization of L-Lactide in Solution. *Makromol. Chem.* **1990**, *191* (5), 1057–1066. https://doi.org/10.1002/macp.1990.021910508.

(19) Kricheldorf, H. R. Syntheses and Application of Polylactides. *Chemosphere* **2001**, *43* (1), 49–54. https://doi.org/10.1016/S0045-6535(00)00323-4.
(20) Kricheldorf, H. R.; Berl, M.; Scharnagl, N. Poly(Lactones). 9. Polymerization Mechanism of Metal Alkoxide Initiated Polymerizations of Lactide and Various Lactones. *Macromolecules* **1988**, *21* (2), 286–293. https://doi.org/10.1021/ma00180a002.
(21) M. S.; Södergård†, A. Use of Monocarboxylic Iron Derivatives in the Ring-Opening Polymerization of l-Lactide. *Macromolecules*. **1999**, *32* (20), 6412-6417 https://doi.org/10.1021/ma9902753.
(22) Dechy-Cabaret, O.; Martin-Vaca, B.; Bourissou, D. Controlled Ring-Opening Polymerization of Lactide and Glycolide. *Chem. Rev.* **2004**, *104* (12), 6147–6176. https://doi.org/10.1021/cr040002s.
(23) Connor, E. F.; Nyce, G. W.; Myers, M.; Möck, A.; Hedrick, J. L. First Example of N-Heterocyclic Carbenes as Catalysts for Living Polymerization: Organocatalytic Ring-Opening Polymerization of Cyclic Esters. *J. Am. Chem. Soc.* **2002**, *124* (6), 914–915. https://doi.org/10.1021/ja0173324.
(24) Ajellal, N.; Carpentier, J.-F.; Guillaume, C.; Guillaume, S. M.; Helou, M.; Poirier, V.; Sarazin, Y.; Trifonov, A. Metal-Catalyzed Immortal Ring-Opening Polymerization of Lactones, Lactides and Cyclic Carbonates. *Dalton Trans.* **2010**, *39* (36), 8363–8376. https://doi.org/10.1039/C001226B.
(25) Witzke, D. R.; Narayan, R.; Kolstad, J. J. Reversible Kinetics and Thermodynamics of the Homopolymerization of L-Lactide with 2-Ethylhexanoic Acid Tin(II) Salt. *Macromolecules.* **1997**, *30* (23), 7075–7085. https://doi.org/10.1021/ma970631m.
(26) Penczek, S.; Duda, A.; Kowalski, A.; Libiszowski, J.; Majerska, K.; Biela, T. On the Mechanism of Polymerization of Cyclic Esters Induced by Tin(II) Octoate. *Macromol. Symp.* **2000**, *157* (1), 61–70. https://doi.org/10.1002/1521-3900(200007)157:1<61::AID-MASY61>3.0.CO;2-6.
(27) Nijenhuis, A. J.; Grijpma, D. W.; Pennings, A. J. Lewis Acid Catalyzed Polymerization of L-Lactide. Kinetics and Mechanism of the Bulk Polymerization. *Macromolecules.* **1992**, *25* (24), 6419–6424. https://doi.org/10.1021/ma00050a006.
(28) Penczek, S.; Szymanski, R.; Duda, A.; Baran, J. Living Polymerization of Cyclic Esters – a Route to (Bio)Degradable Polymers. Influence of Chain Transfer to Polymer on Livingness. *Macromol. Symp.* **2003**, *201* (1), 261–270. https://doi.org/10.1002/masy.200351129.
(29) CFR - Code of Federal Regulations Title 21 https://www.accessdata.fda.gov/scripts/cdrh/cfdocs/cfcfr/CFRSearch.cfm?fr=175.300&SearchTerm=fumaric%20acid (accessed 2022 -05 -03).
(30) Rittinghaus, R. D.; Schäfer, P. M.; Albrecht, P.; Conrads, C.; Hoffmann, A.; Ksiazkiewicz, A. N.; Bienemann, O.; Pich, A.; Herres-Pawlis, S. New Kids in Lactide Polymerization: Highly Active and Robust Iron Guanidine Complexes as Superior Catalysts. *ChemSusChem* **2019**, *12* (10), 2161–2165. https://doi.org/10.1002/cssc.201900481.
(31) Chamberlain, B. M.; Cheng, M.; Moore, D. R.; Ovitt, T. M.; Lobkovsky, E. B.; Coates, G. W. Polymerization of Lactide with Zinc and Magnesium β-Diiminate Complexes: Stereocontrol and Mechanism. *J. Am. Chem. Soc.* **2001**, *123* (14), 3229–3238. https://doi.org/10.1021/ja003851f.
(32) Williams, C. K.; Brooks, N. R.; Hillmyer, M. A.; Tolman, W. B. Metalloenzyme Inspired Dizinc Catalyst for the Polymerization of Lactide. *Chem. Commun.* **2002**, *18*, 2132–2133. https://doi.org/10.1039/B206437E.
(33) Chen, H.-Y.; Tang, H.-Y.; Lin, C.-C. Ring-Opening Polymerization of Lactides Initiated by Zinc Alkoxides Derived from NNO-Tridentate Ligands. *Macromolecules* **2006**, *39* (11), 3745–3752. https://doi.org/10.1021/ma060471r.
(34) Wheaton, C. A.; Hayes, P. G. Cationic Zinc Complexes: A New Class of Catalyst for Living Lactide Polymerization at Ambient Temperature. *Chem. Commun.* **2010**, *46* (44), 8404–8406. https://doi.org/10.1039/C0CC03463K.

(35) Jensen, T. R.; Schaller, C. P.; Hillmyer, M. A.; Tolman, W. B. Zinc N-Heterocyclic Carbene Complexes and Their Polymerization of d,l-Lactide. *J. Organomet. Chem*. **2005**, *690* (24), 5881–5891. https://doi.org/10.1016/j.jorganchem.2005.07.070.
(36) Börner, J.; Flörke, U.; Huber, K.; Döring, A.; Kuckling, D.; Herres-Pawlis, S. Lactide Polymerisation with Air-Stable and Highly Active Zinc Complexes with Guanidine-Pyridine Hybrid Ligands. *Chem. Eur. J.* **2009**, *15* (10), 2362–2376. https://doi.org/10.1002/chem.200802128.
(37) Börner, J.; dos Santos Vieira, I.; Pawlis, A.; Döring, A.; Kuckling, D.; Herres-Pawlis, S. Mechanism of the Living Lactide Polymerization Mediated by Robust Zinc Guanidine Complexes. *Chem. Eur. J.* **2011**, *17* (16), 4507–4512. https://doi.org/10.1002/chem.201002690.
(38) Doddi, A.; Peters, M.; Tamm, M. N-Heterocyclic Carbene Adducts of Main Group Elements and Their Use as Ligands in Transition Metal Chemistry. *Chem. Rev.* **2019**, *119* (12), 6994–7112. https://doi.org/10.1021/acs.chemrev.8b00791.
(39) Tamm, M.; Petrovic, D.; Randoll, S.; Beer, S.; Bannenberg, T.; Jones, P. G.; Grunenberg, J. Structural and Theoretical Investigation of 2-Iminoimidazolines Carbene Analogues of Iminophosphoranes. *Org. Biomol. Chem.* **2007**, *5* (3), 523. https://doi.org/10.1039/b615418b.
(40) Stearns, J. F.; Rapoport, H. Reduction of Acylguanidines to Alkylguanidines with Lithium Aluminum Hydride. *J. Org. Chem.* **1977**, *42* (22), 3608–3614. https://doi.org/10.1021/jo00442a036.
(41) Kuhn, N.; Fawzi, R.; Steimann, M.; Wiethoff, J.; Bläser, D.; Boese, R. Synthese Und Struktur von 2-Imino-1,3-Dimethylimidazolin / Synthesis and Structure of 2-Imino-1,3-Dimethylimidazoline. *Z. Naturforsch. B.* **2014**. *50*, 1779-1784.
(42) Tamm, M.; Randoll, S.; Bannenberg, T.; Herdtweck, E. Titanium Complexes with Imidazolin-2-Iminato Ligands. *Chem. Commun.* **2004**, *7*, 876. https://doi.org/10.1039/b401041h.
(43) Li, M.; Cai, Z.; Eisen, M. S. Neutral Nickel(II) Complexes Bearing Aryloxide Imidazolin-2-Imine Ligands for Efficient Copolymerization of Norbornene and Polar Monomers. *Organometallics* **2018**, *37* (24), 4753–4762. https://doi.org/10.1021/acs.organomet.8b00752.
(44) Tamm, M.; Randoll, S.; Herdtweck, E.; Kleigrewe, N.; Kehr, G.; Erker, G.; Rieger, B. Imidazolin-2-Iminato Titanium Complexes: Synthesis, Structure and Use in Ethylenepolymerization Catalysis. *Dalton Trans.* **2006**, *3*, 459–467. https://doi.org/10.1039/B511752F.
(45) Trambitas, A. G.; Panda, T. K.; Jenter, J.; Roesky, P. W.; Daniliuc, C.; Hrib, C. G.; Jones, P. G.; Tamm, M. Rare-Earth Metal Alkyl, Amido, and Cyclopentadienyl Complexes Supported by Imidazolin-2-Iminato Ligands: Synthesis, Structural Characterization, and Catalytic Application. *Inorg. Chem.* **2010**, *49* (5), 2435–2446. https://doi.org/10.1021/ic9024052.
(46) Nomura, K.; Bahuleyan, B. K.; Zhang, S.; Veeresha Sharma, P. M.; Katao, S.; Igarashi, A.; Inagaki, A.; Tamm, M. Synthesis and Structural Analysis of (Imido)Vanadium(V) Dichloride Complexes Containing Imidazolin-2-Iminato- and Imidazolidin-2-Iminato Ligands, and Their Use as Catalyst Precursors for Ethylene (Co)Polymerization. *Inorg. Chem.* **2014**, *53* (1), 607–623. https://doi.org/10.1021/ic402747d.
(47) Yi, J.; Yang, W.; Sun, W.-H.; Nomura, K.; Hada, M. Vanadium NMR Chemical Shifts of (Imido)Vanadium(V) Dichloride Complexes with Imidazolin-2-Iminato and Imidazolidin-2-Iminato Ligands: Cooperation with Quantum-Chemical Calculations and Multiple Linear Regression Analyses. *J. Phys. Chem. A* **2017**, *121* (47), 9099–9105. https://doi.org/10.1021/acs.jpca.7b08328.
(48) Tskhovrebov, A. G.; Solari, E.; Scopelliti, R.; Severin, K. Insertion of Zerovalent Nickel into the N–N Bond of N-Heterocyclic-Carbene-Activated N2O. *Inorg. Chem.* **2013**, *52* (20), 11688–11690. https://doi.org/10.1021/ic401524w.
(49) Larocque, T. G.; Dastgir, S.; Lavoie, G. G. Coordination and Reactivity Study of Titanium and Zirconium Complexes of the First Imidazol-2-Imine Ethenolate Ligand. *Organometallics* **2013**, *32* (15), 4314–4320. https://doi.org/10.1021/om4004708.

(50) Back, O.; Henry-Ellinger, M.; Martin, C. D.; Martin, D.; Bertrand, G. 31P NMR Chemical Shifts of Carbene–Phosphinidene Adducts as an Indicator of the π-Accepting Properties of Carbenes. *Angew. Chem., Int. Ed*. **2013**, *52* (10), 2939–2943. https://doi.org/10.1002/anie.201209109.
(51) Zhao, F.; Wang, Y.; Zhang, W.-X.; Xi, Z. Metal-Free Synthesis of Cyclic Di-Oxoguanidines via One-Pot Sequential Transformation of Amines, Carbodiimides and Acyl Dichlorides. *Org. Biomol. Chem.* **2012**, *10* (31), 6266. https://doi.org/10.1039/c2ob25799h.
(52) Dolomanov, O. V.; Blake, A. J.; Champness, N. R.; Schröder, M. OLEX: New Software for Visualization and Analysis of Extended Crystal Structures. *J Appl. Cryst.* **2003**, *36* (5), 1283–1284. https://doi.org/10.1107/S0021889803015267.
(53) Sheldrick, G. M. A Short History of SHELX. *Acta. Crystallogr. A.* **2008**, *64* , 112–122. https://doi.org/10.1107/S0108767307043930.
(54) Nakanishi, W.; Ishikawa, T.; Margetic, D. Approaches to the Potential Chirality of Bisguanidinobenzenes by Dynamic NMR Analysis. *BCSJ* **2007**, *80* (6), 1187–1193. https://doi.org/10.1246/bcsj.80.1187.
(55) Kessler, H. Thermal Isomerization about Double Bonds: Rotation and Inversion. *Tetrahedron* **1974**, *30* (13), 1861–1870. https://doi.org/10.1016/S0040-4020(01)97319-3.
(56) Gamov, G. A.; Aleksandriiskii, V. V.; Sharnin, V. A. Inhibited Rotation of Amide Group around C N Bond of Nicotinamide in Different Solvents by 1 H NMR Data. *J. Mol. Liq*. **2017**, *231*, 238–241. https://doi.org/10.1016/j.molliq.2017.01.078.
(57) Rittinghaus, R. D.; Schäfer, P. M.; Albrecht, P.; Conrads, C.; Hoffmann, A.; Ksiazkiewicz, A. N.; Bienemann, O.; Pich, A.; Herres-Pawlis, S. New Kids in Lactide Polymerization: Highly Active and Robust Iron Guanidine Complexes as Superior Catalysts. *ChemSusChem* **2019**, *12* (10), 2161–2165. https://doi.org/10.1002/cssc.201900481.
(58) Arduengo, A. J.; Harlow, R. L.; Kline, M. A Stable Crystalline Carbene. *J. Am. Chem. Soc.* **1991**, *113* (1), 361–363. https://doi.org/10.1021/ja00001a054.
(59) Laidig, K. E.; Cameron, L. M. What Happens to Formamide during C—N Bond Rotation? Atomic and Molecular Energetics and Molecular Reactivity as a Function of Internal Rotation. *Can. J. Chem.* **1993**, *71* (6), 872–879. https://doi.org/10.1139/v93-116.
(60) Yang, L.; Powell, D. R.; Houser, R. P. Structural Variation in Copper(I) Complexes with Pyridylmethylamide Ligands: Structural Analysis with a New Four-Coordinate Geometry Index, T4. *Dalton Trans.* **2007**, *9*, 955–964. https://doi.org/10.1039/B617136B.
(61) Weigend, F.; Ahlrichs, R. Balanced Basis Sets of Split Valence, Triple Zeta Valence and Quadruple Zeta Valence Quality for H to Rn: Design and Assessment of Accuracy. *Phys. Chem. Chem. Phys.* **2005**, *7* (18), 3297–3305. https://doi.org/10.1039/B508541A.
(62) Zhao, Y.; Truhlar, D. G. The M06 Suite of Density Functionals for Main Group Thermochemistry, Thermochemical Kinetics, Noncovalent Interactions, Excited States, and Transition Elements: Two New Functionals and Systematic Testing of Four M06-Class Functionals and 12 Other Functionals. *Theor Chem Account* **2008**, *120* (1), 215–241. https://doi.org/10.1007/s00214-007-0310-x.
(63) Relativistic Pseudopotentials: Their Development and Scope of Applications | *Chem. Rev*. Chem. Rev. **2012**, *112*, 403–480. https://pubs.acs.org/doi/abs/10.1021/cr2001383.
(64) Halgren, T. A. Merck Molecular Force Field. I. Basis, Form, Scope, Parameterization, and Performance of MMFF94. *J. Comput. Chem.* **1996**, *17* (5–6), 490–519. https://doi.org/10.1002/(SICI)1096-987X(199604)17:5/6<490::AID-JCC1>3.0.CO;2-P.
(65) Allen, F. H.; Kennard, O.; Watson, D. G.; Brammer, L.; Orpen, A. G.; Taylor, R. Tables of Bond Lengths Determined by X-Ray and Neutron Diffraction. Part 1. Bond Lengths in Organic Compounds. *J. Chem. Soc., Perkin Trans.* **1987**, *12*, S1–S19. https://doi.org/10.1039/P298700000S1.

(66) Martin, F.; Zipse, H. Charge Distribution in the Water Molecule?A Comparison of Methods. *J. Comput. Chem.* **2005**, *26* (1), 97–105. https://doi.org/10.1002/jcc.20157.
(67) Glendening, E. D.; Landis, C. R.; Weinhold, F. NBO 6.0: Natural Bond Orbital Analysis Program. *J. Comput. Chem.* **2013**, *34* (16), 1429–1437. https://doi.org/10.1002/jcc.23266.
(68) Nikolova, V.; Cheshmedzhieva, D.; Ilieva, S.; Galabov, B. Atomic Charges in Describing Properties of Aromatic Molecules. *J. Org. Chem.* **2019**, *84* (4), 1908–1915. https://doi.org/10.1021/acs.joc.8b02908.
(69) Fuentealba, P.; Preuss, H.; Stoll, H.; Von Szentpály, L. A Proper Account of Core-Polarization with Pseudopotentials: Single Valence-Electron Alkali Compounds. *Chem. Phys. Lett.* **1982**, *89* (5), 418–422. https://doi.org/10.1016/0009-2614(82)80012-2.
(70) Rakhi, R.; Suresh, C. H. A DFT Study on Dihydropyrazine Annulated Linear Polyacenes: Aromaticity, Stability and HOMO–LUMO Energy Modulation. *Phys. Chem. Chem. Phys.* **2016**, *18* (35), 24631–24641. https://doi.org/10.1039/C6CP03723B.
(71) Metz, A.; Heck, J.; Gohlke, C. M.; Kröckert, K.; Louven, Y.; McKeown, P.; Hoffmann, A.; Jones, M. D.; Herres-Pawlis, S. Reactivity of Zinc Halide Complexes Containing Camphor-Derived Guanidine Ligands with Technical Rac-Lactide. *Inorganics* **2017**, *5* (4), 85. https://doi.org/10.3390/inorganics5040085.
(72) Mandal, M.; List, M.; Teasdale, I.; Redhammer, G.; Chakraborty, D.; Monkowius, U. Palladium Complexes Containing Imino Phenoxide Ligands: Synthesis, Luminescence, and Their Use as Catalysts for the Ring-Opening Polymerization of Rac-Lactide. *Monatsh Chem* **2018**, *149* (4), 783–790. https://doi.org/10.1007/s00706-017-2119-1.
(73) Florczak, M.; Michalski, A.; Kacprzak, A.; Brzeziński, M.; Biedroń, T.; Pająk, A.; Kubisa, P.; Biela, T. MALDI-TOF Analysis of Lactide Oligomers with Functional End Groups. *React. Funct. Polym*. **2016**, *104*, 71–77. https://doi.org/10.1016/j.reactfunctpolym.2016.05.010.
(74) Fortun, S.; Daneshmand, P.; Schaper, F. Isotactic Rac-Lactide Polymerization with Copper Complexes: The Influence of Complex Nuclearity. *Angew. Chem., Int. Ed. Engl*. **2015**, *54* (46), 13669–13672. https://doi.org/10.1002/anie.201505674.

6 Appendix

Crystal data and structure refinement for 3a

Compound	3a
Empirical formula	$C_{88}H_{112}Cl_8N_{16}O_{12}Zn_4$
Formula weight	2131.01
Temperature/K	173.0
Crystal system	monoclinic
Space group	$P2_1/c$
a/Å	10.013(3)
b/Å	18.759(5)
c/Å	13.922(4)
α/°	90
β/°	105.730(8)
γ/°	90
Volume/Å^3	2516.9(12)
Z	1
ρ_{calc}g/cm^3	1.406
μ/mm^{-1}	1.218
F(000)	1104.0
Crystal size/mm^3	0.4 × 0.3 × 0.3
Radiation	MoKα (λ = 0.71076)
2Θ range for data collection/°	4.986 to 52.744
Index ranges	-12 ≤ h ≤ 12, -23 ≤ k ≤ 23, -17 ≤ l ≤ 17
Reflections collected	61946
Independent reflections	5154 [R_{int} = 0.1482, R_{sigma} = 0.0463]
Data/restraints/parameters	5154/0/293
Goodness-of-fit on F^2	1.042
Final R indexes [I>=2σ (I)]	R_1 = 0.0675, wR_2 = 0.1835
Final R indexes [all data]	R_1 = 0.0839, wR_2 = 0.2028
Largest diff. peak/hole / e Å^{-3}	1.20/-0.94

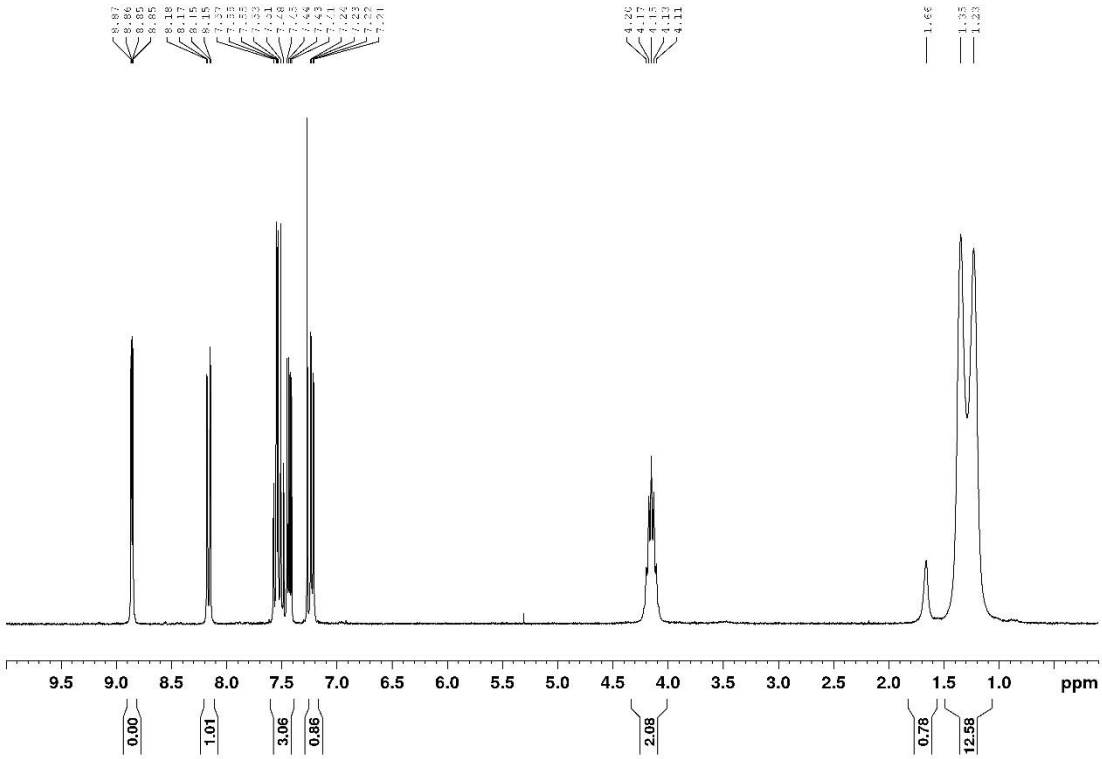

Figure A1: ^{1}H NMR spectrum of **2a** (300 MHz in $CDCl_3$). Signal at δ = 1.66 ppm is H_2O solvent impurity.

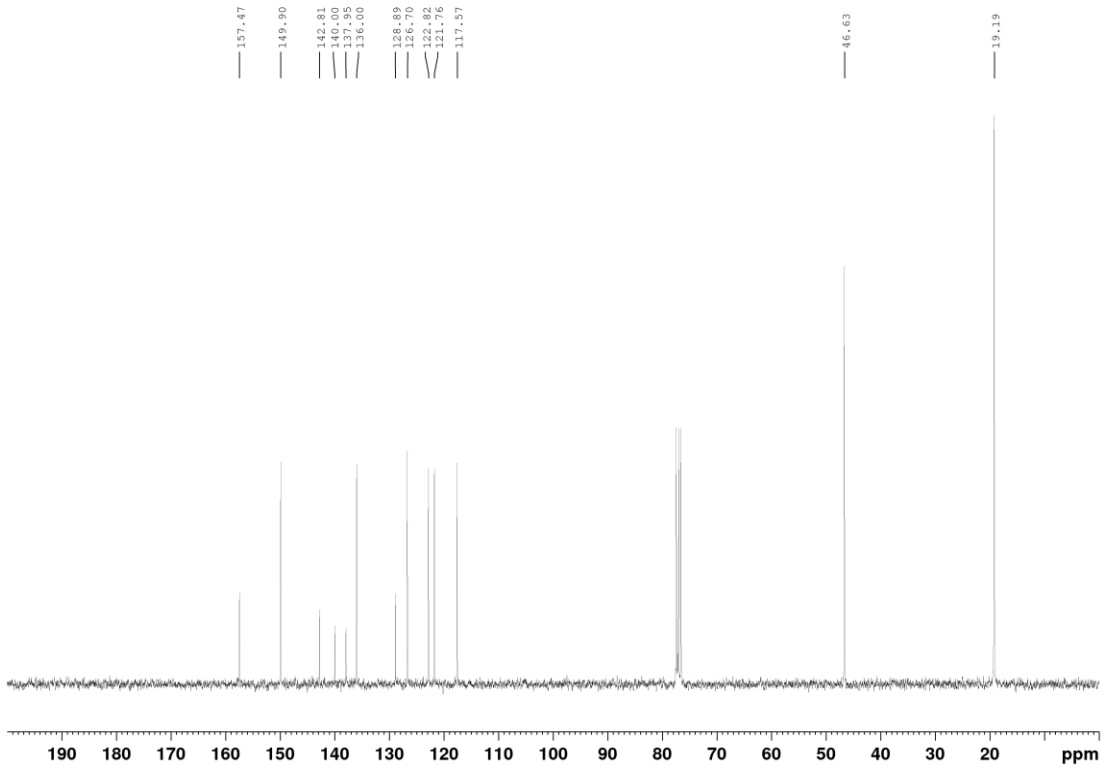

Figure A2: $^{13}C\{^{1}H\}$ NMR spectrum of **2a** (75 MHz in $CDCl_3$).

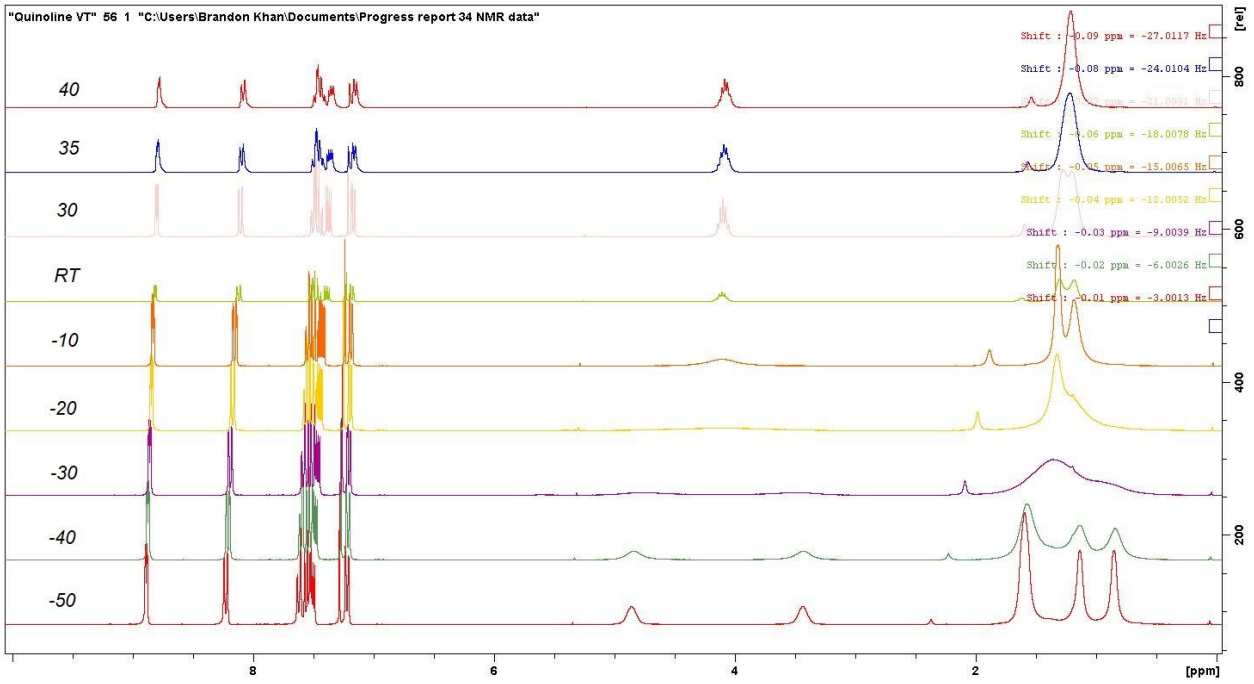

Figure A3: ^{1}H VT-NMR spectrum of **2a** (300 MHz in $CDCl_3$).

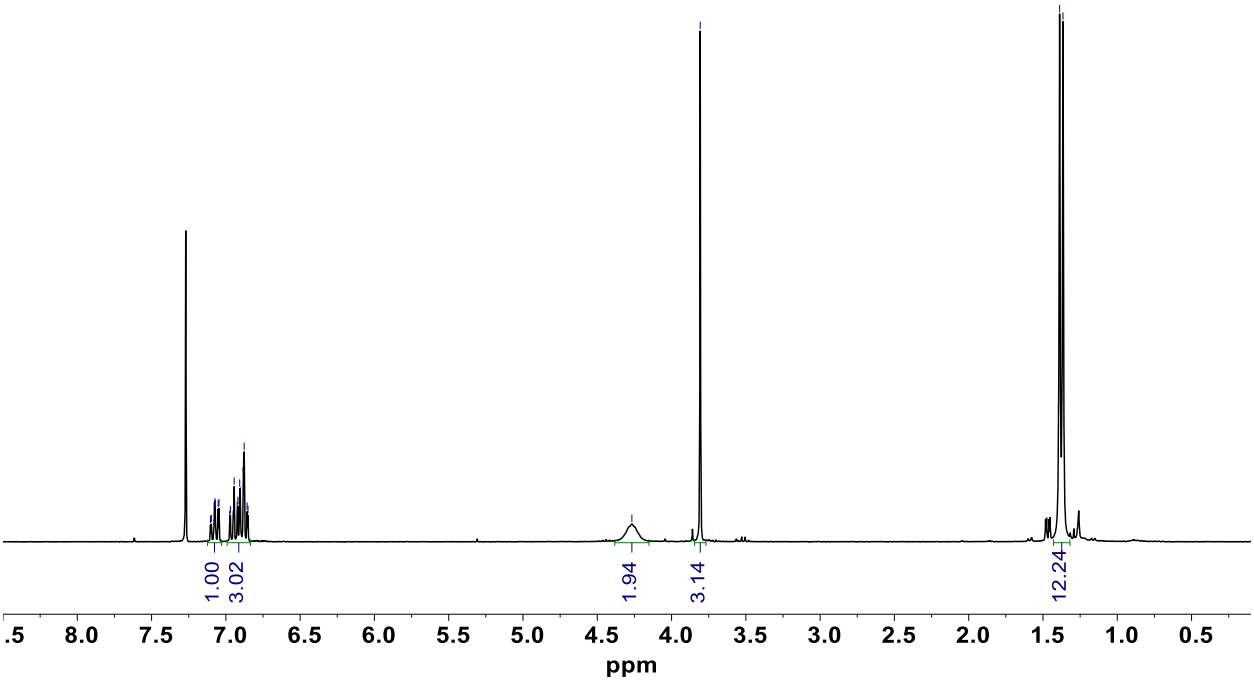

Figure A4: ^{1}H NMR spectrum of **2b** (300 MHz in $CDCl_3$).

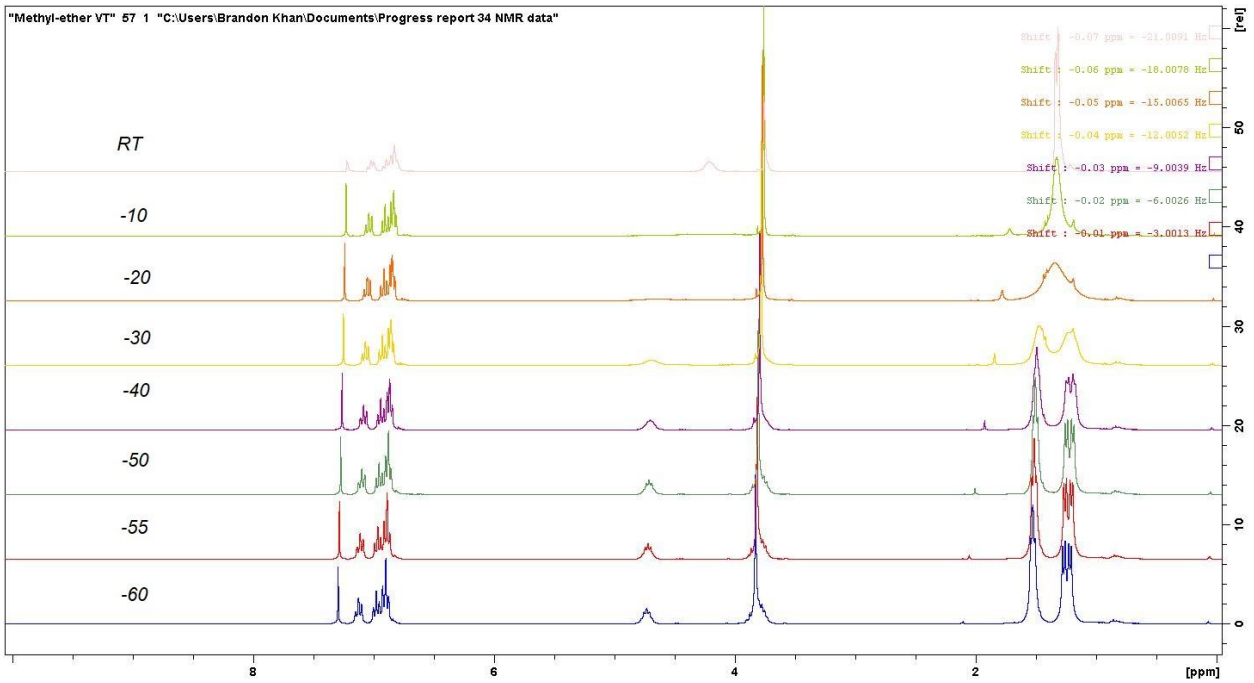

Figure A5: ^{1}H VT-NMR spectrum of **2b** (300 MHz in $CDCl_3$).

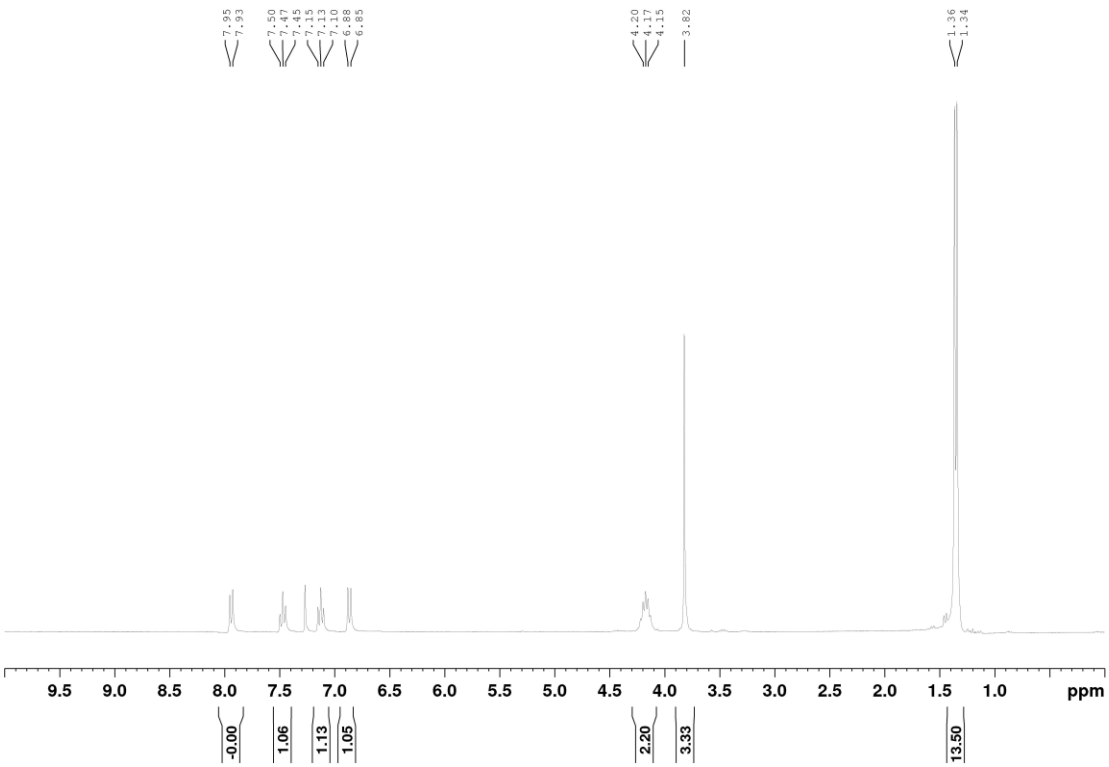

Figure A6: ^{1}H NMR spectrum of **2c** (300 MHz in $CDCl_3$).

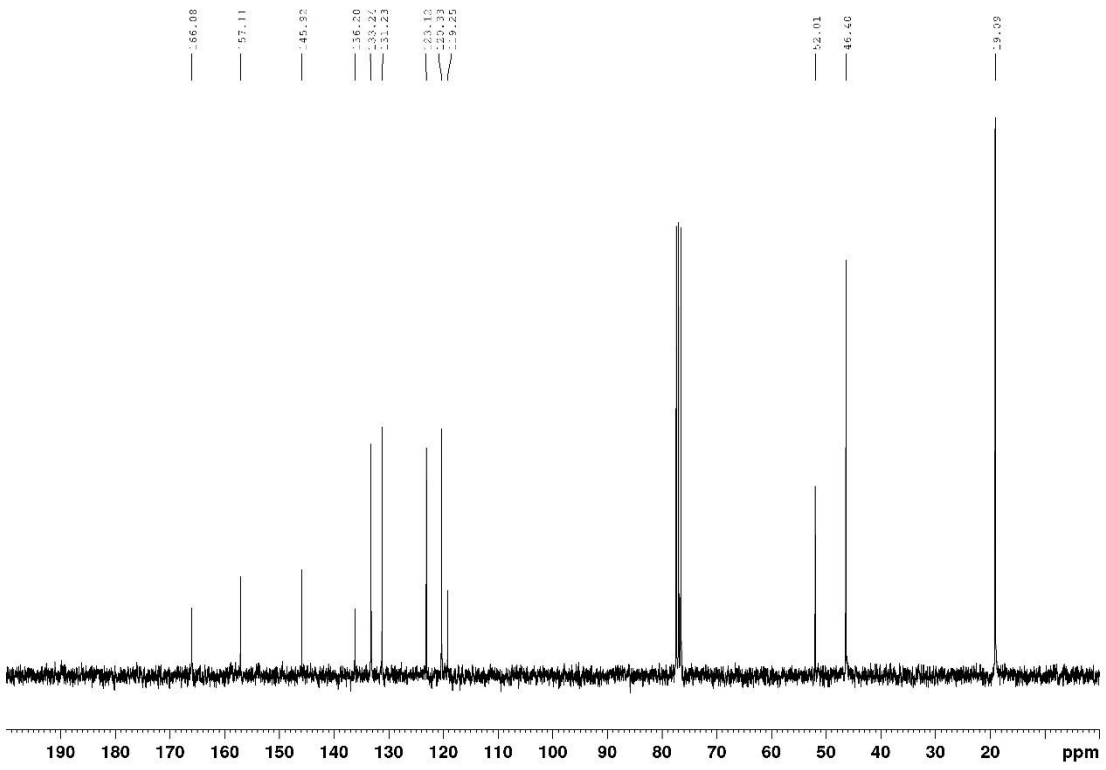

Figure A7: $^{13}C\{^{1}H\}$ NMR spectrum of **2c** (75 MHz in $CDCl_3$).

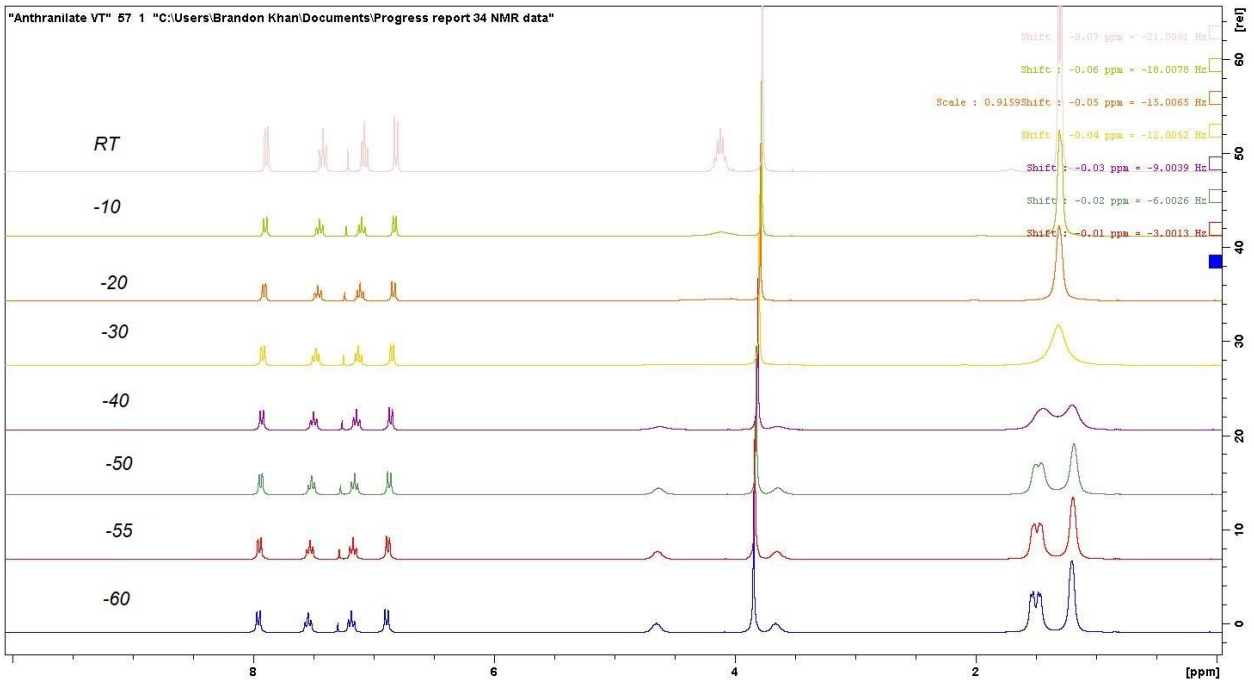

Figure A8: ^{1}H VT-NMR spectrum of **2c** (300 MHz in $CDCl_3$).

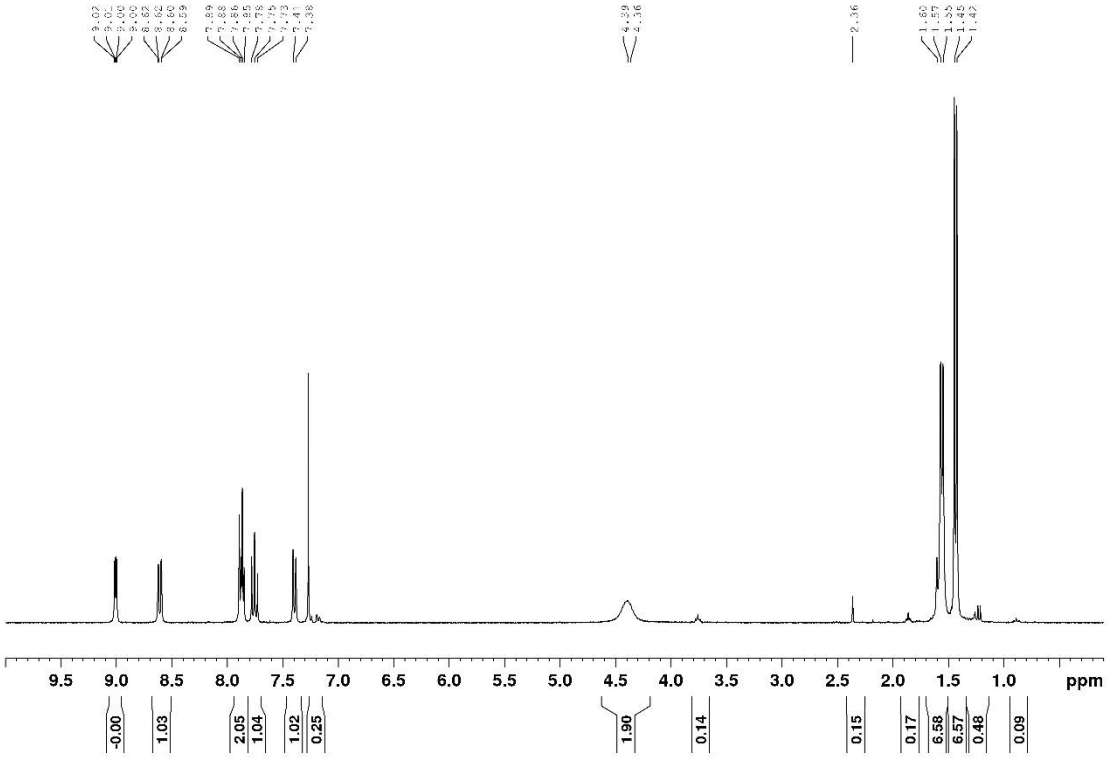

Figure A9: ^{1}H NMR spectrum of **3a** (300 MHz in $CDCl_3$) (δ 5.31 is DCM).

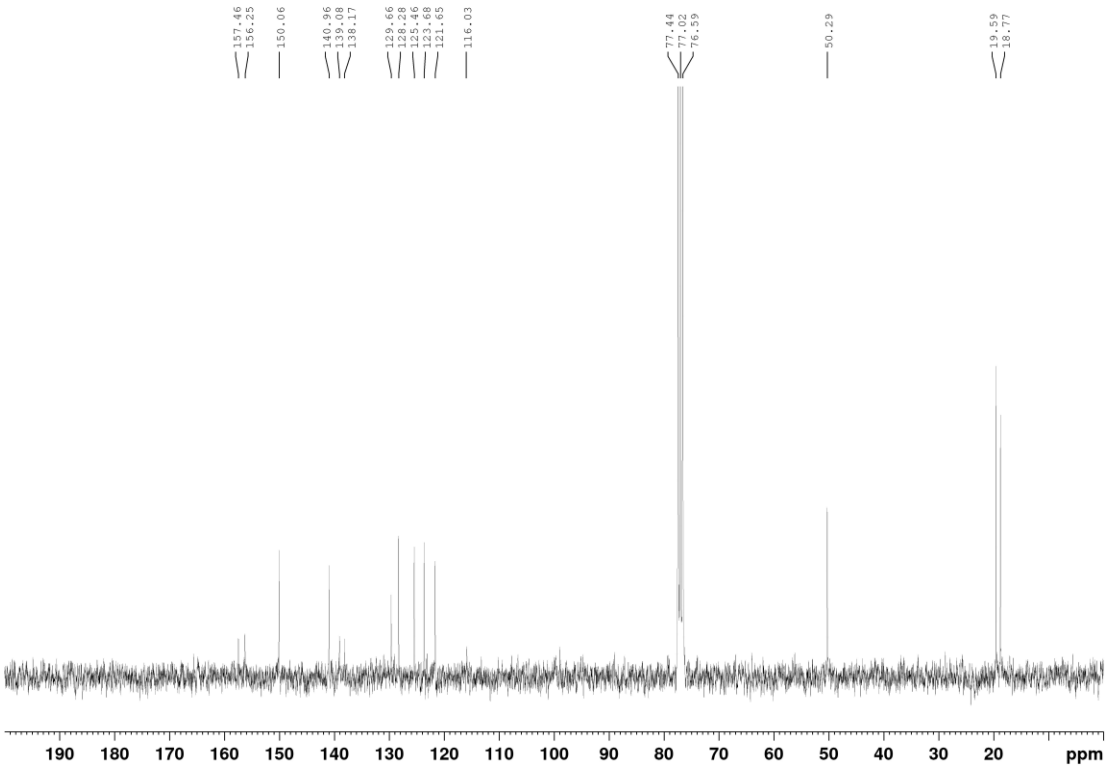

Figure A10: $^{13}C\{^{1}H\}$ NMR spectrum of **3a** (75 MHz in $CDCl_3$).

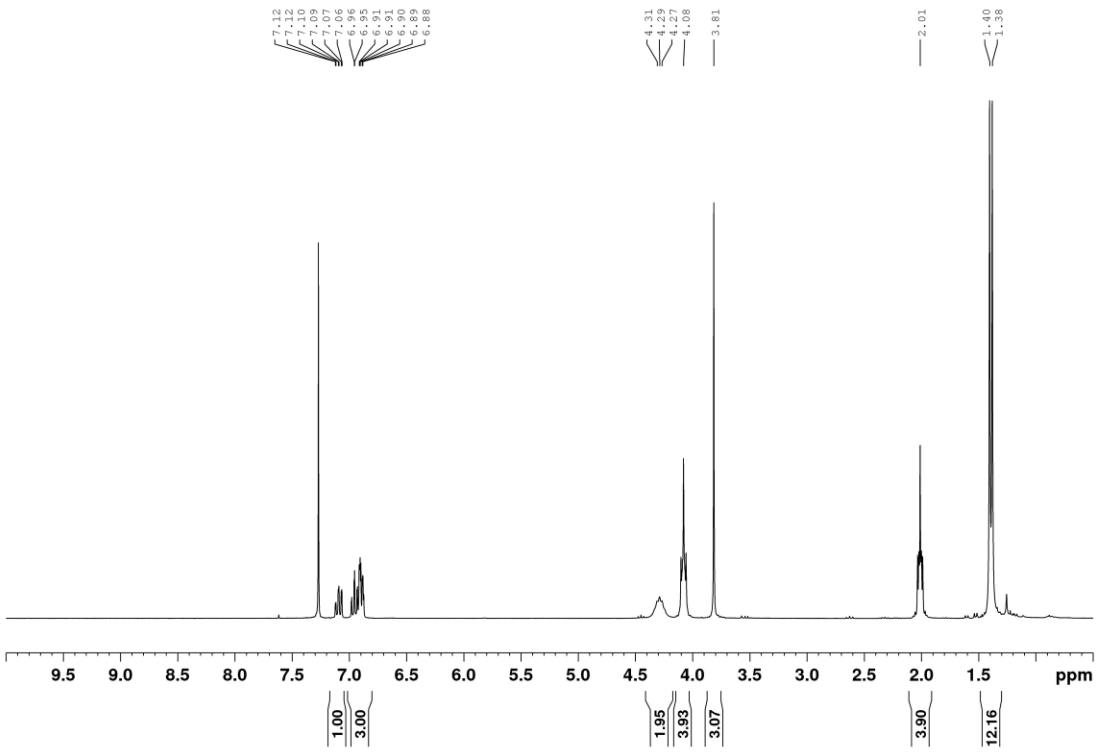

Figure A11: ^{1}H NMR spectrum of **3b** (300 MHz in $CDCl_3$).

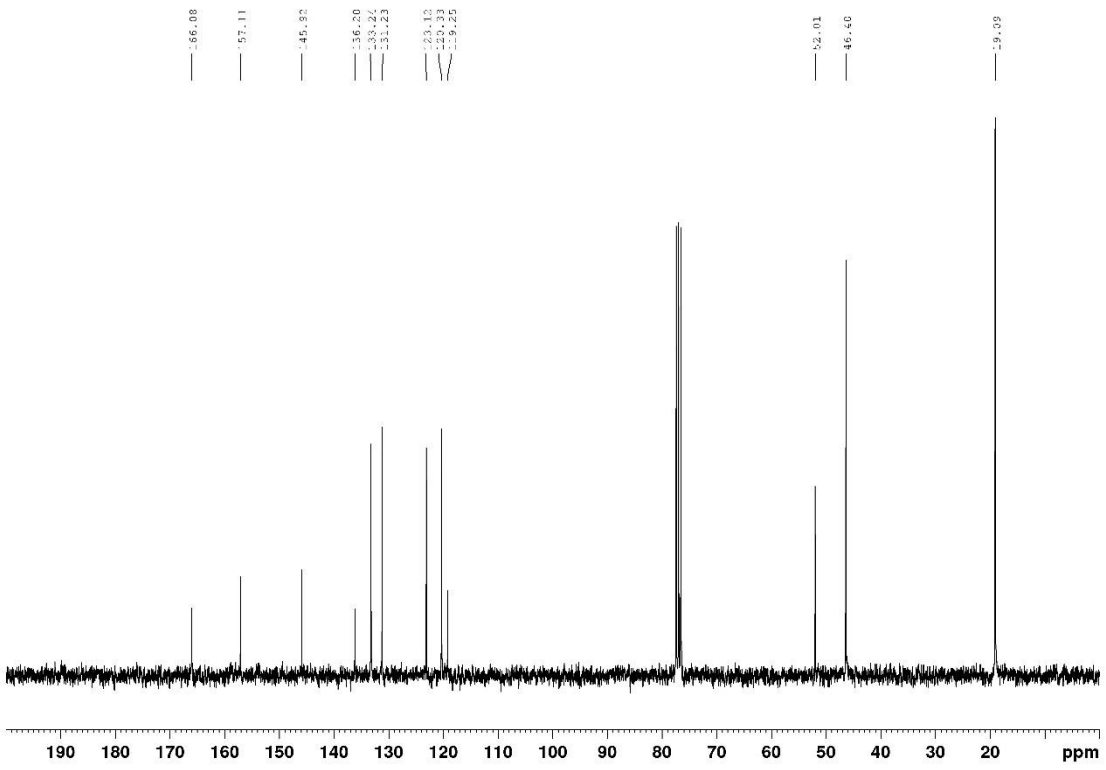

Figure A12: ^{13}C NMR spectrum of **3b** (75 MHz in $CDCl_3$).

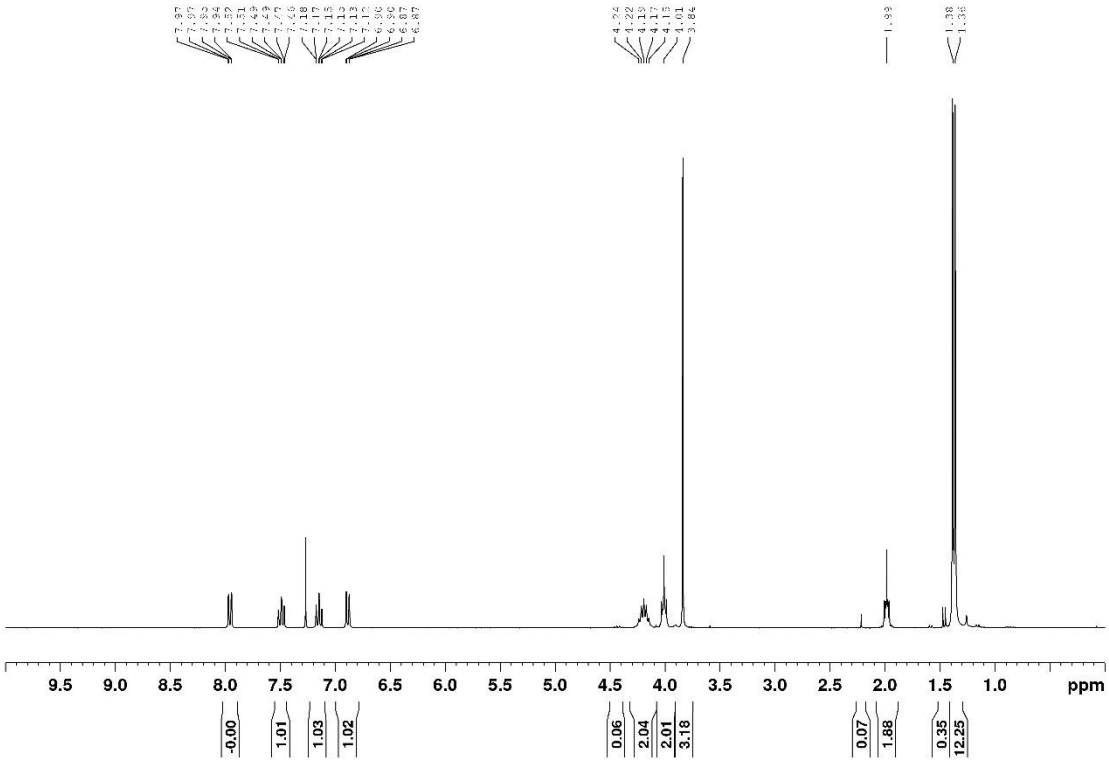

Figure A13: ^{1}H NMR spectrum of **3c** (300 MHz in $CDCl_3$).

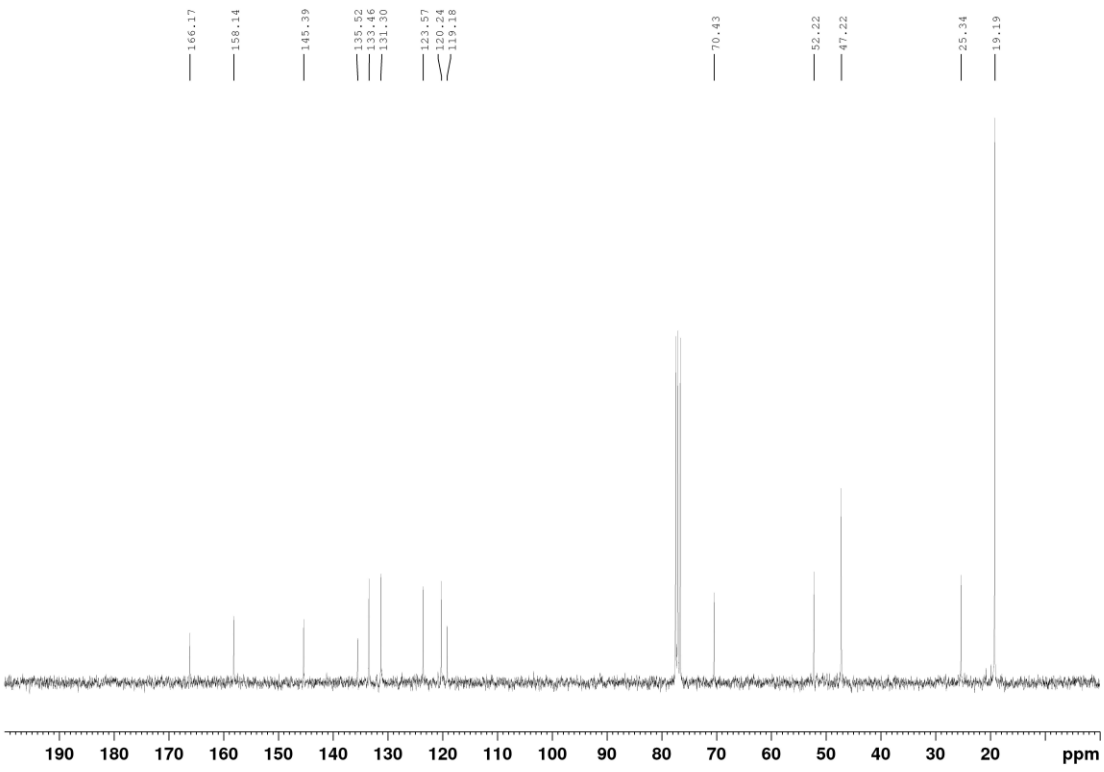

Figure A14: $^{13}C\{^{1}H\}$ NMR spectrum of **3c** (75 MHz in $CDCl_3$).

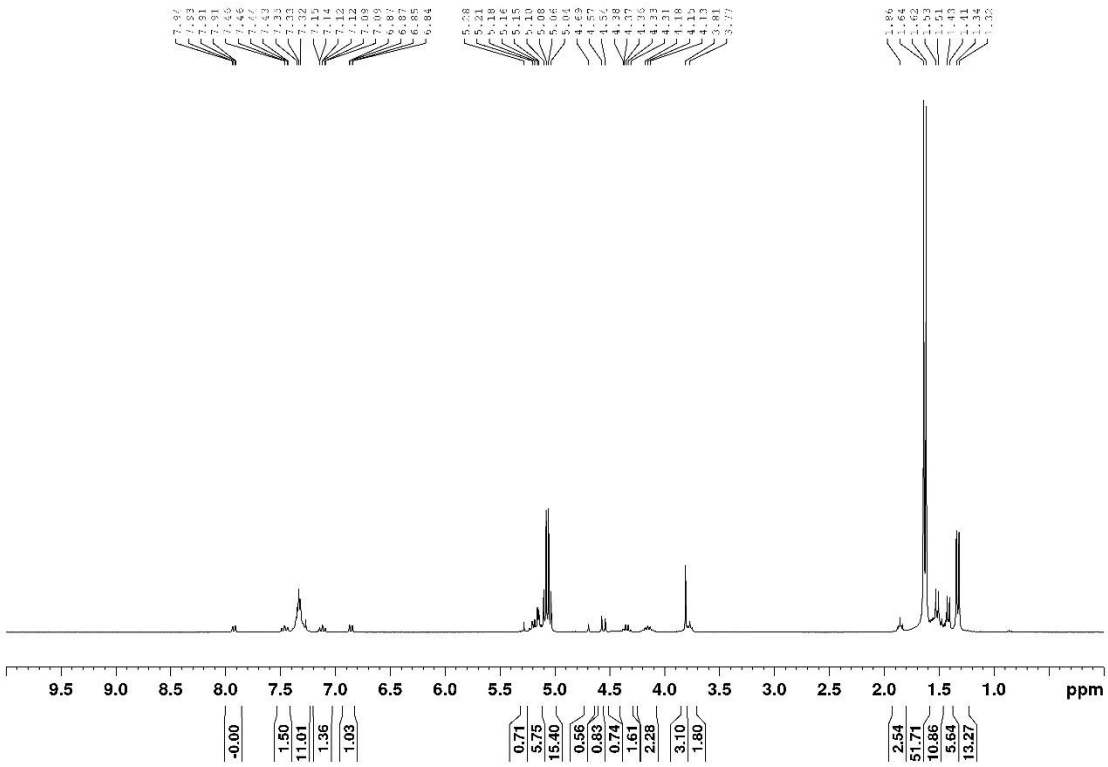

Figure A15: ^{1}H NMR spectrum of reaction of **3c**, BnOH and LA (300 MHz in $CDCl_3$).

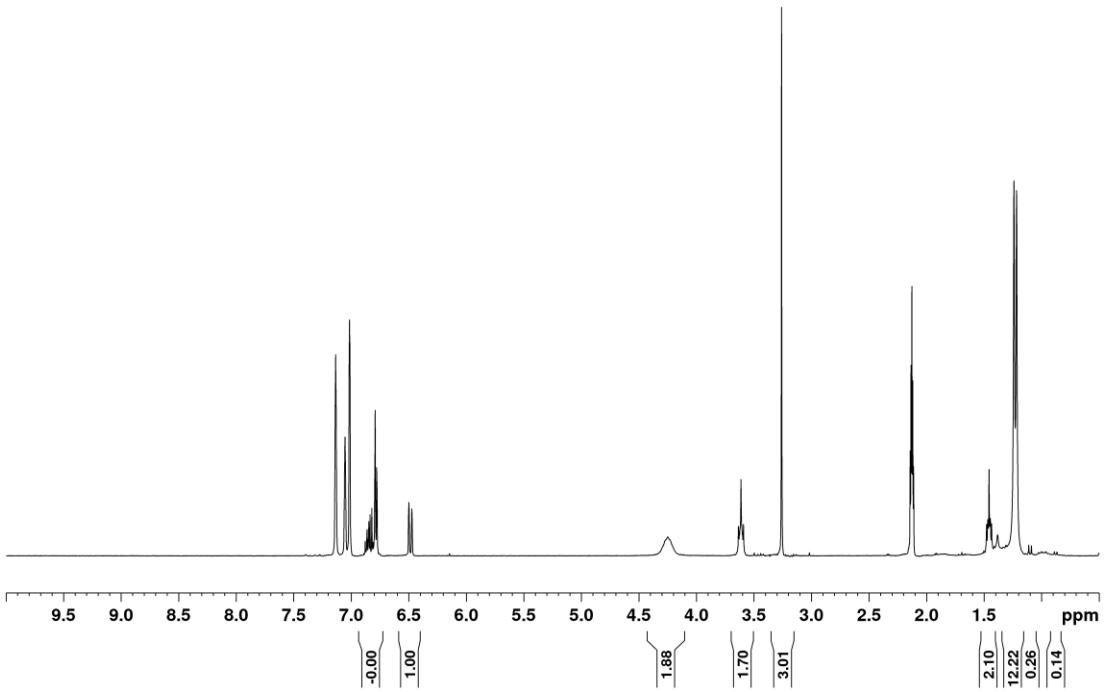

Figure A16A: ^{1}H NMR spectra of **3b** dissolved in tol-d_8 at room temperature (300 MHz intol-d_8).

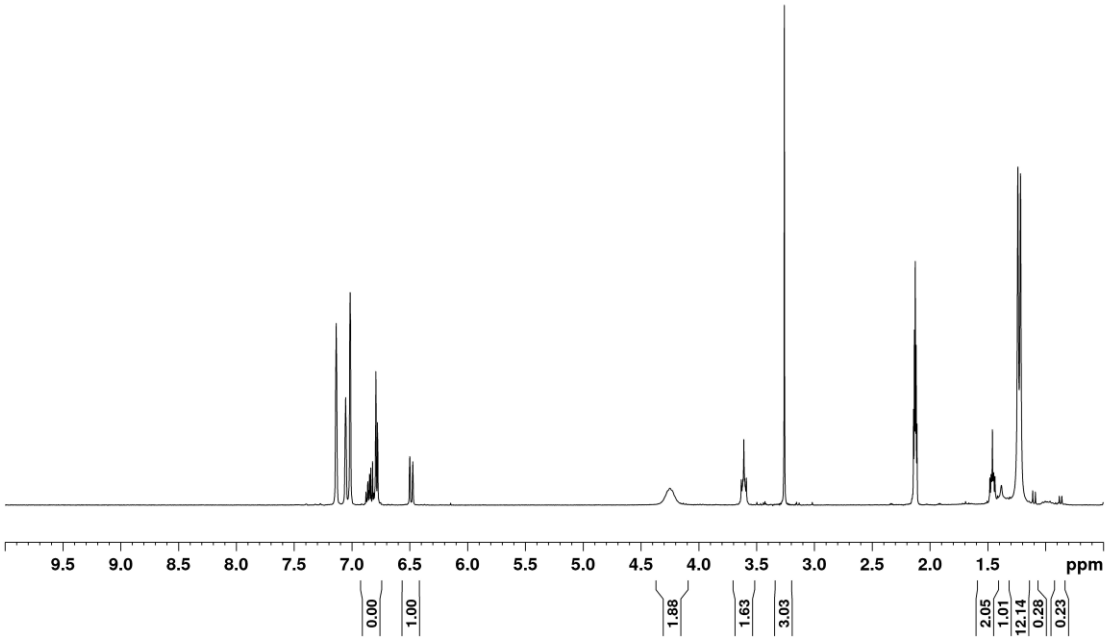

Figure A16B: ^{1}H NMR spectra of **3b** dissolved in tol-d_8 and held at 110 °C for 2 h (300 MHz intol-d_8).

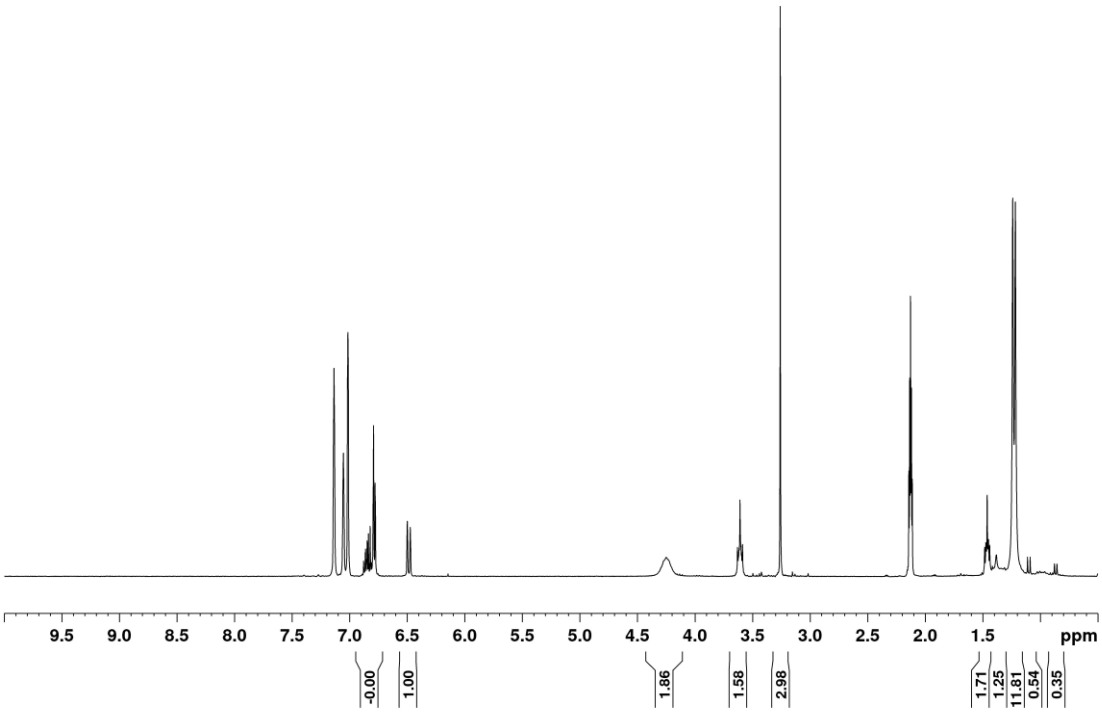

Figure A16C: ^{1}H NMR spectra of **3b** dissolved in tol-d_8 and held at 110 °C for 3 h (300 MHz intol-d_8).

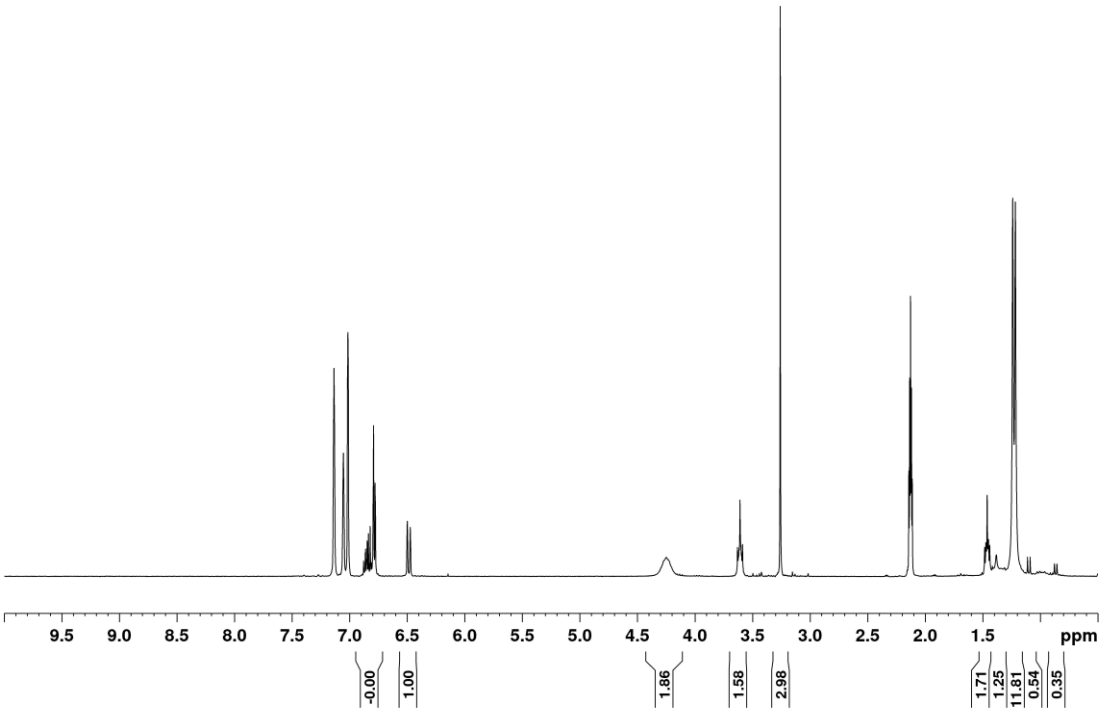

Figure A16D: ^{1}H NMR spectra of **3b** dissolved in tol-d_8 and held at 110 °C for 5 h (300 MHz intol-d_8).

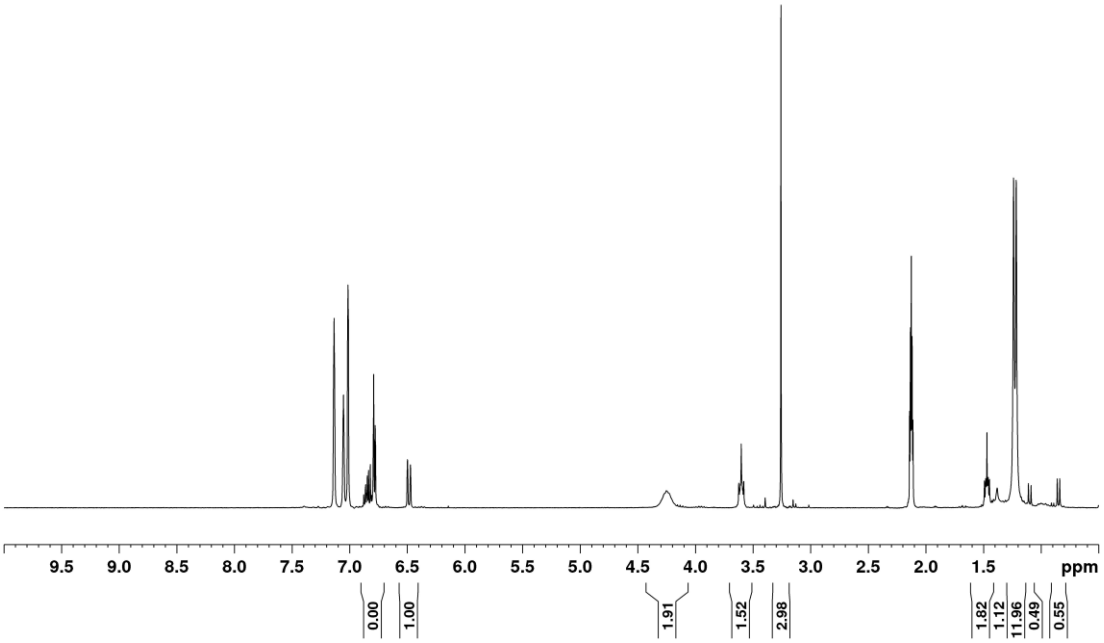

Figure A16E: ^{1}H NMR spectra of **3b** dissolved in tol-d_8 and held at 110 °C for 24 h (300 MHz intol-d_8).

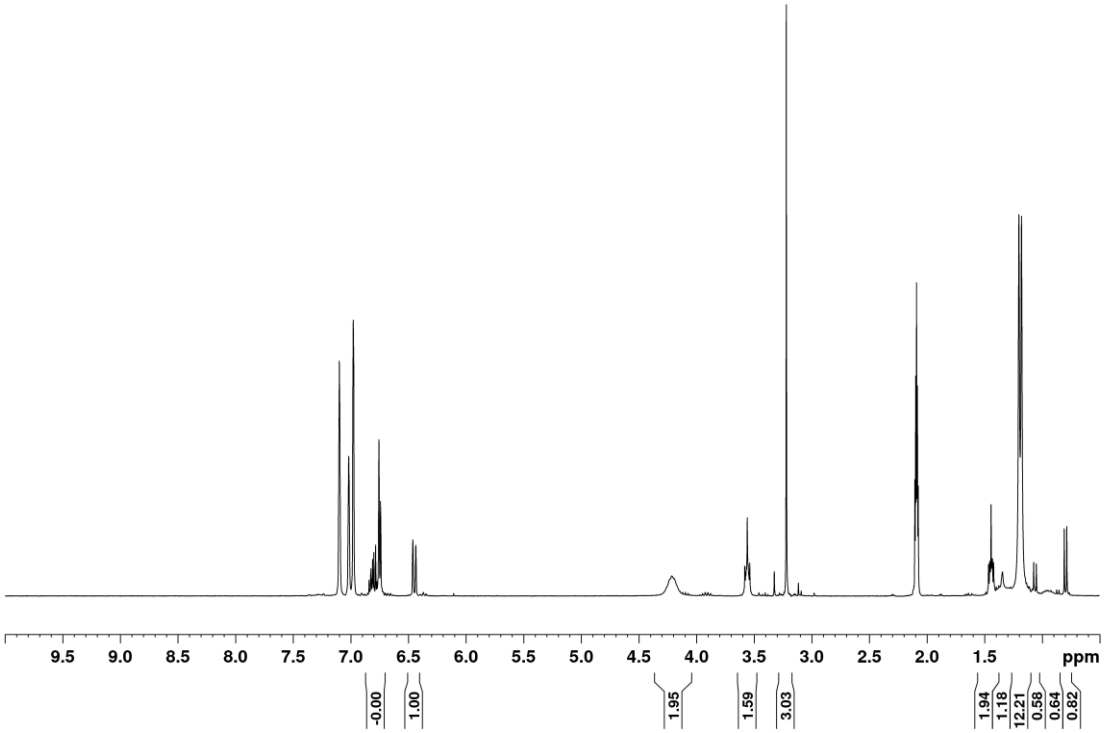

Figure A16F ^{1}H NMR spectra of **3b** dissolved in tol-d_8 and held at 110 °C for 96 h (300 MHz intol-d_8).